TAMPERE UNIVERSITY OF TECHNOLOGY
Degree Programme in Electrical Engineering

ARTTU RASKU

MULTI-ANTENNA SOLUTIONS FOR AUTOMOTIVE ENVIRONMENT

Master of Science Thesis

Examiner: professor Lauri Kettunen
Examiner and topic were approved
in the meeting of faculty council on 5
November 2008

ABSTRACT

TAMPERE UNIVERSITY OF TECHNOLOGY
Master's Degree Programme in Electrical Engineering
RASKU, ARTTU: Multi-antenna solutions for automotive environment
Master of Science Thesis, 103 pages
January 2009
Major: Radio frequency electronics
Examiner: Professor Lauri Kettunen
Keywords: MIMO, beamforming, automotive antenna, multi-antenna, BF MIMO, diversity

MIMO systems have emerged in the last few years as a means to improve the quality of service and spectral efficiency of wireless communication systems. This thesis examines the use of multi-antenna systems on vehicles. The main objectives of this thesis are to develop a procedure for the design of multi-antenna systems, compare the benefits of different multi-antenna systems in automotive environment, study the suitability of the chosen electromagnetic simulation method to modelling and simulation of automotive antennas, and also to give ample references for the reader, in case a more in-depth understanding in the areas of multi-antenna techniques and automotive antennas is needed.

The electromagnetic simulation of the antenna systems are based on the finite integration technique with commercial software, while link level performance simulation is performed on a MATLAB implementation of the SCME radio channel model. The finite integration technique is found to provide accurate radiation pattern results, and it can be recommended for the purpose of simulation of automotive antenna systems at the 700 MHz carrier frequency. On link level simulations the focus is on simulating 2×2 multiantenna systems. These simulations imply a noticeably improved BER when a BF MIMO system is employed, compared to the traditional MIMO system. The BF MIMO is a new concept that combines the best sides of beamforming and MIMO. This is the first study where the BF MIMO concept is applied to antennas in automotive environment. The results for the different antenna array configurations were indeterminate. In general, it can be said that the radio channel (or channel model) is one of the most significant factors in determining the performance of a multi-antenna systems, and it is highly unlikely that any single array configuration can provide optimal performance in every channel conditions.

The first part of this thesis, Chapters 2 and 3, provides background of multi-antenna systems. Theoretical concepts of multi-antenna systems are introduced in Chapter 2 to enable the analysis of such systems. In the third chapter, a literature survey is presented as a summary of related studies on the areas of automotive antennas, multi-antenna systems, related information theory and electromagnetic simulation methods of antennas. In the latter part of this thesis, Chapter 4 describes the electromagnetic and link level simulation software packages and the simulation of the antennas. The results are presented in Chapter 5, and conclusions are drawn in Chapter 6.

TIIVISTELMÄ

TAMPEREEN TEKNILLINEN YLIOPISTO
Sähkötekniikan koulutusohjelma
RASKU, ARTTU: Moniantennijärjestelmät autoympäristössä
Diplomityö, 103 sivua
Tammikuu 2009
Pääaine: Suurtaajuustekniikka
Tarkastaja: professori Lauri Kettunen
Avainsanat: MIMO, keilanmuodostus, autoantenni, moniantennijärjestelmä, BF MIMO, diversiteetti

Moniantennijärjestelmiä, erityisesti niin kutsuttuja MIMO-järjestelmiä, on kehitetty muutamien viime vuosien aikana langattomien tiedonsiirtojärjestelmien palvelun laadun (quality of service) ja spektritehokkuuden parantamiseksi. Tässä diplomityössä tutkitaan moniantennijärjestelmien käyttöä ajoneuvoissa. Ajoneuvoissa käytettäväksi suunniteltujen antennien tulee vastata tiukkoihin ulkonäöllisiin ja ympäristöllisiin vaatimuksiin, mikä tekee niiden suunnittelusta toisaalta erikoisosaamista, toisaalta poikkitieteellisyyttä vaativaa. Tämän työn tavoitteena on kehittää menetelmä moniantennijärjestelmien suunnitteluun, tutkia ajoneuvoon asennettujen antenniryhmien tyypin ja sijainnin vaikutusta järjestelmän suorituskykyyn, vertailla eri moniantennijärjestelmillä saavutettavia hyötyjä autoympäristössä, analysoida valitun mallinnusmenetelmän soveltuvuutta autoantennien mallintamiseen sekä antaa lukijalle kattava lähdeviitteiden kokoelma, jonka avulla täydentää asiantuntemustaan auto- ja moniantennijärjestelmistä.

Luvuista 2 ja 3 muodostuva työn ensimmäinen osio rakentaa pohjatietämystä moniantennijärjestelmistä, jota tullaan tarvitsemaan jälkimmäisissä luvuissa. Moni-antennijärjestelmiin liittyviä teoreettisia käsitteitä esitellään luvussa 2. Koska moderneilta autoihin asennettavilta antenneilta vaaditaan usein pientä fyysistä kokoa, tässä luvussa esitellään lyhyesti myös sähköisesti pienten antennien erikoisominaisuuksia erityisesti säteilyhyötysuhteen ja kaistanleveyden osalta. Kolmannessa luvussa käydään läpi kirjallisuusselvityksen perusteella löydettyjä julkaisuja seuraavilta alueilta: antennit ajoneuvoissa, moniantennijärjestelmät, informaatioteoria soveltuvilta osin sekä menetelmät antennien sähkömagneettiseen simulointiin. Kirjallisuusselvityksessä keskitytään tieteellisiin artikkeleihin, joskin myös muutamiin alan perusteoksiin ja oppikirjoihin tullaan viittaamaan. Kirjallisuusselvityksen tärkein anti liittyy MIMO-järjestelmien suorituskyky-mittauksiin, joiden perusteella näyttää vahvasti siltä, että radiokanava – tai simuloinneissa kanavamalli – vaikuttaa hyvin huomattavissa määrin saavutettuihin suorituskykyarvoihin. On siis todennäköistä, että millään yhden tyyppisellä antenniryhmällä ei voida saavuttaa parasta mahdollista suorituskykyä kaikissa ympäristöissä, vaan radiokanava (käyttöympäristö) vaikuttaa erittäin merkittävissä määrin siihen, kuinka hyvä tietyn antenniryhmän suorituskyky on verrattuna muihin antenniryhmiin.

Työn jälkimmäinen osio, sisältäen luvut 4–6, käsittelee ajoneuvoissa käytettävien moniantennijärjestelmien simulointia, suunnittelua, toteutusta ja analysointia. Luvussa 4 analysoidaan nykyaikaisia sähkömagneettisen mallintamisen menetelmiä ja ohjelmistoja. Antennijärjestelmien sähkömagneettisessa mallintamisessa käytettiin kaupallista, niin kutsuttuun finite integration menetelmään perustuvaa ohjelmistoa. Kyseisen ohjelmiston ominaisuuksia analysoidaan ottaen huomioon erityisesti auto antennin asennusympäristönä.

Sähkömagneettisen mallintamisen lisäksi työssä tutkitaan moniantennijärjestelmien vaikutusta palvelun laatuun mallintamalla järjestelmää radiolinkkitasolla, joka ottaa huomioon signaalin lähettäjän ja vastaanottajan välisen radiokanavan. Linkkitason suorituskyvyn mallinnus suoritettiin SCME-kanavamallin MATLAB-toteutuksella, joka on kehitetty tämän työn ulkopuolella. Suorituskykyä mitataan linkkitasolla tässä työssä bittivirhesuhteella. Simuloitujen sekä mitattujen antenniryhmien atsimuuttitason säteilykuvioiden perusteella laskettava bittivirhesuhde kertoo, kuinka paljon virheitä tiedonsiirrossa tietyllä kohinatasolla tilastollisesti tapahtuu.Linkkisimulointien tärkeimpiä tuloksia on perinteisen MIMO järjestelmän ja niin kutsutun BF MIMO järjestelmän suorituskyvyn vertailu. BF MIMO on varsin uusi konsepti, jonka ajatuksena on yhdistää keilanmuodostuksen ja MIMOn parhaita puolia. Tässä työssä keskitytään 2×2 antennijärjestelmien simulointiin ja mittaamiseen. Luvussa 5 esitellään valittujen antennimallien sähkömagneettisen ja linkkitason simulointien tuloksia, sekä suoritetaan vertailu prototyypillä saavutettuihin mittaustuloksiin. BF MIMO-järjestelmän linkkitason suorituskykysimulointia ei ole aikaisemmin sovellettu autoympäristössä oleviin antenniryhmiin. Johtopäätökset esitellään luvussa 6.

Simuloinneissa käytettiin kahta automallia: ensimmäinen koostuu tasomaisista paneeleista ja on muutenkin hyvin pelkistetty – ”laatikkomalli”. Toinen on ulkokuoreltaan hyvin yksityiskohtainen CAD-tietoihin pohjautuva malli BMW perheautosta, mutta tämäkään ei sisällä lainkaan sisustaa. Toisaalta tässä työssä ei haluta keskittyä tietyn automallin antennien mallintamiseen, vaan tarkoituksena on kartuttaa yleisluontoista tietoa auton korin vaikutuksista antennien säteilyominaisuuksiin. Tähän tarkoitukseen kummankin automallin nähtiin soveltuvan hyvin. Myös antennimalleissa keskityttiin samoista syistä hyvin pelkistettyihin monopolimalleihin.

Mittauksia varten ei ollut saatavilla oikeaa autoa, joten käytetty automalli koostuu teräspalkein yhteen hitsatuista konepellistä, katosta ja takaluukusta. Nämä osat – teräspalkkeja lukuun ottamatta – olivat peräisin oikeista autoista. Automalli ei siis sisällä sivupaneeleja eikä myöskään minkäänlaista sisustaa penkkeineen, joten näiden vaikutusta antennien suorituskykyyn ei kyetty mittaamaan.

Vertaamalla simuloituja ja mitattuja antennien säteilykuvioita käytetyn mallinnusmenetelmän voidaan todeta tarkkuutensa puolesta soveltuvan hyvin antennien mallintamiseen autoympäristössä. Mallinnusmenetelmällä on kuitenkin myös haasteita, joista suuri osa liittyy mallinnusalueen kokoon ja mallinnettujen yksityiskohtien määrään. Mallinnettavan alueen koon tai mallin yksityiskohtaisuuden lisääntyessä vaadittu tietokoneen keskusmuistin tarve kasvaa hyvin nopeasti. Tästä syystä

mallinnusalue joudutaan käytännössä rajoittamaan mahdollisimman pieneksi, jolloin esimerkiksi maanpinnan todenmukainen mallintaminen on haasteellista. Myös auton sisustan mallintaminen saattaa lisääntyvän keskusmuistin tarpeen johdosta osoittautua hankalaksi. Käytetyillä automalleilla päästään säteilykuvioiden osalta melko hyvään tarkkuuteen, mutta antennien sisäänmenosuureiden tarkan mallintamisen havaittiin vaativan tiheämpää laskentaverkkoa antennin syötön kohdalla. Tällaista ei kuitenkaan käytetty, koska antennien sisäänmenosuureiden tarkka mallintaminen ei kuulu tämän työn ydinalueeseen.

Linkkitason simulointien perusteella näyttää siltä, että BF MIMO-järjestelmä parantaa suorituskykyä hieman verrattuna vastaavaan MIMO-järjestelmään. Antenniryhmäkonfiguraatioiden osalta tuloksia on vaikeampi tulkita. Näyttäisi kuitenkin siltä, että antennien sijoituspaikalla katossa on melko vähän merkitystä: sijoittamalla antennit mahdollisimman keskelle kattoa saavutettiin vain hyvin lievä parannus bittivirhesuhteeseen verrattuna tilanteeseen, jossa antennit oli sijoitettu katon reunalle. Useissa tapauksissa näyttää myös siltä, että paras suorituskyky saavutetaan antennielementtien välisen etäisyyden ollessa alle yksi mutta yli puoli aallonpituutta. Joissain tapauksissa tulokset eri automallien ja simulointien tai mittausten välillä ovat kuitenkin ristiriitaisia, ja lisätutkimukset tältä osin ovat tarpeen.

ACKNOWLEDGEMENTS

This thesis was written during the course of the year 2008. It is the results of much hard work, some sweat, occasional fits of frustration (hello, word processor!), a lot of writing and even more learning. The year has been a hectic one, but also more interesting than perhaps any one before it. I have learned a great deal during this year, and not just from antennas, but from working in general and the infamous "realities of life". Of course, that is one of the main goals of theses'.

First and foremost, I would like to thank Elektrobit, for giving me a chance to work on such an interesting research area. Besides being very contemporary, in the best case my thesis will also provide real added value to the development of multi-antenna systems on vehicles at Elektrobit. And that has been a major motivating factor for me.

Another key factor in the development of this thesis has been my instructor, Dr. Taavi Hirvonen, Elektrobit, whose professional skill has allowed this thesis to avoid the potential pitfalls that I by myself would surely have fallen victim to. His feedback has been an invaluable asset in improving this thesis from scientific as well as linguistic points of views.

From Elektrobit I would further like to express my gratitude to Dr. Juha Ylitalo and Mr. Tuomo Haarakangas. Juha has developed the link level performance simulation code used in this thesis and he has also provided important feedback on the sections dealing with link level system performance. Tuomo has diligently answered my questions about CST MWS simulation software, provided feedback on Chapter 4 as well as designed the Butler matrix that was used in the measurements. Furthermore, I would like to acknowledge CST for providing the CAD-data based car model.

A great big thank you goes also to my family. You all mean a lot to me! In particular, I would like to thank my father for giving the Computer a chance, all the while ushering me to go play outside; my mother, who always knew the best way to encourage and comfort me; and my sister, who I know will always be there for me. Finally, very special thanks to Hanna for showing me what else there is in life.

TABLE OF CONTENTS

ABBREVIATIONS AND NOTATION

2.5D	Two- and a half Dimension(al)
3D	Three Dimension(al)
3GPP	3rd Generation Partnership Project
3GPP2	3rd Generation Partnership Project 2
ABC	Absorbing Boundary Condition
ACM	Advanced Car Model
AM	Amplitude modulation
AoA	Angle of Arrival
AoD	Angle of Departure
AS	Angle Spread
AWGN	Additive White Gaussian Noise
BC	Boundary Condition
BCM	Basic Car Model
BER	Bit-Error Rate
BF	Beamforming
BS	Base Station
BW	Bandwidth
CAD	Computer-aided design
Ccdf	Complementary Cumulative Distribution Function
DAB	Digital Audio Band or Digital Audio Broadcasting
DFT	Discrete Fourier Transform
DoA	Direction of Arrival
DS	Delay Spread
DVB-T	Digital Video Broadcasting, Terrestrial
EM	Electromagnetic
FDTD	Finite Difference Time Domain
FEM	Finite Element Method
FFT	Fast Fourier Transform
FIT	Finite Integration Technique
FM	Frequency Modulation
FS	Fixed Station
GPS	Global Positioning System
GSM	Global System for Mobile communications
I.i.d.	Independent, Identically Distributed
ISI	Intersymbol Interference
ISM	Industrial, Scientific, and Medical
LAN	Local Area Network
LOS	Line-Of-Sight
LTI	Linear, Time-Invariant
MEMS	Micro-Electro-Mechanical Systems

MIMO	Multiple-Input—Multiple-Output
MISO	Multiple-Input—Single-Output
MoM	Method of Moments
MS	Mobile Station
NLOS	Non-Line-Of-Sight
PBA	Perfect Boundary Approximation®
PEC	Perfect Electrical(ly) Conductor/Conducting
PCB	Printed Circuit Board
PIFA	Planar Inverted-F Antenna
PML	Perfectly Matched Layer
RF	Radio Frequency
SCM	Spatial Channel Model
SCME	Spatial Channel Model Extended
SIMO	Single-Input—Multiple-Output
SINR	Signal-to-Interference-and-Noise Ratio
SISO	**S**ingle-Input—Single-Output
SNR	Signal-to-Noise Ratio
SM	Spatial Multiplexing
Rx	Receive
TST	Thin Sheet Technology™
Tx	Transmit
VSWR	Voltage Standing Wave Ratio
UMTS	Universal Mobile Telecommunications System
WiMAX	Worldwide Interoperability for Microwave Access
*****	Transpose conjugate
min(x,y)	The smaller of the values x, y
$\boldsymbol{a}$	The radius of a sphere inside which a small antenna lies
$\hat{\boldsymbol{a}}_r$	Unit vector, *r*-directed
$\boldsymbol{c}$	Speed of light
$\boldsymbol{f}$	Frequency
$\boldsymbol{f}_{lower}$	Lower half-power frequency
$\boldsymbol{f}_{min}$	Minimum frequency limit
$\boldsymbol{f}_{upper}$	Upper half-power frequency
$\boldsymbol{h}_{i,j}(\tau,t)$	Channel impulse-response at time t to an impulse applied at time $t-\tau$, between the j:th transmit antenna and the i:th receive antenna
$\boldsymbol{i}$	Index number
$\boldsymbol{j}$	Imaginary unit
$\boldsymbol{j}$	Index number
$\boldsymbol{k}$	Wave number

l	Length
n	Index number
n	Positive integer number
n_i	Additive noise in the i:th receiver
q	Percentage value between 0 and 100
r	Radial distance of the spherical coordinate system
$s_j(t)$	Signal-vector transmitted from the j:th transmit antenna at the time instant t
t	Time instant
w_e	Electric-energy density
w'_e	Non-propagating electric-energy density
$w^{rad}{}_e$	Radiated electric-energy density
w_m	Magnetic-energy density
$y_i(t)$	Signal-vector received by the i:th receive antenna at the time instant t
A_r	Magnetic vector potential, r-directed
B_c	Coherence or correlation bandwidth
E	Electric field
E_θ	Electric field, θ-component
E_θ^{rad}	Radiated electric field, θ-component
E_r	Electric field, r-component
H	Magnetic intensity
H	Complex gain vector of a SIMO or a MISO channel
H	Complex transmission coefficient matrix of a MIMO channel
H	Height
H_φ	Magnetic intensity, φ-component
H_φ^{rad}	Radiated magnetic intensity, φ-component
I_n	Identity matrix with n columns and n rows
L	Length
M	Total number of radiating elements
M_R	Number of receive antennas
M_T	Number of transmit antennas
N	Number of unknowns
N	Integer positive number
P_{rad}	Total radiated power
P_{in}	Input power accepted by an antenna
Q	Quality factor
Q_0	Unloaded quality factor
Q_c	Conductor quality factor
Q_d	Dielectric quality factor

Q_r	Radiation quality factor
R	Transmission rate
W	Width
W_e'	Total nonpropagating electric energy
W_m'	Total nonpropagating magnetic energy
Z	Wave impedance
ε	Permittivity
ε_r	Relative permittivity
η	Efficiency
θ	Elevation angle of the spherical coordinate system
λ	Wavelength
μ	Permeability
μ_r	Relative permeability
ρ	Average signal-to-noise ratio
σ	Electric conductivity
φ	Azimuth angle of the spherical coordinate system
τ	Delay between the transmission and receiving of a signal
ω	Angular frequency
Δt	Time step
Δx	Length interval
Δy	Width interval
Δz	Height interval

1. INTRODUCTION

The invention of transistor radio in the early 1950s enabled small and, above all, durable and shock resistant radios. At the same time the automobile industry was recovering from the Second World War. An in-car radio quickly became a popular option and even standard equipment of automobiles in the 1950s. The AM/FM radio was for long the only equipment requiring an antenna in a car. However, this began to change during the early 1990s with the advent of mobile phones, as well as other emerging terrestrial and satellite broadcasting services. At the beginning of the year 2009 it seems that the pace is only increasing, as more and more new technologies requiring wireless access directly to vehicles are emerging. A new development in the field of automotive antennas (and indeed mobile antennas in general) is the use of multiple antenna elements as an array to enhance the quality of service and spectral efficiency of the wireless communication system. These systems are often referred to as MIMO (short for multiple-input–multiple-output) systems.

The shift to omnipresent mobile Internet has increased the requirements for increased data rates in "online" devices in the recent years. It is anticipated that within the next few years services provided through an Internet-based IP protocol will expand to include digital radio and (high definition) television broadcasting, and more. These new services will require drastically higher data rates than what is possible with traditional single antenna systems. Basically, only two options exist to increase the data rates of single antenna systems: increase the bandwidth or increase the signal-to-noise ratio of the signal. Both of these methods work reasonably well up to a certain point. However, the usable radio spectrum is limited in width, and spectral efficiency of traditional systems must be radically improved to accommodate new data-intensive services. On the other hand, health concerns limit the maximum available transmission power, so that signal-to-noise ratio cannot be increased indefinitely, even under the best propagation conditions.

Drawing near to the end of the 1990's a radically new approach was devised: if multiple antennas were used at both the transmitter and the receiver, it could be possible to effectively multiply the transfer rates of single-antenna systems. Better yet, the scaling of the transfer rate would ideally be linear with the number of antennas at both ends of the communication link. Since these first results the technology, now dubbed MIMO, has enjoyed an almost unforeseen research and development interest. Most incredibly, in much less than ten years the first applications and products taking good use of this new technology were already available for anyone to purchase. For such a large-scale standards-driven industry these are rapid developments indeed.

This thesis is a part of Elektrobit Corporation's technology development related to state-of-the-art car connectivity solutions. It is the first step in the development of a complete automotive antenna system solution. This work is done in parallel with EB's radio channel characterization and air interface technology development projects. The tasks of this thesis are to develop a procedure for the design of multi-antenna systems, examine the effects of antenna array type and location on the performance of multi-antenna systems, study the suitability and accuracy of a commercial electromagnetic simulation software package for automotive antenna simulation and also to conduct a literature survey to provide references to be used in further development of the automotive antenna system. The antenna elements and models thereof that are used in this thesis are not very refined designs, because the results of this thesis should be applicable to various antenna element types. For the same reason most of the research efforts were directed at the less detailed of the two car models—the results should be valid for as broad a range of vehicles as possible. However, a more realistic car model does provide valuable input as to what kind of changes in the performance of the system may be expected when the system is located on a real vehicle.

The literature survey that was done for this thesis provided initial information on what kind of antenna array configurations and locations should be investigated. The best candidates were then selected for simulation. The criterions used were mostly based on potential performance (radiation properties) and feasibility (including aesthetics and cost). A very basic car model was designed by the author for use in this thesis, while a CAD-data based model was provided by CST. Different features of the simulation software was studied, and subsequently used in simulation of different parts of the system from the antenna feed to an intermediate-sized ground plane beneath the car model. The antennas were fed as a beamforming (BF) array, which creates, when combined with MIMO, a beam domain MIMO channel that has the potential to increase the capacity of MIMO systems even further. This state-of-the-art concept is called BF MIMO, and it has not been simulated in automotive environment before this thesis.

While increasing the number of antenna elements can increase performance in favourable conditions, the car manufacturers wish to keep the number of antennas as low as possible mainly for aesthetic reasons. Also, most of the current advanced wireless communication systems, like UMTS and mobile-WiMAX, concentrate on two-element mobile units. Due to these reason, primarily two antenna elements are employed in the simulation models of this thesis, creating 2×2 BF MIMO systems. The simulation results are also validated through measurements, where possible.

MIMO systems are all about increasing the quality of service and spectral efficiency, and plain radiation properties of antennas do not carry this information in them. Consequently, higher level simulations were needed to provide information on how the selected array configurations would perform together with the radio channel. The radio channel characterization project at Elektrobit provided the tools for this kind of performance simulation, namely a suitable channel model with a MATLAB implementation and the actual code for link level performance calculation. The link

level performance calculation code simulated a BF MIMO communication system. The link level performance is characterized in this thesis with the bit-error rate, which describes how many errors happen, statistically, in the transmission of a signal under certain channel conditions. This thesis represents the first case when a BF MIMO concept is applied to antennas in automotive environment.

Theoretical concepts of multi-antenna systems are introduced in Chapter 2 to enable the analysis of such systems. This chapter will also present some theory related to small antennas, since in most cases vehicle antennas are preferred to be as small and invisible to the eye as possible. In the third chapter a literature survey is presented as a summary of related studies on the areas of automotive antennas, multi-antenna systems, related information theory and electromagnetic simulation methods of antennas. The latter part of this thesis deals with the design, simulation, prototyping and analyzing of multi-antenna systems, and includes the chapters 4 and 5. Chapter 4 describes the features of the simulation software, the simulation of the antenna and car models, and the link level simulation of the multi-antenna systems. The results of these simulations will be presented in Chapter 5, which also shortly describes the design and measuring of the prototypes. Conclusions and some recommendations for subjects of future research will be made in Chapter 6.

2. THEORY OF MULTI-ANTENNA SYSTEMS

In this chapter a quick look is taken at the theory involved in designing automotive antenna systems. The purpose of this chapter is to develop a basic understanding of the special characteristics of automotive antennas and to establish some of the primary concepts related to multi-antenna systems. A rigorous derivation of the related field equations, as well as most of the more advanced antenna concepts will be omitted. Also, some information theoretic concepts will be introduced, as these are an integral part of any multi-antenna systems.

2.1. Small antennas

An optimal antenna from car manufacturers' point of view would obviously be low-cost, invisible to the eye and able to cover every wireless service. Cost aside, the latter two—and indeed many other central antenna properties—are connected through what is called a "fundamental limit in the radiation quality factor (Q_r) of electrically small antennas". The purpose of this section is to give a basic understanding of how the different electrical characteristics of small antennas are related to each other and to the "smallness" of the antenna.

Though most of the electronics industry pushes for seemingly never ending miniaturization of its products, antennas have largely avoided this development. There are, however, several applications where electrically small antennas are the only viable choice, such as in pagers. In these situations, a compromise must be made on the antenna linear dimensions and at least one other antenna property, such as bandwidth. An antenna is considered electrically small if the antenna can fit inside a sphere of radius $a = 1/k$ where k is the wave number $(2\pi/\lambda)$ associated with the electromagnetic field.

The key dependence lies between the antenna size and the radiation quality factor, Q_r, of the antenna. A Q of a system is defined as 2π times the ratio of the maximum energy stored to the total energy lost per cycle. The radiation Q is defined through the unloaded quality factor, Q_0, which describes the internal losses of the resonator, and the conductor and dielectric quality factors, Q_c and Q_d respectively, that describe conductor and dielectric losses:

$$\frac{1}{Q_0} = \frac{1}{Q_r} + \frac{1}{Q_c} + \frac{1}{Q_d}. \tag{2.1}$$

A connection between the lowest radiation Q of an antenna and the size of the antenna is derived by McLean [1]. The derivation of the radiation Q in this section

follows that in [1]. The limit of the lowest radiation Q is fundamental, and can be only approached, but never exceeded. McLean's work is a development of that by Chu [2] and Hansen [3].

It has been shown that the lowest possible radiation Q of any linearly polarized antenna is achieved by an antenna which excites only the n = 1 mode (either TE_{01} or TM_{01}) external to the smallest virtual sphere that can confine the antenna [1]. The radiation Q of an antenna can be expressed, from the general definition of Q, as:

$$Q_r = \frac{2\omega W_e'}{P_{\text{rad}}}, \tag{2.2}$$

where ω is the angular frequency, W_e' is the total nonpropagating electric energy and P_{rad} is the total radiated power. This definition assumes that the total nonpropagating magnetic energy W_m' is insignificant compared to W_e'. The derivation of the latter two, unknown, quantities begins with the fields of the TM_{01} spherical mode with even symmetry about θ = 0, which can be obtained from an r-directed magnetic vector potential, A_r:

$$A_r = -\mu \cos\theta e^{-jkr}\left(1 - \frac{j}{kr}\right), \tag{2.3}$$

$$H_\varphi = \sin\theta e^{-jkr}\left(\frac{j}{kr^2} - \frac{1}{r}\right), \tag{2.4}$$

$$E_\theta = \frac{1}{j\omega\varepsilon}\sin\theta e^{-jkr}\left(-\frac{1}{r^2} - \frac{jk}{r} + \frac{j}{kr^3}\right), \tag{2.5}$$

$$E_r = \frac{1}{\omega\varepsilon}2\cos\theta e^{-jkr}\left(\frac{1}{kr^3} + \frac{j}{r^2}\right). \tag{2.6}$$

The field components are to be taken as root-mean-square (RMS) values. There seems to be a slight error in [1] in the equation corresponding to Equation (2.3), in that the term μ is missing, though the following equations seem correct. Next, the electric- and magnetic-energy densities w_e and w_m, respectively, are calculated as

$$\begin{aligned} w_e &= \frac{1}{2}\varepsilon\vec{E}\cdot\vec{E}* = \frac{1}{2}\varepsilon\left(\left|E_\theta\right|^2 + \left|E_r\right|^2\right) \\ &= \frac{1}{\omega}Z\frac{1}{2}\left[\sin^2\theta\left(\frac{1}{k^3r^6} - \frac{1}{kr^4} + \frac{k}{r^2}\right) + 4\cos^2\theta\left(\frac{1}{k^3r^6} + \frac{1}{kr^4}\right)\right], \end{aligned} \tag{2.7}$$

$$w_m = \frac{1}{2}\mu\vec{H}\cdot\vec{H}* = \frac{1}{2}\mu\left|H_\varphi\right|^2 = \frac{1}{2}\mu\sin^2\theta\left(\frac{1}{k^2r^4} + \frac{1}{r^2}\right), \tag{2.8}$$

where $Z = \sqrt{\mu/\varepsilon}$ is the wave impedance. Now, it is easiest to get a hold of the nonpropagating electric-energy density by first calculating the propagating electric-energy density. This energy density is calculated from only the radiation fields (the field components which produce radiated power):

$$H_{\varphi}^{\text{rad}} = -\sin\theta \frac{e^{-jkr}}{r}, \tag{2.9}$$

$$E_{\theta}^{\text{rad}} = -Z\sin\theta \frac{e^{-jkr}}{r}, \tag{2.10}$$

$$w_e^{\text{rad}} = \frac{1}{2}\varepsilon \left|E_{\theta}^{\text{rad}}\right|^2 = \frac{Z^2}{r^2}\sin^2\theta\,. \tag{2.11}$$

Now, defining the nonpropagating electric-energy density as the difference between the total electric-energy density and the propagating electric-energy density one obtains

$$w_e' = w_e - w_e^{\text{rad}} = \frac{Z}{2\omega}\left[\sin^2\theta\left(\frac{1}{k^3r^6} - \frac{1}{kr^4}\right) + 4\cos^2\theta\left(\frac{1}{k^3r^6} + \frac{1}{kr^4}\right)\right]. \tag{2.12}$$

The total nonpropagating electric energy W_e' is

$$W_e' = \int_0^{2\pi}\int_0^{\pi}\int_a^{\infty} w_e' r^2 \sin\theta dr d\theta d\varphi = \frac{4\pi Z}{3\omega}\left[\frac{1}{k^3a^3} + \frac{1}{ka}\right]. \tag{2.13}$$

The only missing term from the expression (2.2) now is the total radiated power, but that can be determined by integrating the real part of the Poynting vector over a spherical surface of any radius:

$$P_{\text{rad}} = \int_0^{2\pi}\int_0^{\pi} \text{Re}\left(\mathbf{E}\times\mathbf{H}*\right)\cdot\hat{a}_r r^2\sin\theta d\theta d\varphi = \frac{8\pi}{3}Z. \tag{2.14}$$

Finally, the radiation Q is

$$Q = \frac{2\omega W_e'}{P_{\text{rad}}} = \frac{1}{k^3a^3} + \frac{1}{ka}\,. \tag{2.15}$$

This is the minimum attainable radiation Q of a single-mode antenna. It should be noted that this minimum Q_r can be derived in three different ways, each arriving at exactly the same expression [1].

For the calculation of the lowest achievable radiation Q of circularly polarized fields the same definition and procedure as above can be used. This follows from the fact that combinations of TM_{0n} and TE_{0n} produce (with appropriate complex weighing) circularly polarized fields. Furthermore, it has been shown that the lowest achievable radiation Q for a circularly polarized antenna is given by that of the combination of TE_{01} and TM_{01} modes, which produces circular polarization. The expression for radiation Q, in the case of circular polarization, is

$$Q_r = \frac{1}{2}\left(\frac{1}{k^3a^3} + \frac{2}{ka}\right). \tag{2.16}$$

For small values of ka the radiation Q for circular polarization (TE_{01} and TM_{01}) is approximately one-half of the radiation Q associated with the TM_{01} mode acting alone. The fundamental lower limits of radiation Q of small antennas for both linear and circular polarizations are illustrated in Figure 2.1.

One way to derive the effect of Q_r on impedance bandwidth of a small antenna is to construct an equivalent circuit model of the antenna as in [2]. Now, if the antenna

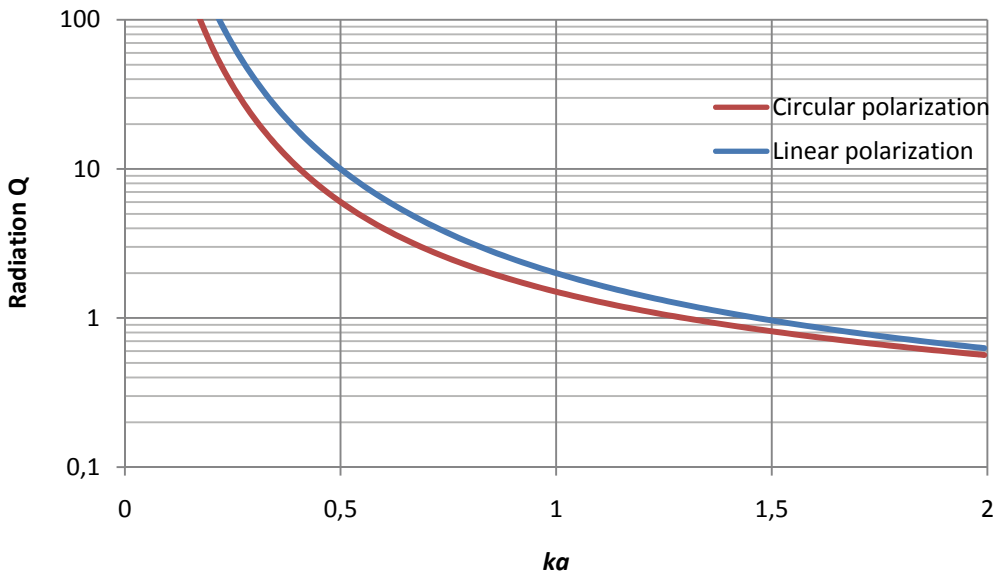

Figure 2.1. *Minimum attainable radiation Q of linearly polarized and circularly polarized antenna, respectively, that fits inside a sphere of radius* a.

equivalent is treated as a resonant circuit with fixed values, the fractional bandwidth of the antenna can be expressed as [2, 3]:

$$BW = \frac{f_{upper} - f_{lower}}{f_{centre}} = \frac{1}{Q_r}. \tag{2.17}$$

Here, the bandwidth BW is defined as the normalized spread between the half-power frequencies. The Equation (2.17) however does not consider the effect of impedance matching at the input terminals of the antenna. From practical point of view, a more useful definition is one that considers the VSWR at the input terminals [4]:

$$BW = \frac{\mathrm{VSWR} - 1}{Q_0 \sqrt{\mathrm{VSWR}}}. \tag{2.18}$$

Here the VSWR is the maximum desired value, and Q_0 is the unloaded quality factor, which includes the effects of losses (for a more detailed description of Q_0 , see [4]). The reciprocal nature of the connection between bandwidth and Q clearly illustrates the importance of both defining the fundamental limits of Q as well as studying how these limits can be approached. It is useful to notice that in the derivation of the radiation Q of a small antenna, the antenna size is characterized only by its largest linear dimension. Consequently, among antennas that fit inside a sphere of fixed radius, those that most efficiently utilize the spherical volume also achieve the best bandwidth. The typical monopole and loop antennas are quite poor in this respect, and accordingly achieve only mediocre bandwidth. The bandwidth of monopoles and similar designs can be increased by increasing the thickness of the radiating element. This effect results from better utilization of the spherical volume, without increasing the radius of the sphere. Other designs, such as spirals, can achieve significantly wider bandwidths due to more effective utilization of the available space. [3]

The quality factor Q also has a connection to the radiation efficiency of a small antenna [5]:

$$\eta_{rad} = \frac{P_{\text{rad}}}{P_{\text{in}}} = \frac{1/Q_r}{1/Q_{tot}} = \frac{Q_{tot}}{Q_r}, \tag{2.19}$$

where Q_{tot} is the total Q of the antenna, which is a sum of the unloaded and the external quality factors. By Equations (2.18) and (2.19), improving the bandwidth of a small antenna is only possible by better utilization of the volume in establishing a TE and TM mode, or by reducing efficiency [3].Of course, one has to remember that the equations in question only define the maximum attainable bandwidth, and as a result the bandwidths of real design will always be less than the limits set by these equations. One way to actually increase the bandwidth of an antenna is to use multiresonant structures. Adding a second resonator to the antenna circuitry as a separate matching circuit or by constructing a multiresonant antenna can increase the available bandwidth by up to about 60 % [5]. The downside of multiresonant structures is increased complexity in both design and manufacturing. Multiresonant structures, and small antennas in general, are discussed at length in [6].

2.2. Antennas in automotive environment

This section gives the reader an overview of some of the practical aspects of automotive antennas. The possible antenna locations, design considerations and different antenna designs will be discussed. Actual automotive antenna designs, with analyses, will be reviewed in Chapter 3.

An antenna in a vehicle must satisfy certain requirements. These requirements can be categorized as follows:

- *Ease of manufacturing.* Necessitated by the requirements of mass production. Also drastically affects the cost of the antenna system.
- *Operating environment.* Faultless operation must be maintained in different environments, from hot and humid to subzero conditions. Also, antenna must endure impact damage from stones and debris, as well as being protected against contamination by dirt and water. Excessive wind noise should be not be generated either.
- *Aesthetics.* The antenna should not interfere with the shape and aesthetics of the vehicle.
- *Radiation properties.* The antenna radiation pattern, input impedance, bandwidth, and other similar parameters must be optimized according to each required service. Care must be taken to include the effects of coupling of the antenna to the vehicle body.

It should be clear from the list above that a single antenna type and location is extremely unlikely to satisfy all the prerequisites in all cases. Different services in different vehicles will call for different types of designs. Nevertheless, it is also likely that some basic designs can be identified, which can be used in similar cases with only minor modifications and development to achieve good performance.

Traditional locations for the FM mast antenna in vehicles have been either the front fender or the roof. While these have worked out adequately for FM-radio services in the frequency range of 80–108 MHz, neither the locations nor the mast antenna type may be ideal for modern/future data-centric services. The modern data-intensive applications require higher bandwidths and, consequently, higher carrier frequencies. Because antenna size is inversely proportional to carrier frequency, a higher frequency can enable whole new classes of antennas that are unfeasible at lower frequencies due to excessive physical sizes.

Conformal antennas are optimal from aesthetics point of view, and have become more common in recent years. Most conformal designs are on-glass FM-antennas, usually located in the rear side window. On the other hand, on-glass antennas for higher-frequency applications are scarce as of yet, and are mostly limited to low-bandwidth applications, such as telematics systems. Consequently, it would seem that the rear edge of the roof is still the preferred location for other than FM antennas. Most of these designs are patch or blade antennas, or a combination of both. Helix and other vertically short monopole type antennas are also common, though these are usually FM antennas. The distance between the rear edge of the roof and the antenna can be anywhere from zero to at least 20 cm.

Electromagnetic coupling to the vehicle body is inevitable with most of the automotive antennas. This can be used to advantage, as in the case of typical mobile phones, where most of the radiation is actually originated from the chassis and not the antenna element itself. The coupling can be exploited especially when employing electrically small antennas. If the coupling is strong, the parts of the vehicle body where the RF currents flow act as a part of the antenna, which increases the size and hence the achievable bandwidth of the antenna system. On the other hand, coupling to the vehicle body can inadvertently and detrimentally affect the radiation properties of the antenna if proper measures are not taken during the design of the antenna to account for these effects.

2.3. Multi-antenna systems

This section is an overview of multi-antenna techniques. An in-depth presentation of each technique is out of the scope of this thesis, but rather a short introduction with pros and cons discussion of each will be given.

2.3.1. Diversity

Diversity is a concept that aims to mitigate fading. Fading can be characterized as variation in signal strength as perceived at the receiver, and it is generally categorized into fast and slow fading. Slow fading is typically caused by shadowing, that is, large obstacles (partially) blocking the line-of-sight between transmitter and receiver. Fast fading, on the other hand, is attributed to constructive and destructive interference at the receiver, or other effects that change the channel during very short times. [7]

All diversity systems employ some form of redundancy to mitigate the effects of fading. The basic idea is to transmit a signal over multiple (ideally) independently fading paths. Because the transmission paths are independently fading it doesn't matter if one path experiences a deep fade—it is highly unlikely that all the other paths will be in a fade at the same time. It should be stressed that diversity systems rely on *uncorrelated* signals—the different paths change independently, and hence the signals arriving at the receiver should be uncorrelated. Obviously, the larger the number of independently fading transmission paths, the better the probability of at least one signal arriving at the receiver without experiencing a deep fade.

Diversity systems are traditionally categorized as operating over time, frequency or space, according to which dimension they rely on transmitting and receiving the multiple signals. Only space diversity will be discussed here, due to the fact that all MIMO systems depend on this particular diversity, although other diversity methods can be utilized in addition. A thorough discussion of diversity systems can be found in [8] and, with reference to modern wireless communication systems, including MIMO, [9].

Space diversity is based on multi-element antenna arrays and on the fact that due to the different locations of each element, the propagation paths to each element are slightly different. It is relatively easy to implement and does not require any additional frequency spectrum. Parameters available to the designer include array configuration, interelement spacing, number of elements, and load impedance. The optimal array configuration depends on the application and the propagation environment. Interelement spacing must be sufficient to ensure uncorrelated individual signals. Number of elements in the array can be arbitrarily high, but the improvement in the fading characteristics, per element, will decrease as the total number of elements increases. The diversity array can be located either at the transmitter (transmit diversity), the receiver (receive diversity) or both (transmit-receive diversity). [8]

A diversity combiner will have to be used to recover the original signal from the multiple received signal instances. The simplest method of diversity reception is the selection diversity. In this case, the receiver having the highest baseband signal-to-noise-ratio (SNR) (sampled at the antenna, for example) will be sent to the output. This method is very simple, but suboptimal. In the second method, called Maximal Ratio Combining (MRC), the signals are weighted with regard to their signal voltage to noise power ratios and then summed. Compared to selection diversity, an additional cophasing and summing element is required. It does, however, provide some additional diversity gain. In fact, MRC gives the best statistical reduction of fading of any known linear diversity combiner. The mean SNR of the combined signal now varies linearly with the number of antennas, which is a marked improvement over selection diversity. Other types of diversity reception methods exist, but will not be discussed here. [7, 8]

2.3.2. MIMO

The idea behind MIMO—that is multiple-input—multiple-output—is simple: in an arbitrary wireless communication system the transmitting end as well as the receiving end is equipped with multiple antenna elements. Together with the use of a combination of space-time modulation and coding techniques it improves the quality (bit-error rate or BER) or the spectral efficiency (b/s/Hz) of the communication system. When talking about MIMO it is easy to get excited about the possible capacity increases. However, it is worthwhile to remember that MIMO, as a system inherently capable of both transmit and receive diversity, can be used to increase the quality of the signal as well. One of the strongest points of MIMO systems is that the ratio between capacity and signal quality can be altered according to prevailing channel conditions.

Although MIMO is related to spatial diversity, its benefits go far beyond the added diversity gain or array gain benefits. The key factor is called *spatial multiplexing* (SM): under certain channel conditions a linear (in $\min(M_T, M_R)$) increase in capacity is possible, for no additional power or bandwidth expenditure, over a matrix channel created by M_T transmit and M_R receive antennas. This increase is realized by transmitting $\min(M_T, M_R)$ independent data streams simultaneously over the (matrix) channel. The SM channel is illustrated in Figure 2.2. [10, 11]

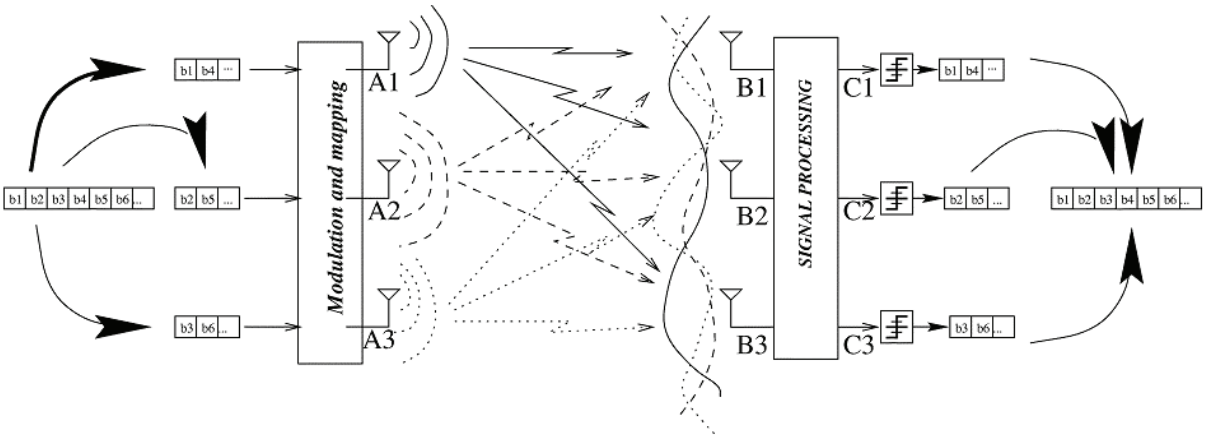

Figure 2.2. *Illustration of a basic spatial multiplexing channel with three transmitting and three receiving antennas. Theoretically, a three-fold improvement in spectral efficiency is possible with this setup. [10]*

To appreciate the capacity gains offered by MIMO, let us work our way through the capacity of different systems from single-input—single-output (SISO) systems to $M_T \times M_R$ MIMO systems. The traditional Shannon capacity of a 1×1 SISO system is [10]

$$C = \log_2\left(1 + \rho|H|^2\right), \tag{2.20}$$

where ρ is the SNR at the receive antenna, and H is the normalized complex gain of a fixed wireless channel or, in the case of a random channel, that of a particular

realization of the channel. The capacity is given in b/s/Hz. If the number of receive antennas is increased to M_R, the capacity of the subsequent $1 \times M_R$ SIMO system is given by [10]

$$C = \log_2\left(1 + \rho \sum_{i=1}^{M_R} |H_i|^2\right). \tag{2.21}$$

Comparing this to Equation (2.20), it is evident that increasing the number M_R results in a logarithmic increase in average capacity. Similarly, the capacity of $M_T \times 1$ MISO transmit diversity system is [10]

$$C = \log_2\left(1 + \frac{\rho}{M_T} \sum_{i=1}^{M_T} |H_i|^2\right). \tag{2.22}$$

Here, the normalization by M_T ensures that the total transmitter power is not increasing with M_T. Equation (2.22) holds if the transmitter does not have channel knowledge. Again, only logarithmic increase over the SISO case is observed. However, if we have transmit *and* receive antenna arrays with M_T and M_R elements, respectively, we get the following capacity equation [10, 12]

$$C = \log_2\left[\det\left(\mathbf{I}_{M_R} + \frac{\rho}{M_T}\mathbf{H}\mathbf{H}*\right)\right], \tag{2.23}$$

where (*) means transpose-conjugate and $\mathbf{H}$ is the $M_T \times M_R$ channel matrix. The channel matrix will be presented in more detail in Section 2.4.1. It has been demonstrated [12] that the capacity of Equation (2.23) increases linearly with $m = \min(M_T, M_R)$. Of course, these results assume ideal channel conditions, and in realistic channel conditions the capacity of MIMO systems is sometimes significantly lower. However, MIMO does offer substantial performance gains over SISO, MISO or SIMO systems under most channel conditions. The downsides are added complexity and manufacturing cost, as well as (in most cases) increased physical size of the antenna system. Examples of MIMO systems in a few references will be discussed in Section 3.3, and some remarks on multi-antenna systems will be made in Section 3.4.

2.3.3. Beamforming

Beamforming (BF) is another multi-antenna technique that has been in use for decades. The basic idea is to individually control the phase and amplitude excitations of a number of radiators in a closely spaced (correlated) array. Unlike MIMO and diversity systems, BF arrays take advantage of coherent combining of signals. Diversity and MIMO systems exploit the multipaths of a radio channel to transmit the signal through different paths to the receiver. On the contrary, beamforming utilizes array gain of the multi-element system to form a concentrated beam pattern with high gain in a certain direction, or few directions. The beam pattern can be adaptive or fixed, depending on whether the phase and amplitude of the excitation can be altered or not. A more comprehensive introduction to phased arrays is given in reference [13].

The main design parameters in beamforming arrays are: number of radiating elements, array configuration, element spacing, element type (radiation pattern), phasing and the so-called excitation amplitude taper. Most of these are self-explanatory, but the last one may require a short explanation: The excitation of different radiating elements affects the beam pattern. The set of amplitude weights of each radiating element is called amplitude taper, and it affects the sidelobe level, (mainlobe) beamwidth and the aperture efficiency. With regards to the antenna type, it should be taken into account that the mutual coupling of the antennas in a closely spaced array affects the radiation properties of the individual elements. [13]

Various methods of feeding the BF array exist. Most feeding methods can be classified as either optical space feeds or constrained feeds. The optical space feeds distribute the source signal through space, illuminating an array of horn-elements that are connected to the radiating elements. Constrained feeds, on the other hand, rely on transmission lines, such as waveguides and microstriplines, to couple the RF energy from the generator to the radiating elements. The constrained feeds can be further divided to parallel and serial feeds. The biggest advantage of the optical space feeds is simplicity, but the downsides are the lack of amplitude-tapering control and large physical size. Further information on the optical space feeds is available in [13].

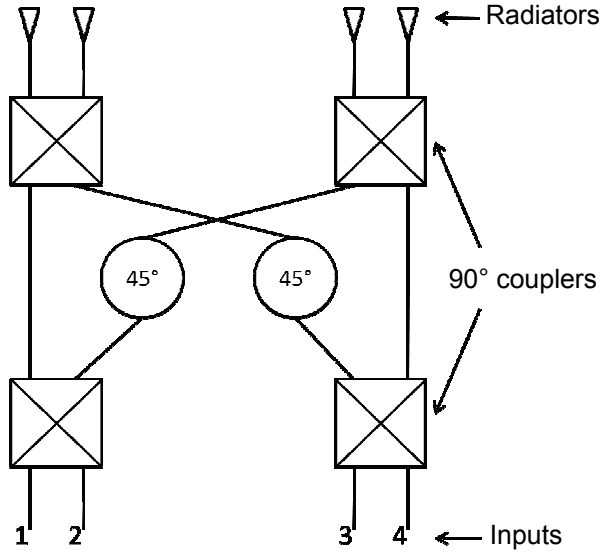

Figure 2.3. *A 4×4 Butler matrix capable of creating four orthogonal beams.*

Constrained feeds can be single- or multi-beam feeds. The former produces a single beam from a single input, while the latter can have several inputs, each of which producing a single beam. Several inputs of the multi-beam feeds can be fed simultaneously, thus producing multiple simultaneous beams. This approach is beneficial in a novel combined BF MIMO system, since, as it turns out, each of these (parallel, orthogonal) beams can be used to create a parallel channel between the transmitter and the receiver [14]. Effectively, in BF MIMO systems uncorrelated *beams* are taken advantage of, instead of uncorrelated antennas, as in traditional MIMO systems. One way to realize the multiple beams is to use the so-called Butler matrix (BM) feeding network, which is a type of parallel-fed multiple-beam-forming feed. The block diagram of a 4×4 BM is illustrated in Figure 2.3. The BM uses directional couplers with 90° degree phase-shift property and fixed phase-shifters to excite all the radiating elements equally in amplitude and with a fixed phase difference between adjacent elements. The phase difference is in odd multiples of 180°/*M*, where *M* is the total number of radiating elements. Hence, a single 90° coupler

is effectively a 2×2 BM. The array pattern of the M beams is of the form $\sin Mx/\sin x$. The notable advantage of the BM feed network is the fact that the peaks of the beams coincide with the nulls of the other beams. Hence, the beams are orthogonal to each other and there is no cross-coupling loss between beams. [13]

2.4. Radio channel

Radio channel includes everything that happens in between transmit (Tx) and receive (Rx) antennas. After the transmit antenna has radiated power to the channel, the EM waves travel through free-space, scattering and reflecting from objects in their way and interfering with other EM waves in the same space. Some of the transmitted energy may reach the Rx antenna at some later point in time. Parts of the energy received by the Rx antenna may have traveled through different paths, and may have arrived from several directions at different times. All this, and more, constitutes the radio channel.

This section introduces the main parameters of radio channels with emphasis on multipath propagation models. The radio channel is, however, a very complex system and the different channel models themselves have very diverse attributes. One is encouraged to acquaint with reference [15] for an introduction to radio channels, and references [9, 16] for a multi-antenna- and MIMO-specific radio channel analysis. Also, partly coinciding with this thesis, a complete MIMO channel model has been developed as a part of the WINNER II project [17].

2.4.1. Channel models

How and what different aspects of the radio channel are modelled, is a design choice. The basic approach is to consider a complex signal s_j(t) that is launched from the jth Tx antenna and received by the ith Rx antenna as

$$y_i(t) = \sum_{j=1}^{M_T} h_{i,j}(\tau,t) * s_j(t) + n_i(t), \tag{2.24}$$

where n_i is additive (usually AWGN) noise in the i:th receiver and $h_{i,j}(\tau,t)$ denotes the time-varying channel impulse response between the jth (j=1,2,…,M_T) Tx antenna and the ith (i=1,2,…,M_R) Rx antenna, i.e. the response at time t to an impulse applied at time $t-\tau$. In the case of a SISO system, $i = j = 1$. It is useful to notice that the relation of Equation (2.24) is linear and time-invariant (LTI). The MIMO channel is most often modelled in the form of a linear $M_R \times M_T$ complex channel matrix $\mathbf{H}(\tau,t)$:

$$\mathbf{H}(\tau,t) = \begin{bmatrix} h_{1,1}(\tau,t) & h_{1,2}(\tau,t) & \dots & h_{1,M_T}(\tau,t) \\ h_{2,1}(\tau,t) & h_{2,2}(\tau,t) & \dots & h_{2,M_T}(\tau,t) \\ \vdots & \vdots & \ddots & \vdots \\ h_{M_R,1}(\tau,t) & h_{M_R,2}(\tau,t) & \dots & h_{M_R,M_T}(\tau,t) \end{bmatrix}, \tag{2.25}$$

and now the MIMO channel input-output relationship can be written as

$$\mathbf{y}(\tau,t) = \mathbf{H}(\tau,t)\mathbf{s}(\tau,t) + \mathbf{n}(\tau,t). \tag{2.26}$$

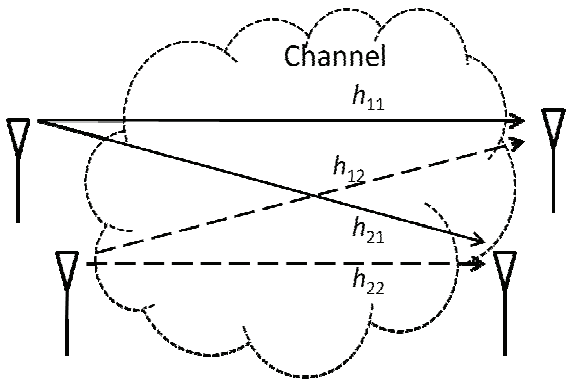

Figure 2.4. *The components of the channel matrix* ***H*** *of a 2×2 MIMO system.*

See Figure 2.4 for illustration of the channel matrix. The channel matrix defines most of the channel's characteristics and propagation properties. Of particular importance to MIMO systems is the eigenvalue distribution of the channel matrix **H**, which characterizes how well the Tx and Rx antennas can distinguish independent, parallel propagation paths. [10, 11]

Equations (2.24) to (2.26) are applicable for most channel models. However, very few assumptions have been made about the variables in these equations. According to the model, for example, the elements of **H** can be constant, deterministic or random. If **H** is random, the distribution of the elements of **H** can change according to the model and the propagation environment. The most common types of random distributions are Rayleigh and Rician, and the corresponding random channels are said to be Rayleigh or Rician fading, respectively. The concept of fading was introduced in Section 2.3.1. Rayleigh faded channel arises when the real and imaginary parts of $h_{i,j}(\tau,t)$ are independent and identically-distributed (i.i.d.) Gaussian random variables (with zero-mean and unit variance). This is a reasonable assumption when there are many scatterers in the propagation environment, and Rayleigh fading channel is clearly the most common type of fading channel that is used to characterise MIMO systems. On the other hand, if a strong line-of sight (LOS) signal is available, a more accurate model is that described by Rician fading. It is actually a generalization of the Rayleigh case, where the channel is represented as a sum of a Rician distributed (LOS) component and a Rayleigh distributed non-line-of-sight (NLOS) component. With Rician fading, an important quantity is the Rician K-factor, which is essentially the ratio of the power of the LOS component to the power of the NLOS (fading) component of the radio channel. [16]

Delay spread

Delay spread (DS) is a widely cited concept that is associated with radio channels. DS is most simply described as the difference in propagation time between the shortest and the longest path (only paths with significant energy are counted). Because of multipath scattering the transmitted signal (impulse response) appears at different time instants at the receiver. With increasing number of scatterers, the discrete received impulses become a continuous signal pulse with a pulse length that is DS. If two independent impulses (say, *a* and *b*) are transmitted within the DS of a channel, it is probable that scattered signals of the impulse *a* are arriving at the receiver at the same time when the first signals of the impulse *b* are arriving. This causes intersymbol interference (ISI). To prevent it, the signalling rate must be slowed down to a rate much less than DS^{-1}.

Similarly, two signals that are closely spaced in frequency can become correlated because of DS in the channel. The minimum frequency interval between two signals that prevents this kind of correlation is called the “coherence” or “correlation” bandwidth B_c. If the frequency changes by an amount of the order of coherence bandwidth, the constructive and destructive interference pattern changes significantly. The coherence bandwidth is reciprocal to the DS, as an order-of-magnitude guide, but the exact definition often differs from one reference to another. [15, 16]

An important aspect of the DS, from the channel modelling point-of-view, is that above frequencies of about 150 MHz it becomes frequency-independent. This behaviour can be explained by the fact that above 150 MHz the sizes of the surrounding structures are always much larger than the wavelength, and thus count as a scatterer. Typically, a structure greater than six to ten wavelengths is claimed as a scatterer, which is capable of reflecting the energy of any incident wave on its surface. Above the frequency of 150 Mhz the number of scatterers counted is independent of the frequency. Therefore the propagation paths of signals of different frequencies are the same and, hence, so are the delay spreads.[15, 16]

Angle spread

Another important channel parameter is angle or angular spread (AS). As its name implies, angle spread describes the angular distribution of impinging power at the receiver. AS may be defined in several ways, but the definition used in this thesis is that described in [18]. The exact definition is a bit unwieldy and unessential from the standpoint of this thesis, and will not be reprinted here, but can be found in [18]. If AS is high there are usually a large number of local scatterers near the receiver. Vice versa, low AS implies few local scatterers (or very closely located scatterers), and this in turn implies a low number of resolvable multipath components and hence lower capacity compared to high AS, everything else being equal.

3. LITERATURE STUDY ON AUTOMOTIVE ANTENNAS AND MULTI-ANTENNA SYSTEMS

Antennas are highly sensitive to location. Antennas located in, or on top of vehicles introduce new design problems that do not exist or are irrelevant with other antennas. Automotive antenna element design has been extensively covered in numerous publications and patents for a wide range of frequencies, element types and uses. Since the late 1990s new ways of exploiting multiple antennas have emerged to improve reception quality, reliability, data rates and/or spectral efficiency. In recent years multi-antenna based technologies have also started to find their way into vehicles. However, while there have been many proof-of-concept and simulations-based studies, a lot of work still remains to be done, especially regarding the MIMO use of multi-antenna systems.

In this chapter, some of the studies in the aforementioned areas of antenna technology are summarized. Focus is on automotive antennas, multi-antenna systems and multi-antenna configurations and simulation methods. The purpose of this chapter is to give an overview of what has already been studied, what remains to be studied, and also to provide a thorough list of references for the interested reader. Although the design part of this thesis is focused on 700 MHz automotive antennas, other types of antennas for various frequencies and uses will be considered in this chapter, but keeping in mind the framework of this thesis.

3.1. An overview of previous work on automotive antennas

The purpose of this section is to introduce a few publications that discuss the design of automotive antenna elements. While these articles present new designs, very few actually new ideas are introduced in them. Instead, the publications in this section discuss the more basic design issues that automotive antenna designers may face.

3.1.1. Wideband automotive antenna elements

A number of specific design issues and challenges need to be solved to successfully integrate antennas to a car body. With the increasing number of radio services available for in car use, the requirements for antennas of different services may be very diverse. However, many similarities also exist. For example, both systems must take into consideration the effects of the car body on the radiation properties and impedance

characteristics of both systems' antennas. Then again, bandwidth requirements are very different e.g. for keyless-entry and mobile-WiMAX systems.

One of the challenges in modern automobiles is the ever increasing number of wireless services. Unfortunately for the car manufacturers, many of the wireless services still need cabling inside the car from the antenna to its transceiver. Car manufacturers are already approaching the limit, where adding more wireless services is hard or even impossible due to limited space for the antennas and cabling. One approach to this problem is to develop broadband antennas with very high bandwidth, so that one antenna can be used by many different services operating within different frequency bands. Examples of this concept are presented in [19-21].

Automotive spiral antennas

In the paper [19] by Gschwendtner & Wiesbeck two spiral antennas for automotive use are presented. Spiral antennas are the smallest of frequency-independent structures relative to wavelength, and this was the main reason for the authors to use the spiral structure. The goal was to design two antenna structures capable of receiving several terrestrial and satellite-based services, including but not limited to terrestrial digital video broadcasting (DVB-T), global system for mobile communications (GSM900/1800), global positioning system (GPS) and universal mobile telecommunication system (UMTS). The services operate over frequencies 470-2200 MHz, so to be able to cover this frequency range with a single antenna requires an extremely wideband solution.

The first design is a two-arm Archimedean spiral, intended for on-glass application in cars. Spiral antennas are usually centre fed, but in the case of on-glass antennas it is generally not possible. Gschwendtner et al. however, extended one arm of the spiral half a turn, so that a two-wire transmission line is formed (Figure 3.1). They then used this transmission line to feed the spiral externally.

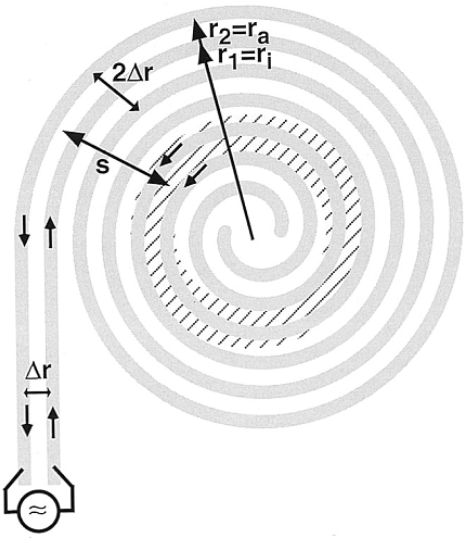

Figure 3.1. *Externally fed two-arm spiral antenna. [19]*

The antenna was demonstrated with a 30 cm-diameter two-arm Archimedean spiral antenna (f_{min}= 318 MHz). The feed network consisted of a fifth order Marchand-Balun. The antenna had good input matching at the frequency range of interest, and it was found to correspond to a centre-fed spiral antenna in terms of radiation characteristics at the lower frequency limit, with circular polarization maximum normal to the spiral plane, and minima in the spiral plane. The maximum moved toward the spiral plane at higher frequencies, and several minima were found at varying angles. Also, despite pattern variations with frequency, the antenna was found

frequency-independent with regard to input parameters. The radiation pattern was also found to be highly dependent on the antenna location in the car, which led the authors to speculate about the antenna's suitability for multi-element MIMO or space diversity systems. The measurement data presented in the paper only covered measurements of the stand-alone antenna. The proposed element is indeed interesting proposition for an automotive antenna system requiring large bandwidth. The diameter of the antenna seems manageable as long as the highest frequencies required are less than or around 1 GHz. Unfortunately the article does not present measurement results of a car-integrated antenna, so one cannot evaluate its performance in actual working environment.

The second spiral antenna introduced by Gschwendtner & Wiesbeck was designed to operate with terrestrial as well as satellite services, and as such required two separate radiation patterns. Unlike the first spiral antenna, this element was intended to be integrated in to the bodywork of a car. This also allowed for central feeding position. Two radiation patterns were realized by multimode four-arm spiral fed by a coplanar transmission line supporting multimode operation. The feed structure allows for independent and simultaneous excitation of both modes.

A 40 cm-diameter four-arm spiral antenna was built and measured. To improve the vertical polarization component in the spiral plane radiation pattern of the four-arm spiral, a metallic cavity was placed below the spiral. This cavity had the effect of increasing vertical polarization in the spiral plane as well as reducing the radiation toward the interior of the car. In the radiation pattern of the first mode of operation, a null is formed to the zenith (normal to the spiral plane), and an omnidirectional maximum toward an elevation of about 20° to 70°. This kind of pattern makes this mode suitable for terrestrial services. In the second mode (for satellite services), the radiation pattern corresponds to that of a conventional two-arm spiral antenna, with a maximum toward the zenith and circular polarization. The spiral was also integrated conformally in the trunk lid of a Mercedes sedan, with the cavity placed below the lid surface, but measurement results for this setup were not discussed in this paper. Instead, radiation characteristics for a corresponding stand-alone antenna were given. Good input matching for the terrestrial mode was achieved from 670 MHz to over 5 GHz, and for the satellite mode from 1.3 GHz up to 2.2 GHz.

The limiting factor for this antenna element in multi-antenna systems would seem to be its size, as an element of around 40 cm in diameter is required for operation near 1 GHz. This makes it impossible to integrate several elements to the body of a car, and as such unsuitable for MIMO use, as attractive as the support for both terrestrial and satellite services in a single element might be.

Automotive blade antenna

Walbeoff & Langley present a wideband blade antenna for multiband telephone application in cars in [20]. The proposed design is a printed PCB blade antenna, with radiation properties close to that of a quarter-wave monopole, and with a little tuning

able to cover the lower (824-960 MHz) and upper (1710-2175 MHz) frequency bands used by mobile telephone systems in the US, Europe and Japan.

As mentioned, the antenna element itself is a double-sided printed blade with circuit elements connecting the element to a ground plane, as can be seen in Figure 3.2. The overall dimensions of the antenna are 48 mm × 28 mm (H×W), offering a greatly reduced height compared to a quarter-wave monopole. The antenna can be tuned to suit different telephone systems worldwide (within the bands specified above) by altering the circuit elements.

The radiation patterns of the blade antenna were measured first over a 1 m square ground plane in an anechoic chamber, and later at an open-field automotive test site. In the latter case, the antenna was mounted to the roof of an estate car, about 30 cm from the rear edge. In both cases, the radiation patterns were found to be in close accordance with those of a reference monopole in similar setups.

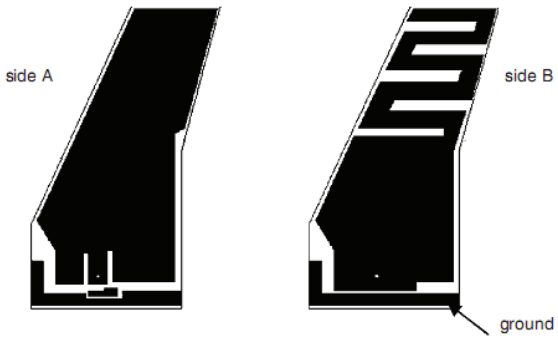

Figure 3.2. *A wideband double-sided printed blade antenna for automotive use. [20]*

Although of unquestionably reduced height compared to a quarter-wave monopole, the omnidirectional radiation pattern of the blade antenna may not be optimal in diversity applications. In these cases a more directional radiation pattern can be beneficial, so as to better make use of different propagation paths in different directions.

Printed planar monopole antenna

A rather similar element is presented by Gamage & Jensen in [21]. Here, the antenna element is a wideband printed planar rectangular monopole with double microstrip line feed, and was designed for the frequency range of 2.2–7.5 GHz, covering all the popular wireless LAN frequencies. It is meant to be mounted on a large ground plane. The element was modelled, simulated and optimized with the finite element method (using Ansoft HFSS version 10 simulation package), and later experimentally validated.

The measurement results of the prototyped antenna agreed well with the simulation results, with wider-than-specified bandwidth and approximately omnidirectional radiation pattern. Cross polarization levels were found to be significant at higher frequencies in some directions but, according to the authors, work is under way to improve this. Compared to the antenna presented in [20], the outer dimensions of this planar monopole antenna—with a total height of at least 30 mm—are actually quite large considering the frequency range of operation is 2.2 GHz and over. And, as with the antenna element in [20], the omnidirectional radiation pattern as reported for this element may be suboptimal for some multi-antenna systems.

Integrated automotive three-antenna system

A slight variation of the wideband theme is introduced by Azaro et al. in [22], where a small sized integrated antenna system with three antennas for different services is simulated and experimentally validated. The intended frequency bands of operation included a Cospas-Sarsat band at 406 MHz, the GSM bands of 880-960 MHz and 1710-1990 MHz as well as the GPS band of 1574-1576 MHz.

A combination of two monopole antennas for Cospas-Sarsat and GSM services and a conical two-arm Archimedean spiral antenna for GPS service was integrated in compact space, as illustrated in Figure 3.3. The different antennas were first simulated separately with standard full-wave method-of-moments (MoM) and finite-difference time-domain FDTD based methods. The dimensions of each antenna were then optimized to achieve set electrical specifications using cost functions (*cost functions* are a way of representing optimization problems; they are also known as *objective* or *energy functions*). Last, the problem of antenna integration was again recast as optimization problem to find the optimal places for each antenna sub-system in the integrated assembly. During the optimization processes the antennas are assumed to be located on an infinite ground plane, although a comparison between an infinite ground plane and a ground plane of approximately the size of a roof of a car was also made (resulting differences were deemed acceptable).

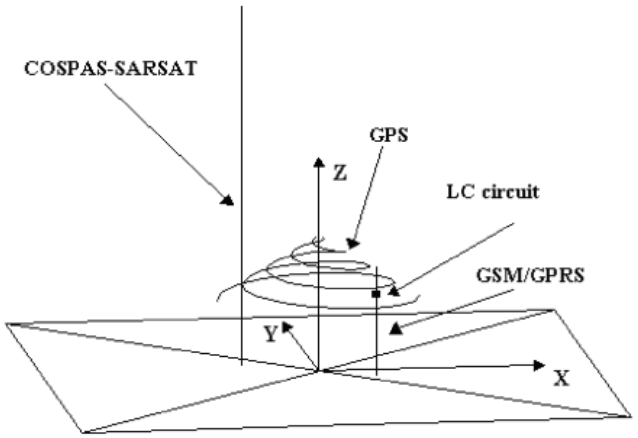

Figure 3.3. *An integrated automotive multifunction antenna. [22]*

Experimental validation of the integrated antenna system was made on a 90×140 cm^2 ground plane. Only vertical cut-plane (elevation) gain patterns were presented for the different antennas, but near-omnidirectional patterns on the horizontal cut plane were suggested. In the vertical cut-planes typical monopole radiation patterns are present, although the null toward the normal of the ground plane is mitigated, especially at the GSM frequencies, by the effect of mutual interferences among the antenna subsystems. The simulation results of the two-arm Archimedean spiral antenna also predicted quite well the shape of the radiation pattern (a wide hemispherical lobe), although the measured gain levels were around 3 dB lower.

The proposed integrated antenna system is an interesting proposition, although its application for multi-antenna systems is perhaps not as clear-cut. It does however demonstrate that a single ultra-wideband antenna is not the only option for covering different or wideband wireless services, even in the extremely limited space conditions the automotive application impose.

3.1.2. General automotive antenna elements

Single-element antennas for automotive applications can give valuable insight into the various challenges of designing an automotive antenna. With a large database of articles discussing single-element antennas for FM, WLAN, GPS, GSM etc. services readily available, it was considered worthwhile to review several articles of these kind. A selection of these will be presented here.

Compact PIFA for automotive applications

A very compact mono- and dual band planar inverted-F antenna (PIFA) for automotive applications is presented by Brzeska & Chakam in [23]. Both simulated and measured results are presented, with simulations being done using the method of moments (FEKO simulation software).

The PIFA element is intended for automotive remote keyless entry and tire pressure monitoring systems. These are narrowband systems operating at 434 MHz and 868 MHz, respectively, for which the resonant-type PIFA elements provide adequate bandwidth. With a height of only 9 mm and biggest dimension of 90 mm (0.26 λ at the higher frequency of 868 MHz, or equally 0.13 λ at 434 MHz), the PIFAs belong to the class of small antennas. This PIFA was designed to be placed between the headliner and the car roof, 10 cm from the rear edge of the roof. Measurements were done in an anechoic chamber with a metal plate above the antenna to simulate the effect of the car roof, and a headliner was also used.

The measurement results were in good agreement with simulations, although again the measured gain levels were often up to 3 dB lower than corresponding simulation results. The radiation patterns were quite similar at the two different frequencies, being a single wide hemispherical lobe (with a null at the plane of the antenna for the horizontal component). This design exemplifies the fact that even with a very small antenna decent radiation properties and input parameters are attainable—although bandwidth will be extremely limited (high quality factor).

Planar printed meander line antenna

Antennas for similar services are presented by Al-Khateeb et al. [24]. The paper describes planar printed meander line antennas, again for remote keyless entry applications in cars. The antennas are designed for 315 MHz frequency range with a 300 kHz bandwidth.

The focus on this article was on comparing different planar printed monopole antennas. The traditional quarter-wave monopole was compared to several different meander line antennas (Figure 3.4). The authors noted that increasing the length of folded (meandered) line length in monopole antenna increases the radiation resistance, and hence input impedance. The goal was to match the antennas to a 50 ohm circuit, and with the input impedance of traditional monopole antennas in the 30 Ω range, increasing the input impedance should affect performance favourably. The antenna parameters were simulated using full-wave MoM-based software IE3D from Zeland Software.

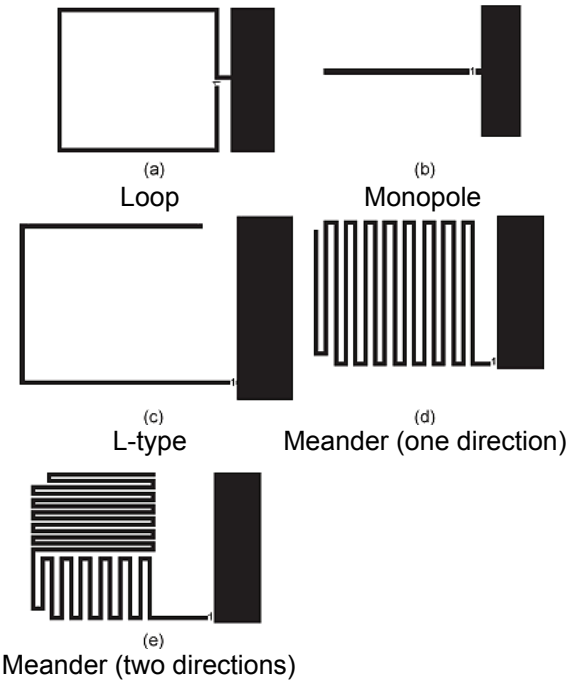

Figure 3.4. *The meander line antenna types that were investigated in [24].*

Measurements were made both with stand-alone antennas in anechoic chamber and with the antennas mounted on a vehicle.

The matching circuits for the antennas were realized with lumped inductor and capacitor elements. The effect of ±5 % component tolerances on the VSWRs of the antennas was examined with Monte Carlo analysis.

The radiation patterns of the different antenna elements were first measured in anechoic chamber without the vehicle. Afterwards, the antennas were also measured mounted to a car on a turntable. The radiation patterns were found highly sensitive to the antenna location in car, although only one antenna type in two locations was measured, and the rest of the antenna locations were only simulated. In both cases the antenna was placed under the front dash, near the windscreen. The measured radiation patterns were expectedly different from the near-ideal ones measured on a simple ground plane in an anechoic chamber. It was also found that not only the antenna location itself, but also the position of the antenna feed cable can significantly contribute to the shape of the radiation pattern, and that an increase of several decibels in antenna gain can be achieved just by optimising the cable position.

The numerous nulls generated in the radiation pattern of the antenna placed inside a car led the authors to investigate space diversity considerations. The proposed diversity scheme consisted of two antennas placed near the windscreen, under the front dash, and a receiver unit located on the steering column. Then, the receiver would periodically connect to either one of the antennas, with connection time long enough to receive the communication protocol. Hence, the diversity antenna radiation pattern is the overlap of individual radiation patterns of antennas 1 and 2. In this manner, the number of the nulls was significantly reduced and the signal level was more consistent overall. The advantage of the diversity system to the end-user was measured with probability of maximum communication range for the antenna system. For a range of 100 meters and vertical polarization, the probability of detection increased from 60–70 % for the single antenna systems to a healthy 90 % for the diversity system.

This paper exemplifies several important points on different topics related to automotive antenna design. Firstly, the meandered line monopole is an interesting alternative as an antenna element because of its small physical but large electrical size. Secondly, a Monte Carlo analysis of the effect of tolerances is often most revealing on

the manufacturability of any RF-designs that include lumped elements, and has become standard procedure in modern-day RF-design. Thirdly, the notion that if the antennas are separated from the receiver and not mounted on a large ground plane, the antenna feed cable may have a considerable effect on the radiation properties of the antenna. Even if in part outside the scope of this thesis (for example, the Monte Carlo analysis), these are important aspects to consider when designing an automotive antenna.

Windscreen integrated antennas

Windscreen integrated antennas require conformality. One such candidate is patch antenna that is not only conformal, but also inexpensive to produce. However, number of publications discussing the performance of windscreen integrated patch antennas is quite limited. A few such studies have nonetheless been made. The effects of window glass on the radiation properties of a circular microstrip patch antenna are studied by Economou et al. in [25]. The studied frequency range was 2–6 GHz, although results are mostly presented only at the frequency of 5.8 GHz. The simulation method was based on spectral domain method of moments, but no commercial software was used. A different approach to conformal automotive antennas is presented in [26, 27], while simulation of on-glass antennas is discussed in [28-30].

Two approaches for the integration of the antennas to the windscreen were considered (see Figure 3.5). Firstly, the antenna may be fabricated separately from conventional dielectrics and finally attached to the windscreen with adhesive. Taking the integration one step further, the antenna can be printed entirely inside the laminated windscreen. Both methods were considered, although the latter only at the simulation level because of the difficulties in manufacturing patches within a commercial windscreen. Nominal thickness for the windscreen was 2.5 mm, though it was reported to vary considerably in practice. Electrical properties were $\varepsilon_r = 6.75$ and $\tan\delta = 0.03$. Additionally a laminate layer and, in the case of the glue attached antenna, a thin adhesive layer were considered in the simulations.

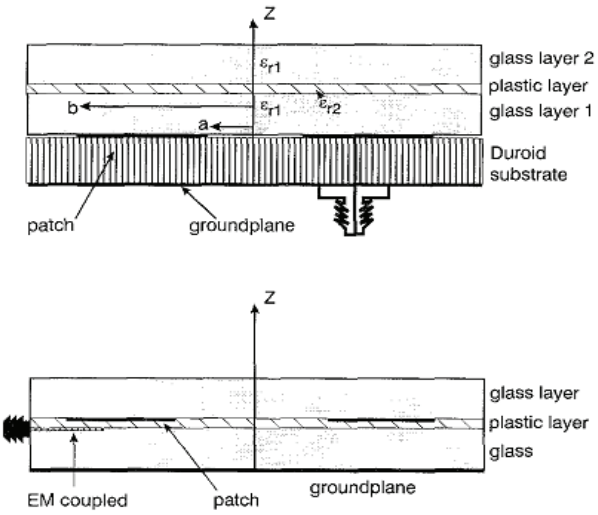

Figure 3.5. *Integration techniques of circular patch antennas on windscreen. Upper picture: coaxial probe fed patch with glass superstrate. Lower picture: electro-magnetically coupled patch with laminated glass. a = patch inner radius, b = patch outer radius. [25]*

A 40 mm circular disc patch was constructed and measured. Attached to a 600 mm square section of flat float glass, the resonant frequency of the patch was found to decrease from 2.79 GHz without the glass cover to 2.63 GHz when attached to it. The

point of these tests was to gain confidence in the simulation method, and results between measurements and simulations did prove to be in close accordance.

Next, a 16 mm circular patch antenna was attached to the windscreen. Compared to a corresponding stand-alone patch, the bandwidth rose from just 1.8 % to a more useful 6.8 %, while resonant frequency decreased from around 6.65 GHz down to about 5.5 GHz. The increase in bandwidth was credited to the thick high dielectric constant glass cover rather than the losses in the glass. Both antennas were measured with a circular ground plane, 120 mm in diameter.

Radiation patterns were only presented for the 16 mm circular patch antenna. When the antenna was attached to a windscreen, the patterns were expected to feature deep ripples due to increased surface wave propagation and -radiation. The study was made at 3.8 GHz and 5.8 GHz, but the differences between these two frequencies were found so minor that only the results for the higher frequency were published in the article. Amplitude ripple across the main forward lobe for the disc attached directly to the back of the windscreen was about 2 dB. Also, some broadening of the main lobe was visible, as was an increase in back radiation. Interestingly, the typical loss measured through the windscreen was only 2 dB. The measurements were repeated with a gap of 1 mm, 5 mm and 10 mm between the patch and the windscreen. No significant differences were recorded with 1 mm of separation, but increasing the distance to 5 and 10 mm produced a notable increase of ripples in the patterns as well as in back radiation. Cross-polarisation patterns for neither principal plane were presented in the article, but according to the author they were typically 10–15 dB below the co-polar ones.

Additionally, the authors investigated the effect of material parameter and manufacturing tolerances on radiation properties of the windscreen attached antenna. Resonant frequency, input impedance and bandwidth were found to be heavily influenced by the permittivity of the windscreen material and the thickness of the inner glass layer (between the patch antenna and the plastic laminate layer). At the resonant frequency of about 5.33 GHz of the measured antennas, overall variation in resonant frequency was reported as 150 MHz (about 3 %), with the bandwidth varying overall by 90 MHz—both significant indeed considering the narrow bandwidth characteristics of the patch antenna. Efficiencies of the antennas attached with different methods to the windscreen were computed. The efficiency of the patch attached to the screen decreased from 91 % for the patch alone to 69 % when attached to the screen. The losses in the glass reduced the efficiency by 10 %, while surface waves warranted a further 12 % reduction. Similar numbers were recorded for the other antennas as well.

Numerous articles and papers have been published on many kinds of automotive antennas for a multitude of radio services. Only a handful has been covered here, and a selection of others was examined by the author for this thesis, and the interested reader is directed to the following publications: [30-37].

3.2. Electromagnetic modelling and simulation of antennas in car environment

As an important part of this thesis, several publications on numerical antenna simulation were reviewed. A couple of these papers that are considered most relevant and informative will be summarized here. A more in-depth understanding of the different electromagnetic field simulation methods can be gained from the various books written on the subject, such as [38].

Simulations of automotive antennas at FM frequencies

A simulation based study of automotive antennas for FM-frequencies is presented by Low et al. in [27]. Although the frequency range in this paper is quite low compared to the 700 MHz that is of primary interest to us, the use of CST Microwave Studio software and the numerous tips on which settings worked and which did not, make this paper highly interesting. Additionally, the antenna system that was used is a new concept where many different antennas are printed on a plastic carrier plate that is installed in a roof aperture, making it fully conformal. The antennas mounted on the carrier included AM, FM, television and Digital Audio Band (DAB) antennas, but the paper referenced here concentrated on the performance of the FM antennas (there were two of them for optional diversity operation).

The car model that was used was obtained from the car manufacturer, and manipulated to obtain a model better suiting electromagnetic simulation needs, as well as available computing resources. The model did not include any internal furnishings or passenger loading. The effects of omitting the furnishings were promptly referenced, but no hard facts were presented or available to the authors at the time. It was duly noted that more work on this needs to be done. In a later study on on-glass automotive antennas by Low, Langley & Batchelor [29] a reference is made to a yet unpublished study, that would seem to show that by including more of the details of the bodywork, as well as internal details, the prediction of nulls is improved more than anything. This is expected, as even the smallest changes in the simulation models or parameters usually have their biggest impact on the nulls.

Simulation of on-glass antennas

A recent study by Savia et al. [28] on on-glass automotive antennas provides some more insight into the effect of the detail of the simulation model. In this study, four different levels of detail of a car body with an on-glass rear window antenna were simulated and the results compared. The simplification of the models was done by using triangular planar faces to model complex surfaces and reducing the number of faces. The most detailed model was largely omitted due to excessive use of computer resources and consequent instability of the simulation software. The simplest model on the other hand was little more than a “box car”.

The results of the second most detailed model were found to be in good agreement with measured values, for the most part, with only a couple of nulls predicted where

they were not measured. Decreasing the model level of detail led to the disappearing of several nulls and a much less detailed radiation patterns. The simplest “box car” model was found to be in gross error most of the time. Overall, best results were obtained for vertical polarization, which is probably explained by the approximation of perfectly conducting ground plane in the simulation models (also used by Low et al. in [27]). The authors concluded that a “sufficient” level of detail is needed and most of the vehicle contours must be included to assure a good agreement with measurements. The inclusion of interior detailing and metal seat frames in particular were deemed important, though the exact effects of these were still under investigation.

Curiously enough, while the effects of the perfectly conducting ground plane are largely dismissed by the authors of both [27] and [28], in [30] its effect is found significant enough that the author describes finite electrical parameter ground plane as “essential”, however the absolute values of permittivity and conductivity were found to be of little importance. The difference between the former two papers and the latter is the simulation method and software. The former two are using FIT-based CST Microwave Studio, while the in the latter paper the simulations are run on NEC version 2 based software. Both simulation methods provided most accurate results for the vertical polarisation. While the model used in [31] included realistic electrical properties of the ground plane, it seems that even with these parameters the simulation method has other inaccuracies that prevent the ground plane from being modelled accurately. On the other hand, using the FIT-based method, the problem lies in modelling the infinite ground plane, which is very difficult from computing resource point of view unless a perfectly conducting ground plane is used. Both methods did however provide comparably accurate radiation pattern results, when viewed against measurements. Also noteworthy is that the NEC-method doesn’t provide simulation of input parameters, such as input impedance.

The article [27] included a lengthy discussion on different simulation settings they used to attain a good computing-resource-to-accuracy trade-off. The thin printed antenna elements were modelled as bond wires, which reduced the simulation time and memory requirements, as well as increased the stability of the calculation when compared to using cuboids with extremely small dimensions to model the elements. Discrete feed ports were used (these will be explained and more thoroughly discussed in the Chapter 4). The simulated input matching and impedance results were quite poor in general, but this was most likely the cause of heavily simplified modelling of the feeds and the metallic parts of the carrier and antenna mountings, as similar problems were also described by Savia et al. in [28]. The authors do point out that these kinds of errors are very common in automotive antenna simulations, as computer resources set limits to how detailed the antenna surroundings can be. For radiation patterns better agreement with measurements was achieved, within 3 dB, but again not all nulls were accurately predicted and/or positioned. A part of the radiation pattern results presented in this paper is also presented in an earlier article [26] by the same author, but with a comparison to another simulation package called FEKO (utilizing method of moments).

Propagation of electromagnetic waves inside vehicles

A new simple path loss model for antennas inside a vehicle such as a car is developed by Harryson in [39]. The new model was based on approximation of edge diffraction and proposed to be used in simulation of mobile communication systems with the antennas located inside vehicles. The resulting model provides mean path loss as a function of angle. Interestingly, attenuation through window glasses was found to be relatively minor (at 1.9 GHz), but Harryson does remind that it would be significantly higher were the windows equipped with metallic coatings.

A paper by Schoof et al. [40] describes the simulation and measurement of the propagation of ISM-signals in automobiles. The field distribution simulations were carried out using a method of moments based software CONCEPT-II. The car model included the passenger cell of a compact car with planar body panels and no windows. In an attempt to quantify the effect of antennas located inside the car body on critical car electronics, such as airbag sensors and electronic drive assistance, induced currents in several different lines inside the passenger cell were measured. Comparing measurements to simulation data, the effect of windows (up to 10 dB) were found significantly higher than speculated. This was, however, attributed to the light shield coating of the windows. Also, the influence of the driver was examined and no "significant changes" in the amplitude was measured, although radiation pattern did change slightly. Measurement data of the internal electric field distributions inside an automobile body is also available [41], if only for a miniaturized box-type automobile, at 4 GHz.

A similar study was conducted by Blöcher et al. [42] with finite integration technique used in the simulations. Of main interest was the electric field distribution caused by a $\lambda/2$ dipole at 2.5 GHz inside a car. Three different body styles and several antenna locations were simulated, and a simplified model for passengers was also adopted. Inside a sedan body style car, the best position for the antenna with regard to even illumination of the interior of the car was found to be in front of the dashboard. The same position was also found to be the best in an estate car, but no definite best position of the antenna was found for the convertible body style.

3.3. Multi-antenna systems in literature

In this section, an overview of papers dealing with the issues arising in multi-antenna system design is presented. The topics of the publications range from information theory and array configurations to multi-antenna element design.

3.3.1. Information theoretic point of view

Efficient utilization of the increased degrees of freedom in multi-antenna systems requires enhanced information theoretic understanding of the radio channel. Extracting most of the available data rate calls for more complex receivers. Papers concentrating

on the performance and performance metrics of these systems will be discussed in this sub-section.

Fundamental limits of capacity of multi-antenna systems

The information theoretic basis of multi-antenna systems' performance is analyzed by Foschini & Gans in [12]. In the paper, they concentrate on fundamental limits of information transmission in idealized Rayleigh fading channel with additive white Gaussian noise (AWGN). Idealized Rayleigh fading channel in this context means that independent Rayleigh paths are assumed. Capacity is defined in terms of mutual information between input and output; it is taken as a random variable and measured by complementary cumulative distribution functions (ccdfs) that are derived in the paper.

All the results are compared to the baseline case of single transmit and single receive (denoted by (1,1)) antenna. The authors evaluate the theoretical capacities of many different antenna and receiver configurations. For example, the capacity ccdfs of 2 and 4 antennas at both transmitter and receiver (denoted (2,2) and (4,4) cases, respectively), were compared to that of 1 antenna at both transmitter and receiver (1,1). A selection of these results is given in Table 3.1. The outage probability for a certain transmission rate R is the probability that the capacity falls below that level R. The q % outage capacity, correspondingly, is the transmission rate that is guaranteed for $(100-q)$ % of the channel realizations. As can be seen from the Table 3.1, the capacity improvements are significant even with comparably low number of antennas. Also, (2,2) and (8,8) cases were compared to systems using only receive (1,n) or transmit (n,1) diversity, and it was found that significant increase in capacity is achievable with the simultaneous use of receive and transmit diversity. The results for the receive diversity tabulated in Table 3.1 are attained with optimum combining. While the advantage in capacity does tend to decrease with lower SNRs and outage probabilities, it was demonstrated that even at 0 dB SNR and low outages the performance difference is considerable.

Table 3.1. *Maximum outage capacities for a few antenna arrays (*SNR = 21 dB*)*. [12]

Antenna array size (Tx,Rx):	**(1,1)**	**(2,1)**	**(1,2)**	**(2,2)**	**(4,4)**	**(8,1)**	**(1,8)**	**(8,8)**
1 % outage capacity [bit/cycle]	1	3	3.5	7	19	5	8	41
5 % outage capacity [bit/cycle]	3	4.5	5.5	8.5	20	6	9	43

Though concentrating on information theoretic aspects, the authors also consider some issues relating to antenna design of multi-element arrays. Specifically, some practical limitations of antennas are briefly introduced. These include the problem of mutual coupling and field transmission matrix (channel matrix) correlation when small (sub-λ, in general) inter-element distances are used in an array. Mutual coupling makes it difficult to match the antenna impedance efficiently, and also increases the correlation between antenna signals. Also noteworthy is that signals of narrow angular spread tend to increase the correlation, and subsequently decrease the available diversity gain even at larger antenna spacings than λ. Nevertheless, according to the authors a worthwhile

improvement over a single antenna can be achieved even with relatively strong mutual coupling and correlation.

BF MIMO approach

A paper by Ylitalo [14] describes the benefits achievable from combining beamforming (BF) and MIMO approaches. As stated by the author, most papers discussing the properties of MIMO systems normally assume ideal channel properties and ignore the effects of actual antennas. This study concentrates on introducing the ideas behind BF MIMO and analyzing the system's simulated BER performance.

One of the key difficulties in realizing the remarkably high potential of MIMO systems is that the capacity is governed by the achievable signal-to-noise-and-interference ratio (SINR). BF focuses the transmitted power to a narrower sector, and so transmit power can be reduced while keeping the received power constant. This is an advantage in itself, but in the case of MIMO it also means that interference caused to other directions—that is, to the other parallel data streams—is decreased, and that increases the SINR.

To achieve the BF operation, the author proposes the use of a Butler matrix that coherently combines signals from different directions while keeping the power constant and independent of the signal direction. In this study, a 4×4 Butler matrix for a four element ULA with half a wavelength antenna spacing was applied in different MIMO channels.

According to the simulations of the 4×4 ULA arrays, combining BF with MIMO provides an additional 5-15 bit/s/Hz of spectral efficiency compared to regular MIMO. The increase was accounted to the increase in effective SINR that is provided by the BF gain. Also, significantly better BER performance was recorded for the BF MIMO, especially at large BER levels. In the case of small angular spread at base station and mobile terminal, a 10 % BER can be achieved with as much as 10 dB worse SNR if BF MIMO is applied, compared to regular MIMO without BF. The BER performance of the simulated BF MIMO system starts to saturate at lower BER levels, due to the suboptimal Rake receiver that was employed. The Rake receiver is a simple and widely used receiver structure that provides additional diversity gain from multipath components (signal components arriving at different times to the receiver) [7]. The suboptimality of the Rake receiver stems from the parallel data streams that cause interference to each other. Additionally, the spatial diversity of BF MIMO is reduced due to the data streams traversing via spatially correlated channels. As noted by the author of the publication, increased performance would be enabled by a more advanced, interference suppressing receiver, such as parallel interference canceller receivers.

Further work on the theoretical aspects of multi-antenna systems

Other articles discussing the benefits, performance, information theory and extrinsic requirements of MIMO systems, and extremely worthy of the interested readers' time, are for example [10, 11, 43-55]. Also, many books have been written on the subject of

multi-antenna systems, comprehensive and recent examples with emphasis on MIMO systems being [9, 16].

3.3.2. Multi-antenna configurations

The process of successfully implementing MIMO systems depends heavily on antennas and array configurations. To realize the capacity offered by the radio channel, diversity at the receiver as well as at the transmitter must be efficiently employed. Also, in addition to space diversity, other types of diversity such as polarization diversity can be used to enhance the performance. The process of finding the optimal antenna configuration, if there is one, is still very much incomplete. Here, a couple of papers will be presented that analyse this problem, and a few more will be given as a reference.

MIMO measurements in microcell and picocell environments

Several different antenna configurations are analyzed by Sulonen et al. in [56]. They investigated the effects of antenna polarization, array configuration, antenna spacing and directivity on Shannon's capacity in picocell and microcell environments. What differentiates this publication from many others is the fact that their results are based on real measurements, whereas several others offer only simulations and theoretical results of MIMO systems [44, 49, 57-63]. Measurement data is available also in [47, 64-66].

The antennas used consisted of a vertically polarized discone reference antenna, up to eight dual-polarized antennas in different linear arrays at the transmitter and up to 32 dual-polarized antennas at the receiver in a spherical array. The spherical receiver array also enabled extraction of incident waves with corresponding properties, which enabled the authors to simulate arbitrary dipole antennas (ignoring mutual coupling, though).

The microcell case was measured in downtown Helsinki. Expectedly, the capacity of directive elements was found highly dependent on the orientation of the antennas. In the worst cases, the capacity was lower than that of the omnidirectional reference antenna. The capacity of cross-polarized channels was found a little better than that of the single polarization, if both the mobile station (MS) and the fixed station (FS) employed dual-polarized elements. If only one orthogonal polarization was used at the FS, no significant difference was measured between vertical and horizontal polarisations.

Antenna spacings of 0.5 to 2.5 λ at the FS were measured, and it was found that increasing the spacing increases the capacity. The largest increase of about 2 bit/s/Hz was measured between 0.5 and 1 λ, after which the increases saturated a bit. According to direction of arrival (DoA) analysis, the signals in the urban microcell case arrived from only few specific directions—the "street canyons". Increasing the FS antenna spacing also increases the variety of propagation paths, and as a result the MIMO capacity.

The effect of increasing the number of FS (Tx) elements was studied by progressively increasing the number of elements at FS, while the MS had four dual-polarized elements. The biggest difference in capacity was recorded as the number of

Tx elements increased from one to four. Increasing the number of Tx elements above that of Rx elements further enhanced the performance somewhat. According to the authors, added performance was due to the increased antenna array gain. Interestingly, the capacity increase in the outdoors case was much less than that of the two indoors cases. Apparently, an indoor environment offers a much more scatter-rich channel that can be effectively utilized by the increased number of antenna elements. On the contrary, the reduced angular spread and limited number of parallel paths in an outdoor environment results in capacity increasing more as a result of increased antenna gain than actual MIMO gain—at least in this kind of urban microcell case.

In the indoor environment misplaced orientation of the directive elements again resulted in significantly reduced capacity, although this time even the worst case provided better capacity than the reference discone. And again, dual-polarized elements provided a little better capacity than copolarized, albeit only slightly. As speculated in the previous paragraph, increasing the FS antenna spacing had only a little influence on the capacity, presumably because of the much more scatter rich environment. Also, all the studied four-dipole arrays had all but the same capacity, with the array of 2 vertical and 2 horizontal polarized elements just edging ahead. The capacity of the omnidirectional dipole arrays was found to be lacking about 2 bit/s/Hz when compared to the arrays of directive patch elements, which is due to the increased element gain of the patches. However, the dipole arrays provided more consistent results, with the variance of the capacity of the dipole configurations being clearly lower. This reflects the significant effect that the azimuth orientation of the patch array had on capacity, coupled with variations in MIMO gain along the measurement route.

Low profile phased array

An interesting idea is introduced by Kronberger et al. in a set of publications encompassing [67-69]. The authors propose a way of realizing a near-omnidirectional radiation pattern using a phased array of only a few low profile (on the order of $\lambda/8$) antenna elements at the upper rim of the rear window of a car. The interesting part is, from MIMO perspective, that this setup can also be used as a beamforming array with configurable beam direction. The achieved radiation patterns are very impressive with approximately 4–5 dB higher gains recorded in the main beam direction using three low profile elements, compared to a single monopole antenna at the roof centre.

A study on arbitrary non-uniform multi-antenna arrays on confined space has been conducted by Muharemovic et al. [70]. They attempt to optimize spectral efficiency of multi-antenna transceiver configurations in a small a-priori fixed volume. Independent and identically distributed signalling with AWGN is assumed, but no apparent fading model is described. A closed-form expression for circular antenna geometries is presented, as well as numerical procedure and examples for designing linear and square arrays. For example, a 37 % increase in spectral efficiency was simulated for a non-uniform linear eight element array, compared to uniform linear array of the same element count (8) and outer dimension (4λ). The communication limits of such systems

are also derived. The study applies to multi-antenna transceivers in the low-power communication mode, in which spectral efficiency and energy per information bit are critical system performance measures. While the channel and antenna models used in the publication do not assume low power regime, the spectral efficiency that is in a key role in the performance assessment sections of the correspondence, is derived with low power assumption in mind. This publication is notable for considering non-uniform arrays, which is a rare find but one that, according to the study, could offer significant performance advantages over uniform arrays.

3.3.3. Multi-element antenna designs

The performance of a MIMO system is also very much dependent on the antenna elements used in the arrays. Of course, other typical standards of measurement for antennas also contribute: size, bandwidth, input characteristics, etc. The purpose of this sub-section is to briefly introduce a few recent publications on antenna elements that were designed specifically with multi-element use in mind. The procedures of measuring multi-element antennas in indoor environment are discussed in [71].

There are two common ways of creating a MIMO-array. The more versatile and more common way is to use a set number of identical antennas in an array configuration of choice. Typical arrays consist of two to up to about ten elements in a uniform linear array or square array. These kinds of elements are presented in [72-75].

Another approach to the multi-element antenna problem is to use an array of—typically—tens of elements and by some criterion select a subset of these to be used at any given time. In this way the effective antenna properties, such as radiation pattern and polarization, can be configured to meet the varying channel conditions. Another benefit is that while cheap-to-produce antenna elements are numerous, the much more expensive RF-chains are limited in number. The downsides are the somewhat increased cost over fixed, small number of antenna elements and by some extend the increased design effort of such systems. The design of a reconfigurable MEMS integrated antenna is described in [76].

3.4. Conclusions and discussion

Previous work that has been done on automotive antennas, electromagnetic simulation of automotive antennas, the underlying information theory of multi-element antenna systems and, finally, multi-element antenna designs have been looked at in this chapter. Here, the chapter will end with a summary of the main points of the publications and discussion on the importance of the findings of some of the papers.

Wideband antenna solutions have been at the focus of increasing interest in recent years. Reducing cost and complexity by having many wireless communications systems covered by a single antenna is one of the main reasons; the high bandwidth requirements of emerging high-speed communication standards being another one. One of the approaches to a high-bandwidth antenna is the Archimedean spiral antenna. It is

the smallest frequency-independent structure relative to the wavelength, and conformally integratable. Even so, the size of the spiral element does limit its usefulness to a narrow frequency range, especially so in multi-antenna use.

Another way of realizing high bandwidth is to use several, more or less integrated antennas for different frequency ranges. This is usually the best method if several radio services at separate frequencies need to be covered, and it is also the most widely used. However, it may suffer from reduced aesthetics due to several antennas of different size and shape possibly interfering with the visual outline of the vehicle—a consideration that is increasingly important in modern vehicles.

Still today the bulk of literature on automotive antennas deals with FM radio antennas. This is of course understandable, as all but every car made in the last 50 years or so has come with such an antenna, and to many the FM radio is still the only means of wireless communications they consider necessary in their cars. Although being around for so long, the FM radio antenna techniques are all but stagnant, and quite significant research resources are still being invested on improving existing solutions as well as on all-new solutions.

The biggest advancements of FM antennas in recent years have been the development of diversity, on-glass and other conformal antennas. Most new antenna systems are evaluated from diversity point of view, as it has the potential to significantly increase the quality of the received signal. Small antennas are well suited to diversity systems because of their small size, but they often have problems with input parameters and require external input matching. The radiation patterns of small antennas are often highly non-omnidirectional and dependent on the antenna's mounting location on the car, but this is actually a benefit in diversity systems. The most limiting factor for most uses of small antennas comes from the fact that the smaller the antenna element is, the narrower the bandwidth is also. This makes it extremely hard to use electrically small antennas in systems requiring high bandwidths.

On-glass antennas are ideal from the car manufacturer point of view, in that they are all but invisible and do not interfere with the design of the models. They also produce zero wind noise and due to their non-omnidirectional radiation pattern are prime candidates for diversity systems. However, early work suggests that the manufacturing tolerances of automotive-grade window glass may have a significant effect on the radiation properties of on-glass antennas. Further work is needed to examine the effects at higher frequencies.

Simulation of automotive antennas—as with any other antenna types—has been rife in recent years. Most common simulation methods that have been applied to these problems are (in no particular order):

- Method of moments (MoM).
- Finite difference time domain and finite integration technique (FDTD/FIT).
- Finite element method (FEM).

Other simulation methods have also been used, but these three enjoy the most widespread use. All methods were found to provide results corresponding to the

modelling complexity of the car; increasing the model complexity provided more consistent results compared to measurements. However, it is noted that the different simulation methods were used with geometries of different levels of complexity. Especially the MoM was used with a low detail car model, and typically at lower frequencies (FM frequencies of 80-108 MHz being the most common). The FDTD/FIT techniques were used with more complex models and at higher frequencies, up to several gigahertz. The accuracy of input parameter simulation results from FIT simulators were clearly inferior to the accuracy provided by the radiation pattern results, and more often than not could only predict the approximate resonant frequencies. Presumably this is the result of relatively low modelling detail of the antenna feed structure, forced by limited computer time and memory resources. An interesting discrepancy between simulation results was found in the simulation modelling of the ground plane. Some studies found that perfect electric boundary compared well with measurement results, while others strongly suggested the use of ground plane with realistic electric properties (this is challenging in any volume mesh based simulator). Most simulation models excluded any interior furnishings and passengers, the authors again referring to simulation time and computer memory limitations, although most agreed that these could have a significant effect on the radiation patterns. This would seem to be a natural subject of future research.

The research of multi-antenna and especially MIMO systems has heated up in the last ten years. Although much work has been done on characterising the basic principles behind the increased capacity achievable with MIMO, defining the fundamental limits of capacity in MIMO systems, defining the radio channel and recognizing the channel properties governing MIMO performance, yet much work remains to be done. In particular, most of the work done so far has assumed ideal channel properties in some respect or the other, and only in the last couple of years have papers that consider real antenna radiation properties been introduced. So far it is largely unknown how the MIMO performance will be affected in real radio channel environment with real antennas. A few papers with such measurements have already been published, and are referenced in this thesis, but with MIMO performance being—according to simulations, at least—so dependent on the channel properties, more measurements are needed in varying environments. Also, although the antenna array configuration has a huge effect on MIMO capacity, only a handful of publications have actually measured the effect of different configurations. Below is a non-exhaustive list of items that have been identified to have an effect on MIMO capacity (a "+" sign at the end of the line signifies a positive effect, a "−" signifies an adverse effect, and a "±" means the effect can be either way):

- the number of local scatterers near the receive array (+)
- the number of parallel (independent) paths between Tx and Rx arrays (+)
- the number of transmitting and receiving antennas (+)
- the separation between antennas in a linear array (±)
- signal-to-noise ratio of the received signal (+)

- receiver architecture (±)
- the radiation patterns of the antennas (±)
- mutual coupling of antenna elements in the Tx/Rx array (±)
- signal correlation between separate antenna elements (−)

Again, this list is not comprehensive, but even so it demonstrates that a lot of very different aspects of the communication system will have to be considered to achieve good capacity out of MIMO, and some of these will be at odds with each other. Take for example the path loss and the complexity of the channel (multipath propagation). As the separation between transmit and receive arrays increases, so does (in most cases) the complexity of the channel, and hence the number of parallel propagation paths. This effect should increase the capacity. However, in some cases, this advantage can be totally consumed by the increase in path loss, so that increasing the separation actually reduces the capacity.

The antenna elements are a crucial part of the MIMO system. The use of dual-polarization has been shown to enhance capacity over single-polarization, albeit only a little. In many cases, directive elements provided somewhat increased capacity when compared to omnidirectional elements. Of course, higher gain will provide more capacity, as with any other wireless communication system. Mutual coupling has been shown to increase capacity for larger antenna spacings (about $\lambda/2$), but reduce it for smaller spacings. Another decisive antenna parameter is the antenna array configuration. While uniform arrays have been demonstrated to work reasonably well, there are still many unknowns, or at least uncertainties. Judging by the major differences between separate simulations and measurements, it would seem that the channel properties affect the results in such a significant way that no definite conclusions can be made based on a single simulation or measurement made under certain channel conditions and/or propagation environment. It has been verified by measurements that most indoor and outdoor environments provide fundamentally different behaviour with regard to antenna configuration and capacity. This would seem to imply that finding a single array configuration that would work optimally in any environment may be impossible. Reconfigurable arrays might be a solution, but this literature survey did not provide enough papers on this subject to be able to make a definitive conclusion. In any case, it is quite clear that much more measurements are still needed to provide reliable data in different environments against which simulation methods can then be gauged and developed.

4. ANALYSIS OF THE MODELLING AND SIMULATION METHODS

Modern design methods of antennas almost exclusively make use of computer-aided design (CAD). In recent years computing power has reached such high levels, that not only structural analysis and electromagnetic simulation of simple systems, but also of rather complex structures are feasible. Electromagnetic modelling and simulation of high frequency antennas in cars becomes computationally challenging when the wavelength is comparable to the dimensions of the car. At 700 MHz, which is the frequency of interest in this thesis, this is very much the case as the wavelength is about 43 cm.

A number of methods for EM simulation of 3D systems exist. The method of moments (MoM), the finite difference time domain method and finite integration technique (FDTD and FIT, respectively), and the finite element method (FEM) being a few of the most widely used. Each has their strengths and weaknesses, and the most suitable method is usually found on a per-case basis. An extensive overview of the different methods can be found for example in [38].

The chapter begins with Section 4.1, which takes a look at antenna simulation features of CST Microwave Studio (MWS), and also discusses some of its electromagnetic field simulation features in general. Next, Section 4.2 provides a quick look at how CST MWS handles multi-antenna situations and what features it has for that. After that, Section 4.3 concentrates on the special characteristics of simulating automotive antenna systems, as well as introduces the simulation models used in this thesis. Finally, Section 4.4 delves into simulating the link level antenna system performance.

4.1. Modelling and simulating antenna systems using CST Microwave Studio

For this thesis work, CST Microwave Studio (MWS) simulation software was chosen. The CST MWS is based on the finite integration technique (FIT). In addition to a time domain transient solver, it also has frequency domain, eigenmode and integral equation solvers, which add to the versatility of this software. The main user interface of MWS is depicted on Figure 4.1. The computer that was used for the simulations had a quad-core Intel Xeon 3.0 GHz processor and 16 GB of system memory. The simulations were run in 64-bit operating environment.

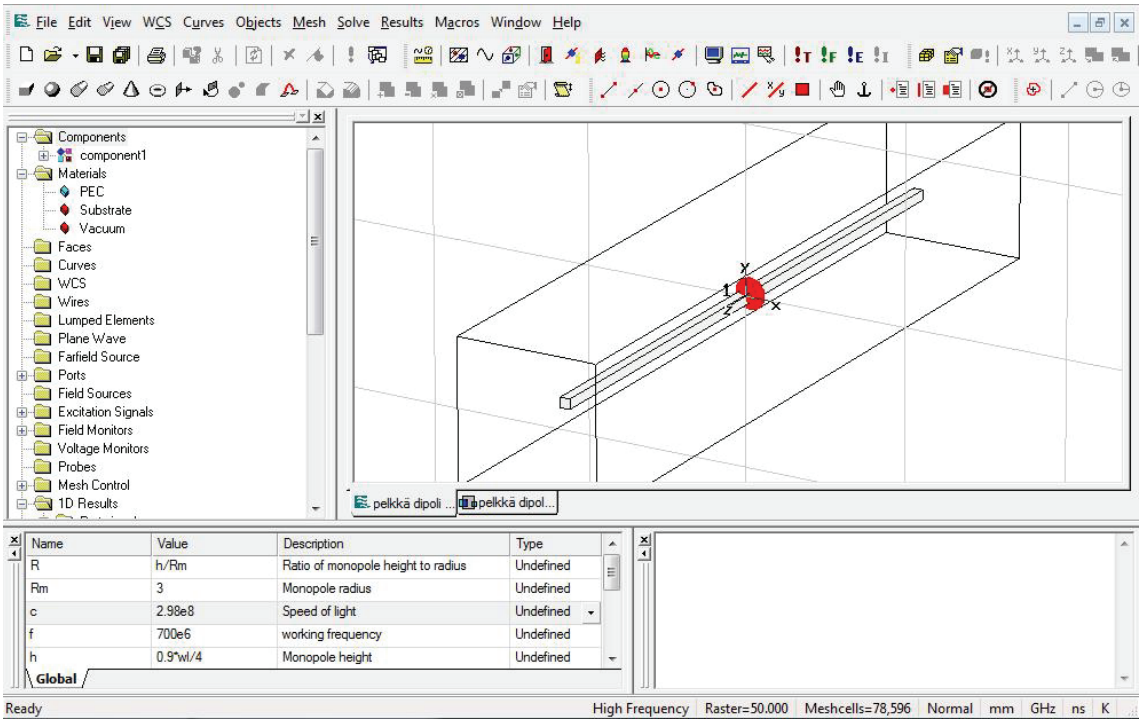

Figure 4.1. *The main user interface of CST Microwave Studio.*

4.1.1. Suitability of FIT to automotive EM modelling

The choice of simulation method and software was based on several reasons. First, as mentioned in the introduction to this chapter, the numerical processing of electromagnetically large objects with techniques using space discretization is always going to be difficult (at least, with contemporary methods and processing power). The solution time of the FIT scales quite linearly with the size of the problem. This comes from the built-in requirement of local orthogonality (i.e. hexahedral mesh), in which case the constitutive law (material matrix) is diagonal. This is opposed to fairly heavy N^2 (where N is the number of unknowns) dependency with MoM, and somewhat heavier (compared to linear) N×log(N) dependency with FEM. On the other hand, if local orthogonality is enforced in FEM, too, the same linear dependency can be achieved as with FIT. Furthermore, most modern FEM software packages are quite efficient even with large mesh sizes, although few (if any) employ local orthogonality. Additionally, the surface mesh of the MoM only discretizes object boundaries, so fairly large structures can be simulated with moderate mesh size, but at the same time true 3D (sometimes nicknamed as 2.5D) modelling is not possible in some situations. Nevertheless, FIT is also well suited to handling large 3D problems in time domain. A strong point of FIT in view of solving large problems is its ability to efficiently distribute the computing load to several processors and/or systems. This comes from the fact that the updating of field components is a local operation. Conversely, the parallelization of a problem where a direct solver or a preconditioning matrix is to be used with FEM or MoM is troubled because these operations are inherently sequential

(assuming local orthogonality and resulting explicit solver is not employed by the FEM). In addition, with time domain methods, such as FIT, a broadband frequency response is generated with fast or discrete Fourier transformations (FFT or DFT, respectively) in a single simulation run. Compared to separate simulation runs for every frequency point when using frequency domain methods, the time domain approach is advantageous when wideband response is desired. Furthermore, the time domain simulators have no problems with nonlinear materials, boundaries or devices. Lastly, the author of this thesis as well as Elektrobit had previous experience with CST software and so, combined with the previous observations, it was a natural choice.

As with any method, FIT is not without its weaknesses. A potential problem with time domain methods lies in solving problems where fine geometrical detail is embedded within a much larger structure—such as an antenna and feed circuits integrated to a car. The problem originates from the fact that the time step for the field updating process has a maximum value specified by the *Courant–Friedrichs–Lewy (CFL) criterion*. The criterion for magnetically and electrically isotropic media characterised by μ_r and ε_r is

$$\Delta t \leq \frac{\sqrt{\mu_r \varepsilon_r}}{c\sqrt{\frac{1}{\Delta x^2}+\frac{1}{\Delta y^2}+\frac{1}{\Delta z^2}}} \tag{4.1}$$

where c is the speed of light, Δx, Δy and Δz are the length, width and height intervals. According to this limit, the time it takes for the field to travel across the largest diagonal dimension of a cell must be greater than the time step. Also, if the mesh has cells of different sizes, the *smallest* cell dictates the largest stable time step for the entire mesh. So, if a large structure requires even a few small cells, the time step must be made very short. In large structures with fine details—and hence a large amount of cells, some of which very small—this condition can quickly increase the computational requirements of the problem. Another problem with FIT is that it does not obey the energy conservation principle, which leads to inaccuracies and long solution times in near-resonant problems. Recognized weaknesses of the FIT also include limitation to hexahedral meshes (staircase approximation of curved surfaces) and the fact that multiple solution runs are needed for multiport *S*-parameters. [38]

Many FIT simulators have certain features that can help with the meshing problems. One such feature is called subgridding, which can alleviate problems with structures with varying degree of detail somewhat. Using subgridding it is possible to create denser mesh around areas with fine detail, and conversely a sparser mesh in less detailed areas. Subgridding is done automatically when enabled. It also enables different time steps to be used in the finer submesh and main grid. This allows for keeping the increase in solving time modest, while the smallest mesh cell size is decreased. It does require some numerical overhead in itself, and thus it's only recommended for use in structures where it can provide a significant reduction in mesh size (about threefold or more). Also, subgridding requires time and space averaging at the boundary between the

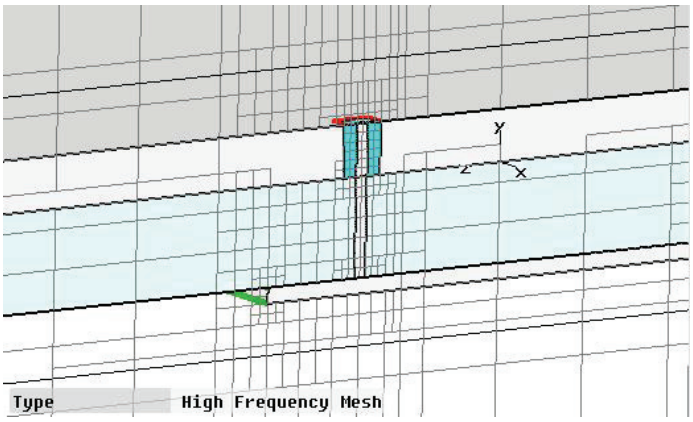

Figure 4.2. *Subgridding has been applied to a structure with a coaxial feed in the middle.*

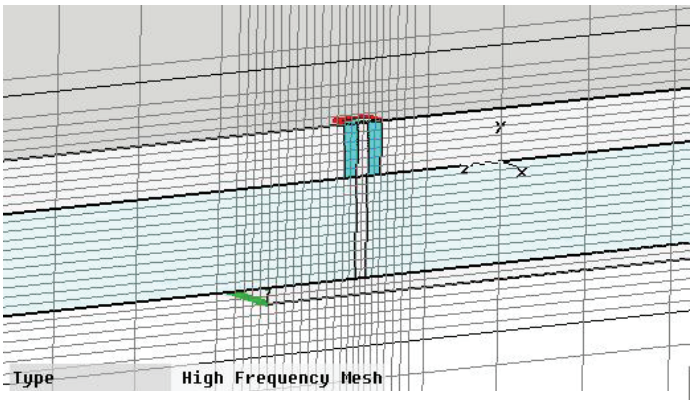

Figure 4.3. *Local mesh refinement has been applied to the same structure as in Figure 4.2 (here without subgridding).*

sub-domains, which can introduce errors. However, in certain cases with the current FIT simulation software it is the only viable choice for significantly reducing the total mesh size while maintaining a dense mesh in some places of the model. Another option is to manually create a denser mesh around some parts of the structure, but in this case the refinement can be local in one coordinate direction only, whereas with subgridding the refinement can be local with respect to all coordinate directions. Also, manually increasing the mesh size has the effect of driving the minimum stable time step down for the whole mesh and hence increasing the solution time. The effect of subgridding and increasing local mesh density manually are demonstrated in Figure 4.2 and Figure 4.3, respectively. [38, 77]

The CST's heuristic implementation for circumventing meshing problems arising from curved surfaces is called Perfect Boundary Approximation® (PBA). The standard mesh in MWS is hexahedral, and so a possible problem lies in curved surfaces that are difficult to mesh with finite mesh size. Normally, the curved surfaces would have to be expressed in staircase approximation. The PBA approximates these kinds of features within the cubic mesh cells using a special kind of conformal boundary cells, and does provide reasonable accuracy in many cases, as long as the approximated structure is greater than the cell size of the mesh. The PBA method appears to truncate larger cells to form polygonal cells to achieve conformal mesh. The reader should note that although it provides expected results in many cases, as is the case with subgridding, the theoretical base of the PBA is not entirely robust. [38, 77]

4.1.2. Modelling with Microwave Studio

The workflow of MWS starts with modelling the geometry of the object to be simulated. One of the strengths of many modern EM simulators are their wide support for importing model data from various CAD file types, and MWS is no exception. In

addition to importing model data from CAD files, MWS also incorporates a few essential tools for creating some basic forms by hand. Both of these methods were used in this thesis, in that a simple "box car" model was modelled using MWS, and a more detailed car model of a 1990s BMW 5 series sedan was imported from CAD data. After the model is ready, ports where the transient signal is fed into the system are defined.

As the MWS is based on FIT, the whole computational space needs to be meshed. In most cases, however, the computational space is not or indeed cannot be limited. For these situations boundary conditions can be implemented in the MWS. These include

- open boundaries (realized as perfectly matched layers, PML), which simulate free space beyond the boundary
- electric and magnetic boundaries, which, respectively, impose on vanishing tangential electric and magnetic fields at the boundary
- periodic boundary condition (BC) that connects two boundaries with a definable phase shift such that the boundaries are point wise identifiable with each other, and hence the calculation domain is simulated to be periodically symmetrical in the corresponding direction [77]
- a conducting wall BC simulates a wall of lossy metal material, and finally
- a unit cell boundary condition that is similar to the periodic BC, with the exception of two-dimensional periodicity.

It is also possible to define electric or magnetic symmetry planes using the electric and magnetic boundary conditions, which can greatly reduce the computational space and hence the memory and time requirements. Thermal boundaries are also definable in MWS. [77]

Excitation of signals and energy to the system is handled by ports in MWS. There are two kinds of ports: waveguide and discrete. The waveguide port is a special kind of boundary condition that enables the stimulation as well as absorption of energy. It simulates an infinitely long waveguide that is connected to the structure, such as a coaxial cable or a micro strip line. These kinds of ports were predominantly used in the simulation models in this thesis. [77]

The discrete port simulates lumped element sources. According to [77], they give a good approximation for the source in the feeding point of antennas. However, larger reflections can occur when using these ports due to the transmission between transmission lines of different geometric dimensions. The discrete port can be one of three different types: a voltage port, a current port or an impedance element. The latter enables the measurement of *S*-parameters, and so it was the one used in the models of this thesis when discrete ports were employed. It consists of a current source with inner impedance and is able to both excite and absorb power.

4.1.3. Solvers

The MWS has four different solvers for use in different kinds of problems. For automotive applications in the sub-1 GHz frequency range, CST recommends using the

transient time domain solver. It is based on the solution of the discretized set of Maxwell's Equations. It determines the progress of fields step-by-step through time by the "leap frog" method at discrete locations. The time-step must satisfy the CFL criterion in Equation (4.1). The transient solver enables broadband simulation of a structure in a single computation run, which makes it very efficient in broadband calculations. However, monitors for different quantities, such as farfields and electric or magnetic fields, at every frequency point of interest need to be defined beforehand. The downside of this is that the results of these monitored quantities can only be viewed at these predetermined frequencies. Nevertheless, some results, most importantly the *S*-parameters, are viewable on the whole simulated frequency range. Because of its linear dependence on the size of the problem it is the best of the MWS's solvers for simulating 3D objects with large dimensions. It is not however ideal for high-Q problems, since it would take a considerable amount of time for the inputted signal to die down in the highly resonant situation. Thankfully autoregressive filtering is available and very helpful with the highly resonant structures, but even that will only help so much. For networks with more than two ports the time domain solver must do a complete solution run for each port in the network if a complete set of *S*-parameter results are needed. This can dramatically reduce the effectiveness of this solver with multi-antenna systems. Hexahedral mesh is used with the transient solver. All in all, the transient solver is the most versatile and a good general purpose solver of the MWS solvers.

For smaller problems of tens of thousands of mesh cells, for highly resonant and for narrowband problems the frequency domain solver can be more efficient than the transient solver. Two other solvers, namely eigenmode and integral equation solvers are also available in MWS. The former is efficient in calculating resonance frequencies and the corresponding fields (eigenmodes) of loss free structures. The integral equation solver is available for *S*-parameter and farfield calculations in the frequency domain.

4.1.4. Simulation of multi-antenna systems

CST MWS sports a few features especially useful in the analysis of multi-antenna systems. While simulation of multi-antenna systems is not fundamentally any different from the single-antenna case, there are some notes to be made on the subject.

As mentioned in the previous section, MWS handles the energy transfer in and out of the system by ports. If more than one active antenna element is desired, there are basically two options on how to feed it. First, it is possible to use one port that will feed all of the elements through power dividers. This isn't a very good approach, since it requires a lot of extra transmission lines to get the power from the port to all the antennas, and the inter-element phase shift is only adjustable by manually changing the length of each of the feeding transmission lines. It may not be the most convenient way of doing it, but in some applications the feeding is arranged in this way. The more practical and more common way of multi-antenna excitation is to use a separate feed for every element. As one would expect, this is done by defining a port, either waveguide or discrete, for every element.

After setting up the ports, the solver is run. There are three options for acquiring the results of a multi-element setup. If the geometry of the problem is very simple, and basically includes only an antenna element and substrate, it is possible to apply pattern multiplication to a calculated far field monitor. In this way, the corresponding results for an array can be calculated very fast in post-processing. The result is formed in the following way:

$$E(\text{tot}) = [E(\text{single element at reference point})] \times [\text{array factor}], \tag{4.2}$$

where E(tot) is the far field of the resulting array, and E(single element at reference point) is the far field of the single element. The reference point is the phase centre of the entire grouping structure. As can be seen from the Equation (4.2), this method does not consider coupling between elements—that is, E(single element at reference point) is assumed to have being determined with no other antennas or objects in its vicinity. However, it is a very fast method for quickly obtaining a coarse approximation of the farfields of an array. The position and phase of each element can be separately defined in order to create an arbitrary array pattern.

If more precise results are desired, or the geometry of the problem includes objects other than the antenna element with substrate, it is recommended to simply model all the required antenna elements. Although this method is very accurate, the solving time of arrays with large number of elements will be heavily increased, as each additional port requires a separate simulation run. Of course, this is only the case in time domain calculations. Another benefit of this method—besides the increased accuracy—is that the results can be computed in post-processing for arbitrary amplitude and phase shift between elements. All the ports can also be simulated in one calculation, if the required amplitudes and phase shifts of each element is known beforehand. In this case, the time domain solver has an option of simultaneous excitation that calculates the output of all the ports in one run. This is very advantageous if the mutual coupling of elements needs to be considered, or if the geometry is too complex for the array factor multiplication method, but the linear increase in solving time with number of ports is not acceptable. It should also be stressed that the combination of excitation amplitudes and phase shifts of the ports can only be configured before the simulation run, and that for each combination the solver must be run again. Unfortunately *S*-parameter calculations are also unavailable with this method.

4.2. Car models

The results of electromagnetic simulators are affected by the accuracy of the geometry used to simulate the subject. With contemporary computers, the level of detail of models is a compromise between accuracy, computation time, and memory requirements. With this in mind, two very different models in level of detail were created for the simulation of the antennas in automobiles, and these will be presented next. This section gives a general overview of the models and their geometry and materials.

4.2.1. Car antenna modelling in simulations

The section starts with a brief introduction of the antenna models that were used with the car models in the simulations. First, the quarter wave monopole presented in Figure 4.4 is discussed. The monopole is, with some exceptions, modelled as parallelepiped to fit the hexahedral mesh perfectly and to keep the computational requirements as low as possible. The relation between the radius of a cylindrical monopole and the side length of a rectangular parallelepiped monopole is given in [78] as $r = 0.59a$, where r is the radius of the cylindrical monopole and a the length of a side of the rectangular monopole. The effects of this approximation on far field pattern and matching were found to be negligible. In some cases a cylindrical monopole was also used. The length of the monopole was varied from about $0.9 \times \lambda/4$ to $0.97 \times \lambda/4$. The purpose of varying the length of the monopole was to achieve input matching of −6 dB or better with the different car models, antenna locations and feed mode. In most of the models used, this threshold was cleared with ease, although in a couple of models it was met only just. The monopoles were excited through short stubs of coaxial cable through the roof panel that were in turn excited with waveguide ports, as in Figure 4.5.

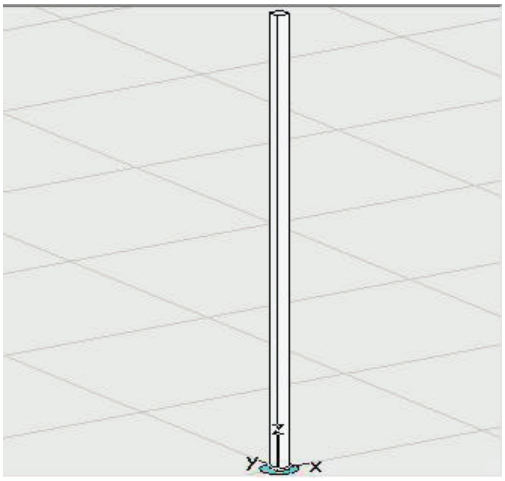

Figure 4.4. *The monopole antenna model as used in most of the simulations.*

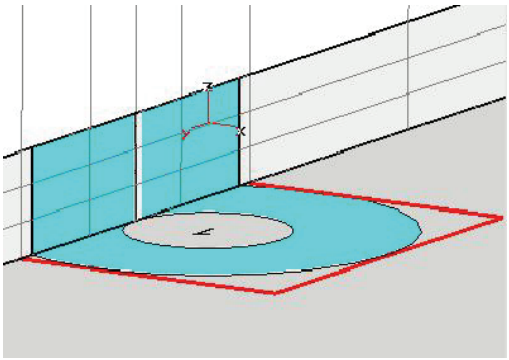

Figure 4.5. *A cut-through image of the coaxial feed model. The red rectangle indicates the outer perimeter of the waveguide port.*

A quarter wave patch antenna was also considered, but achieving decent input matching and bandwidth without using external matching circuits quickly increased the dimensions of the patch to unacceptable levels to be considered for a multi-element array. An array of two dipole elements on the rear window was also of interest, as these kinds of glass mounted antennas are becoming more and more popular on modern cars. The dipole elements were modelled as two mirrored monopoles—with matching dimensions from the previous paragraph—separated by a small air gap. Discrete *S*-parameter ports with impedances of 75 to 77 Ω were used for excitation.

The antenna elements presented so far have all been designed to be installed by the car manufacturer at the factory. However, other types of antennas are also of interest, namely antennas mounted inside the car as after-market items. These include antennas on mobile terminals, such as mobile phones, but also fixed antennas mounted inside the

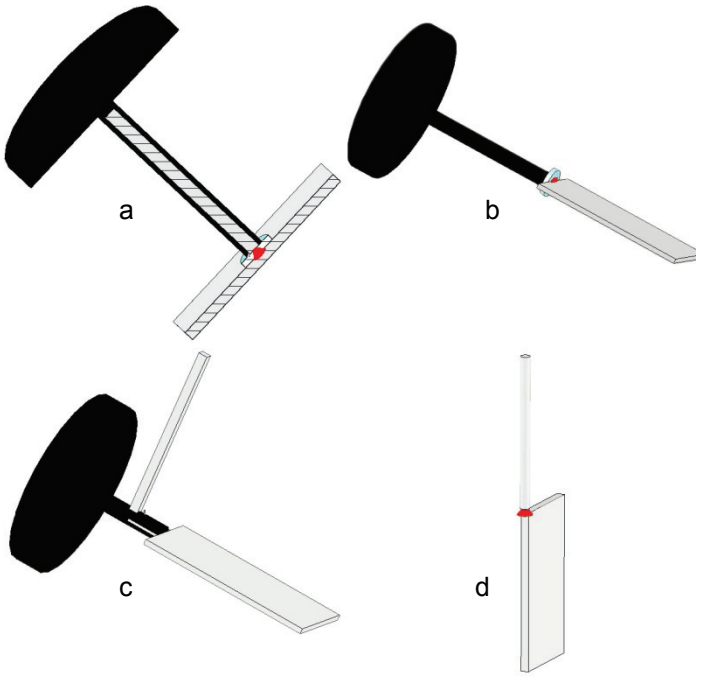

Figure 4.6. *After-market antenna models. Antennas a and b are similar to each other, only the orientation of the small ground plane is changed. Antennas a–c are mounted on the windscreen using the black suction cup. Antenna d is located on the dashboard.*

car (typically inside the passenger compartment). An example of this kind of an antenna would be an antenna element mounted on a suction cup on the windscreen. Four of these kinds of "after-market" antennas were created for the basic car model as presented in Figure 4.6. These antennas were used to examine the effect of finite thickness of window glass on farfield radiation, and also to provide a comparison to the roof mounted multi-element antennas. They will simply be called after-market antennas from now on. The antenna elements themselves are actually just monopoles located on small and asymmetric ground planes, which in most cases leads to poor input matching. Monopole models *a–c* are rectangular, while model *d* is cylindrical.

The simulations were run on single antennas or two-antenna arrays for the most part, although some four-element arrays were also experimented with. This was due in part to the limitations in the MATLAB implementation of the BER calculation code (to be introduced in Section 4.3), which was primarily designed for 2×2 MIMO simulations (1×1 simulation was possible with some minor modifications). Extending this implementation for other antenna configurations is possible, but unfortunately not within the time frame of this thesis. This limitation was not too disappointing, though, because the car manufacturers wish to keep the number of antennas as low as possible, in any case. Moreover, the most advanced wireless communication systems, like UMTS rel. 7 and WiMAX, limit currently to 2×2 MIMO antenna configurations. [79, 80]

4.2.2. Basic car model

The least detailed car model comprised basically only of three boxes—the engine compartment, the passenger cell and the rear compartment. The model is illustrated in Figure 4.7. The passenger cell had A-, B- and C-pillars connecting the roof to the lower part of the car. All the panels were planar, and the passenger cell had no accessories or detailing. The engine as well as rear compartments were disconnected from the passenger cell by a conducting panel. This model is called the basic car model (BCM).

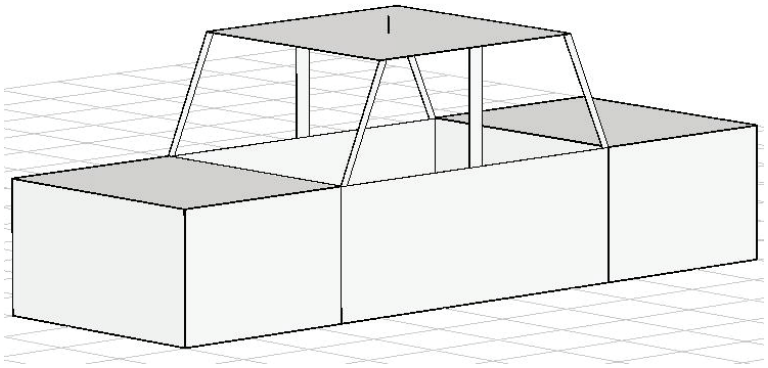

Figure 4.7. *The basic car model.*

The BCM was designed using only the tools provided by MWS. All the panels were 5 mm thick, and made of perfect electrically conducting material (PEC). All the boundaries except for the horizontal plane boundary were always modelled using open boundary conditions. An electrical boundary condition (conducting wall) was used on the horizontal plane boundary in some simulations, though in most cases an open boundary was used in this plane also.

Both waveguide and discrete ports were used with the BCM. With waveguide ports a 5 mm long stub of coaxial cable was used to transfer energy and power to the antenna element. The inner and outer radiuses of the coaxial cable were selected such as to provide optimal input-impedance matching. Discrete port was utilised in between the ground plane and monopole element after lifting the monopole a few millimetres from the ground plane, or straight in between the halves of a dipole antenna. The effect of ground-plane–monopole spacing on input matching is reported in Section 5. Different types of ports in the basic car model are illustrated in Figure 4.8.

4.2.3. Advanced car model

CST kindly provided us with a much more detailed car model, compared to the basic car

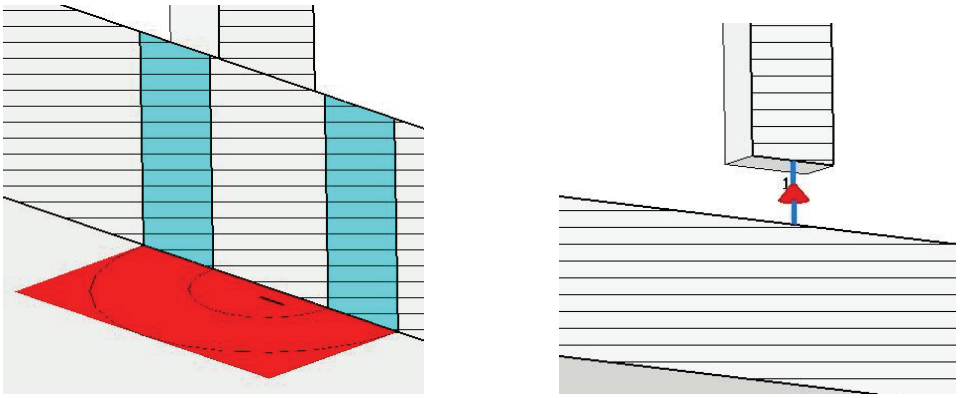

Figure 4.8. *Cut-through images of the antenna excitation models used with the BCM. Waveguide port feed on the left; the red square represents the excitation interface. Discrete S-parameter port excitation is illustrated on the right; the red cone denotes a point-source while the blue lines represent electrical connections.*

model, to be used in this thesis. The modelled vehicle is a third generation (E34) BMW 5 series 4-door sedan from the early 1990's. The model was imported from CAD data, and includes accurate models of all the body panels as well as comprehensive list of accessories, such as wheels, windscreen, and sunroof. The model is, though, only a shell with no interior or panels separating the engine compartment and the rear compartment from the passenger cell, as can be seen from the Figure 4.9. This model is named as the advanced car model (ACM). It is the most accurate vehicle model used in this thesis. Compared to the less detailed BCM, a sufficiently dense mesh could be created with about twice the total cell count, increasing the memory requirements accordingly. In many cases, the subgridding feature was used to reduce the mesh size by a factor of at least two while retaining adequate accuracy (some computational overhead is required, also).

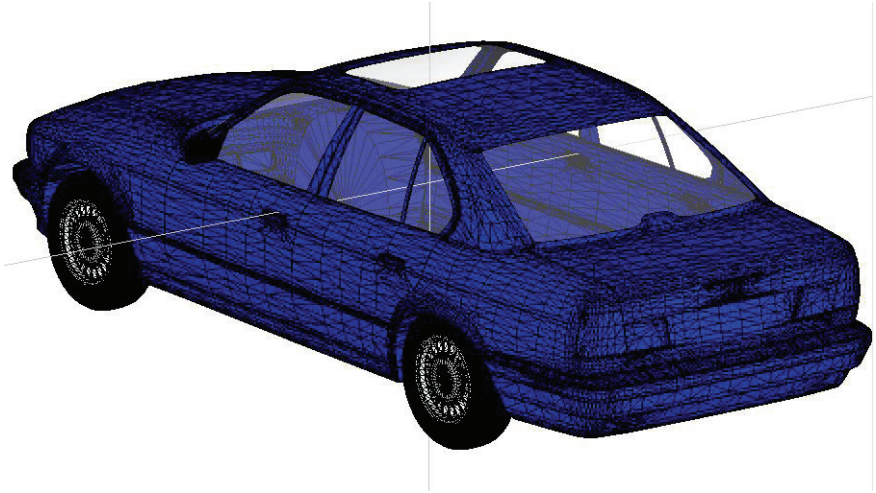

Figure 4.9. *The advanced car model. Note the lack of interior furnishing, engine, dashboard, etc.*

Body panels are of PEC, but tires, all the window glasses and some plastic detailing are modelled with characteristic electrical properties for each respective material. All the surfaces are modelled as infinitely thin.

The antennas simulated with the ACM included the roof monopoles, window dipoles and the after-market antennas. Antenna excitation was modelled for the most part with discrete *S*-parameter ports, though waveguide ports were checked to work as well (the discrete ports should provide some concessions on computing resources).

4.2.4. Keynote concerning the car models

The perceptive reader may have noticed what would seem to be a significant omission in both the ACM and BCM simulation models. That is, in Chapter 3 we discussed several papers that suggested that the interior details and furnishing of the car models are crucial parts of the model and can have a significant effect on the radiation patterns. However, both the simulation models we employ in this thesis are devoid of any interior detailing.

There is a principal difference between the use of the simulation models presented in this thesis and the ones in the referenced articles. That is, in the referenced articles the focus is on finding and/or developing methods for as accurate simulation of a certain antenna model as possible. The success of this task is usually measured by mounting the antenna under test on a vehicle and comparing the simulated radiation patterns to the measured ones. However, the objective of this thesis is not as tightly focused as finding a single antenna element and array configuration that perform the best while driving along in downtown Helsinki. What is important, in the context of this thesis, is to:

- Find the general performance behaviour of multi-antenna systems in automotive environment (not limited to any single car model, make or body style, or to any single antenna type).
- Study the pros and cons of simulating antenna systems with FIT.
- Provide measurement and simulation data of link level performance of automotive multi-antenna systems.
- If possible, establish a few basic design rules or practices that should help to improve the capacity of automotive multi-antenna systems.

None of these objectives were thought to require a "carbon copy" model of a real car. With this background it was judged irrelevant to include much of the details of the vehicle interior as this would only make the results more relevant with that exact car model and increase the already-quite-formidable computer resource requirements.

The same principles actually apply also to the antenna models in this thesis. Again, the objective was to demonstrate the general link level performance of multi-antenna systems, and for this reason only established, easy-to-design elements were even considered.

4.3. Link level performance simulation

The standard performance measures of antennas are the radiation properties. Farfield and even near field antenna pattern, impedance matching and total efficiencies, as well as the antenna gain are important to any system using antennas. However, sometimes these may not adequately describe the system level performance, or the needed information might not be easily extracted from these measurements.

Most modern, wide-spread wireless systems are digital. In these systems the only thing that matters, in the end, is whether or not the correct bits can be recovered from the transmitted signals. Thus, the link level bit-error rate (BER), as described in Chapter 2, is a proper measure for performance evaluation. Indeed, it is rather difficult to predict how many of the transmitted bits can be correctly detected in a certain environment just by looking at the far field antenna patterns. But in a sense, the BER is the ultimate measure of how good an antenna is for a given application. Thus, it is be extremely beneficial to be able to measure the BER in realistic radio propagation environments. A method for extracting an antenna system's BER performance from its far field radiation pattern will be described in this section.

4.3.1. 3GPP Spatial Channel Model

The antenna is not the only part of the communication system that affects the system's performance. The receiver architecture, signal processing algorithms and losses throughout the system (resistive or mismatch) also heavily contribute to the system performance. Furthermore, these are the aspects of the wireless communication system that the system designer has control over. There are other aspects of the wireless communication system that the designer has little or no control over. Probably the most significant is the radio channel. That is, the medium and "path" through which the electromagnetic energy needs to travel to get from the transmitter to the receiver.

Most of the time the designer of a wireless system cannot control the radio channel, instead the system must be designed to cope with the channel or, in the best case, take advantage of it (as in the case of a MIMO system). To make the most out of a radio channel, an accurate model of it needs to be constructed. If such a model is at hand, realistic link and system level performance simulations become possible. Channel models realistically characterise the space- and time-variant effects of radio channels. The main outputs of these models are the channel coefficients between a base station (BS) and a mobile station (MS). These models take into account effects like fading, antenna orientation at MS and angle spread of the multipath signal components at both the BS and MS that affect the performance of the antenna system. One such model is the 3rd Generation Partnership Projects' (3GPP & 3GPP2) Spatial Channel Model (SCM) that was the basis of the link level performance simulations of this thesis. A detailed description of the channel model is available in [18].The path model between the MS and the BS and the related angular parameters (including some that are not covered in this thesis) are illustrated in Figure 4.10.

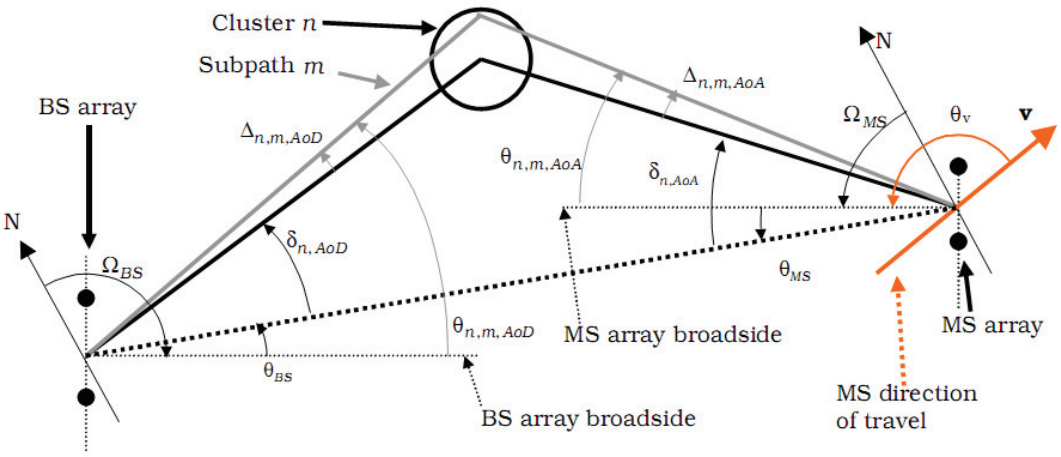

Figure 4.10. *An illustration of the path model and related angular parameters of the Spatial Channel Model (SCM). This figure is carried over from [18], and all the parameters in the figure are introduced and explained in that reference.*

4.3.2. Estimating link level performance

The link level performance simulation of the antenna system was carried out using a MATLAB implementation of the Interim Channel Model for Beyond-3G Systems, denoted as SCME to emphasise the fact that it is an extension of the 3GPP SCM, although it is not associated with the 3GPP working group. This SCM extension and its MATLAB implementation were developed in Work Package 5 of the IST-WINNER project of the European Union's 6th framework program. The main difference between the SCM and the SCME is that the SCME includes additional parameters that enhance its accuracy and enables its use with higher bandwidth systems. Although the SCME implementation is used, it is used in SCM-mode with the associated lower bandwidth. [81]

The SCME includes antenna parameters, together with MIMO radio link parameters and model configuration parameters as input parameters. Outputs of the model are the MIMO channel matrices that give the relationship between the input and the output of the system (radio channel). The model includes three main scenarios which are the suburban macro cell, the urban microcell and the urban macro cell. These scenarios control a few scenario-specific parameters, such as shadow fading characteristics, angle and delay spreads of the multipath components, and path loss. The environment parameters of different scenarios are presented in Table 4.1. The AoA and AoD in this table denote Angle of Arrival and Angle of Departure, respectively, that describe the angle of inbound/outbound power with respect to the broadside. The urban macro cell environment was used in this thesis.

As already mentioned at the beginning of the section, the system's BER performance will be used as the performance metric of choice. The uncoded BER results will be calculated from simulated and also from measured radiation patterns, while the propagation environment is the one characterised by the SCME channel model. The BER calculation code was originally developed at Elektrobit.

The model considers only the azimuth plane radiation pattern as an input, with angular resolution of 1°. This can of course present some inaccuracy to the model, especially if the distance between MS and BS is small in a scenario where the BS is located for example on top of a tall building and the MS antenna radiation pattern has significant variation in elevation plane. Furthermore, the SCME was developed for 2 and 5 GHz frequency bands, while we use it at 700 MHz. Using a channel model at other than design frequency is not unusual—a precedent is found in [82]. The inaccuracy due to the different carrier frequencies is expected to be small since the lower frequency has a substantial effect only on the path loss. In link level simulations, the average radio channel power is normalised to unity regardless of the distance (path loss) between the BS and the MS. Therefore, only Rayleigh or Rician fast fading is considered. The effect of path loss and shadow fading are usually modelled in multi-user system level simulations which are out of scope of this thesis. The author is not

aware of any available MIMO channel models that are specifically designed for the 700 MHz carrier frequency.

The basic procedure for the calculation of BER values is as follows:

- set channel parameters according to the SCM and the antenna radiation patterns
- compute *N* channel samples, where the MS and BS directions/orientations and accordingly the impulse response change randomly
    - for each of the *N* channel samples, compute 200 time realizations, where fast fading characteristics change according to the antenna orientations
        - for every time realization compute noise levels for six predefined SNR values
        - compute the bit errors for every time realization and for each SNR level
    - count the total number of erroneous bits in the 200 time realizations for each of the *N* samples and for each of the six SNR values
    - compute the BER for each sample and SNR value
- for each SNR value, compute the average BER of the *N* samples

In our simulations, *N* was set to 300, and the average BER of five simulation runs (each as described above) was taken as the final BER value. Most of the simulations and measurements were run with 2×2 MIMO configurations, although some 1×1 SISO cases were also studied. In the MIMO cases a minimum mean square error (MMSE) receiver was employed (for further information on the MMSE receiver see [9]).

The MS radiation pattern was obtained from simulations or measurements, while calculated monopole radiation patterns were used for the BS. It is important to note that because of the dramatically different interference characteristics in the radio channel (parallel path interference) the MMSE receiver requires significantly larger SNR level than the simple SISO receiver to achieve the same BER level.

Table 4.1. *Environment parameters of the SCM for different scenarios.* [18]

Channel Scenario	Suburban Macro	Urban Macro	Urban Micro
Number of paths (*N*)	6	6	6
Number of sub-paths (*M*) per-path	20	20	20
Mean AS at BS AS at BS as a lognormal random variable $\sigma_{AS} = 10\text{^}(\varepsilon_{AS}x + \mu_{AS}),\ x \sim \eta(0,1)$	E(σ_{AS})=5° μ_{AS} = 0.69 ε_{AS} = 0.13	E(σ_{AS})=8°, 15° 8° μ_{AS} = 0.810 ε_{AS} = 0.34 15° μ_{AS} = 1.18 ε_{AS} = 0.210	NLOS: E(σ_{AS})=19° N/A
$r_{AS} = \sigma_{AoD} / \sigma_{AS}$	1.2	1.3	N/A
Per-path AS at BS (Fixed)	2 deg	2 deg	5 deg (LOS and NLOS)
BS per-path AoD Distribution standard distribution	$\eta(0, \sigma^2_{AoD})$ where $\sigma_{AoD} = r_{AS}\sigma_{AS}$	$\eta(0, \sigma^2_{AoD})$ where $\sigma_{AoD} = r_{AS}\sigma_{AS}$	U(−40°, 40°)
Mean AS at MS	E($\sigma_{AS, MS}$)=68°	E($\sigma_{AS, MS}$)=68°	E($\sigma_{AS, MS}$)=68°
Per-path AS at MS (fixed)	35°	35°	35°
MS Per-path AoA Distribution	$\eta(0, \sigma^2_{AoA}(\mathrm{Pr}))$	$\eta(0, \sigma^2_{AoA}(\mathrm{Pr}))$	$\eta(0, \sigma^2_{AoA}(\mathrm{Pr}))$
Delay spread as a lognormal random variable $\sigma_{DS} = 10\text{^}(\varepsilon_{DS}x + \mu_{DS}),\ x \sim \eta(0,1)$	μ_{DS} = −6.80 ε_{DS} = 0.288	μ_{DS} = −6.18 ε_{DS} = 0.18	N/A
Mean total RMS Delay Spread	E(σ_{DS})=0.17 μs	E(σ_{DS})=0.65 μs	E(σ_{DS})=0.251μs (output)
$r_{DS} = \sigma_{delays} / \sigma_{DS}$	1.4	1.7	N/A
Distribution for path delays			*U*(0, 1.2μs)
Lognormal shadowing standard deviation, σ_{SF}	8dB	8dB	NLOS: 10dB LOS: 4dB
Pathloss model (dB), *d* is in meters	31.5 + 35*log$_{10}$(*d*)	34.5 + 35*log$_{10}$(*d*)	NLOS: 34.53 + 38*log$_{10}$(*d*) LOS: 30.18 + 26*log$_{10}$(*d*)

5. ANTENNA DESIGN, VERIFICATION AND LINK LEVEL SIMULATIONS

EM simulation software packages have gained a lot from the increased computer resources. Still, simulations often provide us only with crude models, and they may include some non-idealities that can cause some unexpected results. Because of these properties, both simulations and measurements are needed to give information on how a given system will function.

All the simulated antenna radiation patterns presented in this chapter exclude the effects of input mismatch. This decision was made because there was not enough time to optimise the input matching in each separate case, and hence unrealistic differences would be introduced by including the mismatch.

This chapter focuses on the design and construction of a monopole antenna, although other antenna type design and simulation will be touched upon. Measurement results for the antennas described here will also be presented, and compared to the simulations for the purpose of validating the simulation methods described in Chapter 4.

5.1. Design through simulation

This section briefly covers the design process and the simulation results of the antenna elements that have been presented in this chapter. The building and tuning of the antenna elements used in the measurements will also be presented here. The coordinate system used throughout this chapter is illustrated in Figure 5.1 with a 3D far field radiation pattern of the monopole antenna at the centre of the roof of the BCM. The coordinate system is chosen such that the forward direction corresponds to $\varphi = 0°$, and upwards direction (toward the zenith) corresponds to $\theta = 0°$. In all the subsequent 2D radiation pattern figures these angles are at the top of the figures, and the θ angles increase clockwise, φ angles counter-clockwise. Two elevation plane cuts are used in this chapter: *1)* longitudinal cut, $\varphi = 0°$ and *2)* transverse cut, $\varphi = 90°$.

Ground plane

All the single- and multi-antenna configurations presented in this thesis were simulated in free space (open boundary conditions, no ground plane). A couple of ground plane simulation methods were studied, namely: *1)* a finite thickness cuboid, with realistic electrical parameters, representing the ground plane underneath the car model and *2)*

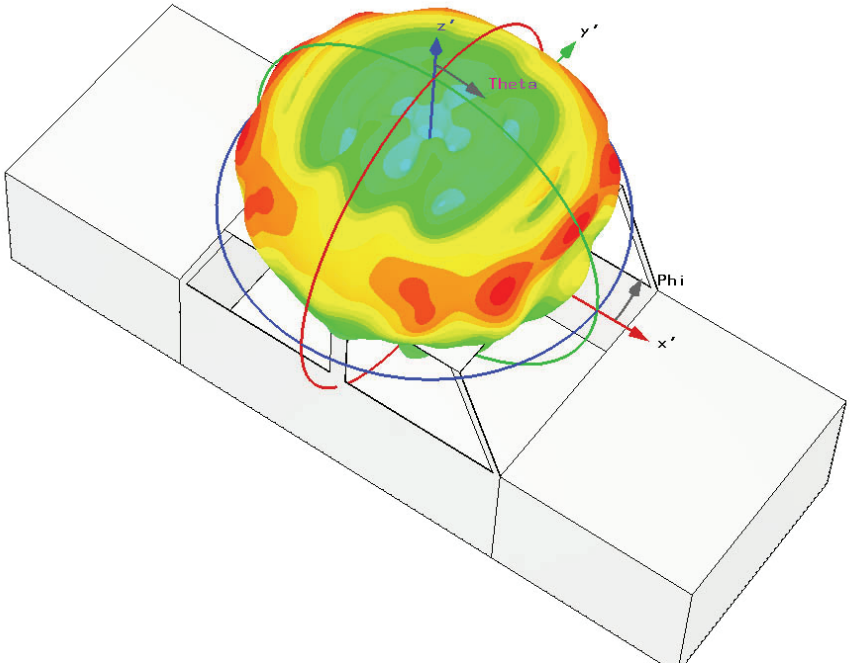

Figure 5.1. *The coordinate system used in this chapter with a 3D radiation pattern.*

electrical boundary condition underneath the car model. The problem with the former approach is that the ground plane radically increases the mesh size of the problem, and so the size of the ground plane is extremely limited (in our case to about twice the length and width of the car model, and approximately 1 m thick). Simulation results of the different modelling methods showed either *a)* no discernable effects in the radiation patterns when method *1* was used, as illustrated in Figure 5.2, or *b)* a significant, to the point of unrealistic, effect on the radiation pattern, as evidenced in Figure 5.3. Besides the heavy ripple, the gain level increased by about 3 dB compared to the free-space model (resulting from no radiation into the lower half space). These effects on the elevation plane radiation pattern were not considered realistic.

According to the material parameters of CST MWS, the electrical conductivity of dry soil should be on the order

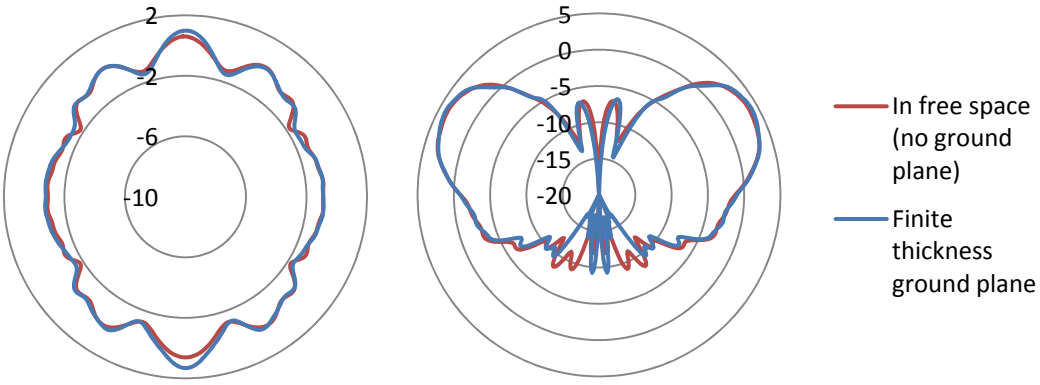

Figure 5.2. *A comparison of the radiation patterns of a monopole on the BCM with finite thickness (80 cm) ground plane and no ground plane below the car model. Azimuth plane pattern on the left and elevation plane 2 ($\varphi = 90°$) pattern on the right.*

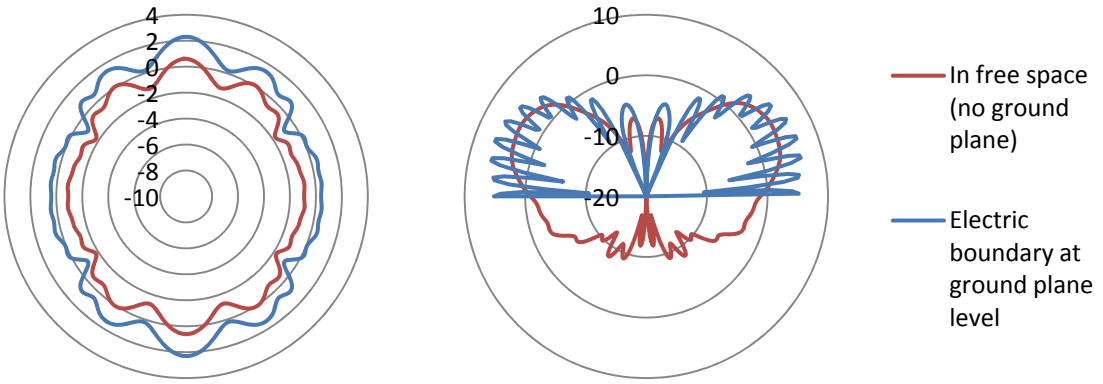

Figure 5.3. *A comparison of the radiation patterns of the BCM with perfectly conducting ground plane (electric boundary condition at z=0) and no ground plane below the car model. Azimuth plane pattern on the left and elevation plane 2 ($\varphi = 90°$) pattern on the right. The azimuth plane pattern is measured at θ=88° in the case where there is an electric boundary at θ=90°.*

of 0.1 mS. Thus, modelling the ground plane with a layer of effectively infinite electrical conductivity would seem unnatural. On the other hand, any noteworthy differences between the radiation patterns of the free-space model and the model with a small ground plane of finite (realistic) conductivity underneath the vehicle were not found. Thus, it was considered reasonable to limit the computation space with open (absorbing) boundaries, and not to model a finite ground plane beneath the car.

Monopole design

The frequency of operation was selected to be 700 MHz due to the recent interest in this frequency range. Bandwidth of the element should be adequate for modern high-speed wireless communication systems, such as WiMAX. The input matching should also be better than −6 dB in the operating frequencies, preferably without complex external matching circuits.

The design process was started with modelling a $\lambda/4$ monopole antenna on an infinite ground plane. As expected, the resonant frequency of the $\lambda/4$ monopole was somewhat below 700 MHz. Tuning the antenna to 700 MHz was achieved by shortening the length of the antenna to about $0.91\times\lambda/4$, or 97 mm. Due to the assumed inaccuracies of the current EM simulators in input impedance prediction—resulting from imprecise feed models and not the simulation methods themselves, as discussed in Section 3.2—input matching was not analyzed in detail in this thesis. With this in mind, it would seem that the port model (waveguide or discrete *S*-parameter), the car model (basic or advanced car model, BCM/ACM), array configuration and the antenna location all had an effect on the resonant frequency. These effects were, however, rather small and the length of the monopole could be held fixed at about 96 mm in most cases and still get better than −10 dB input matching. The logarithmic reflection coefficients of the monopole element on infinite ground plane and on the centre of the roof of the BCM are illustrated in Figure 5.4.

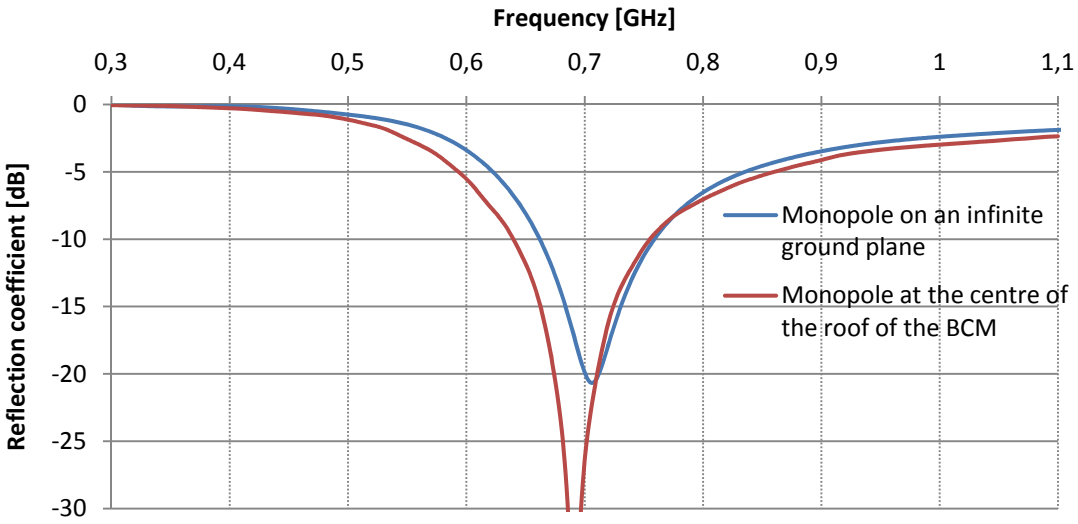

Figure 5.4. *The simulated reflection coefficient of a monopole on infinite ground plane and on the roof of the BCM. Waveguide port feed was used in both cases and the physical dimensions of the monopoles as well as the feed lines were identical.*

In most cases the antenna excitation was handled by the waveguide port (coaxial feed model). The discrete *S*-parameter port was also experimented with, but the waveguide port was used in most cases as it was easy to implement and is assumed more accurate (including at least some physical modelling). The spacing between the roof panel and the lower end of the monopole affected input matching and resonant frequency quite significantly, even though the change in overall monopole length was offset by altering the length of the monopole. The input matching of the monopole with discrete *S*-parameter port excitation at different spacings is presented in Figure 5.5.

Though no strict bandwidth requirements were set, it is known that future high-speed wireless services require relatively high bandwidth of tens of megahertz. Thus the monopole was designed with a fairly large diameter of 3 mm, which provided a −10 dB

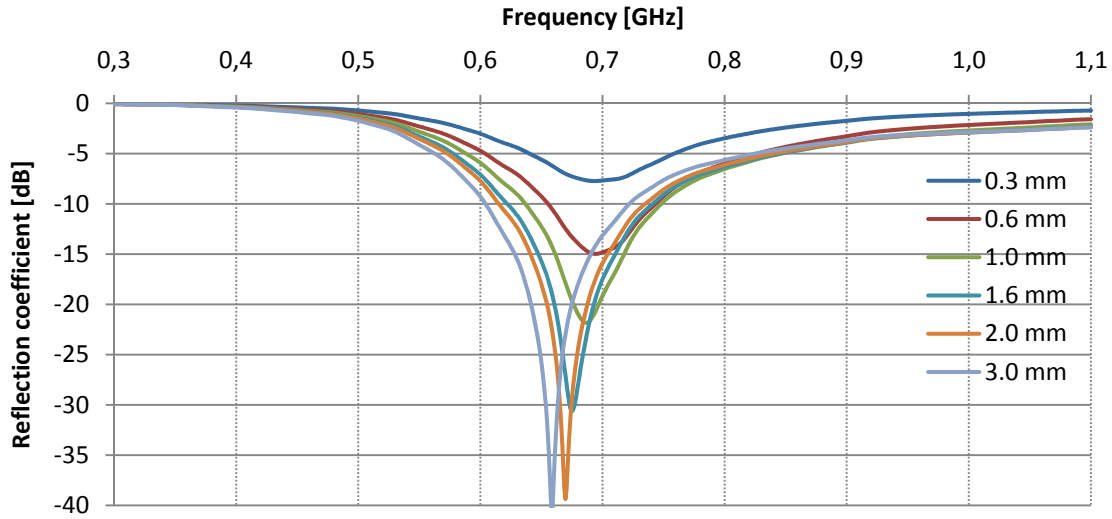

Figure 5.5. *Simulated input matching of the monopole antenna with discrete S-parameter feed. Increasing the spacing between the roof panel and the monopole base enhances the input matching and decreases the resonant frequency.*

impedance bandwidth of about 120 MHz when the antenna was mounted on an infinite ground plane. Again, the location and the car model affected the bandwidth somewhat. Other diameters were experimented with to visualize the bandwidth-diameter dependency of the monopole, and consequently 3 mm was judged to strike a reasonable balance between bandwidth and physical dimensions.

As mentioned in Section 4.2.1, the monopole was modelled in most cases as parallelepiped. The purpose of this was to achieve a better fit with the hexahedral mesh and hence squeeze every last ounce of performance from the simulator without affecting the simulation results noticeably. The relation between the radius of a cylindrical monopole and the side length of a rectangular monopole was taken as $r = 0.59a$ [78], where r is the radius of the cylindrical monopole and a the side length of the rectangular monopole. The rest of the simulated and measured radiation patterns of the monopole elements in different car models are presented in Section 5.2.

5.1.1. Building and tuning the antennas and the feed network

Two types of monopoles—cylindrical and flat bar—were prototyped, and the designs are photographed in Figure 5.6. The radius of the cylindrical monopole is the same as in the simulations—3 mm—while the flat bar's thickness and width are 2×6 mm, respectively. The monopole elements are connected to an SMA female connector that is attached to a small ground plane (50 mm × 50 mm). The small ground plane is used to improve ground connection and ease the installation of the antennas to the car model that is used in the measurements.

The tuning and bandwidth measurements were done in a small RF-laboratory (no shielding, non-anechoic) with Hewlett-Packard 8722D network analyzer. The antennas under test were mounted on a 70×70 cm aluminium ground plane, one at a time. Frequency range of the measurements was set at 200 to 1200 MHz. The bandwidth of the cylindrical and flat bar monopoles was expected to be roughly the same due to the monopoles' largest dimensions (radius and long side, respectively) being about equal.

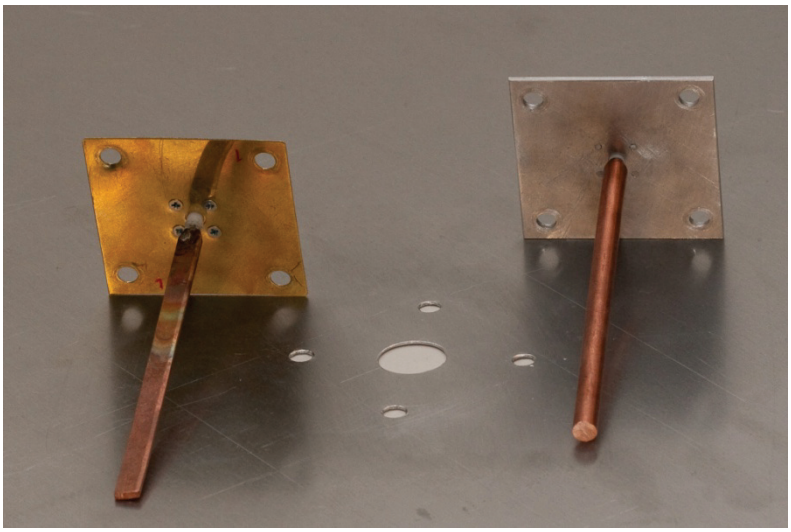

Figure 5.6. *Prototype monopole antennas.*

According to the measurements the cylindrical as well as the flat bar monopole achieved about the same bandwidth of slightly over 100 MHz, as expected. The differences between the monopoles were so small that due to easier length tuning of the flat bar monopole it was selected for the measurements with the car model.

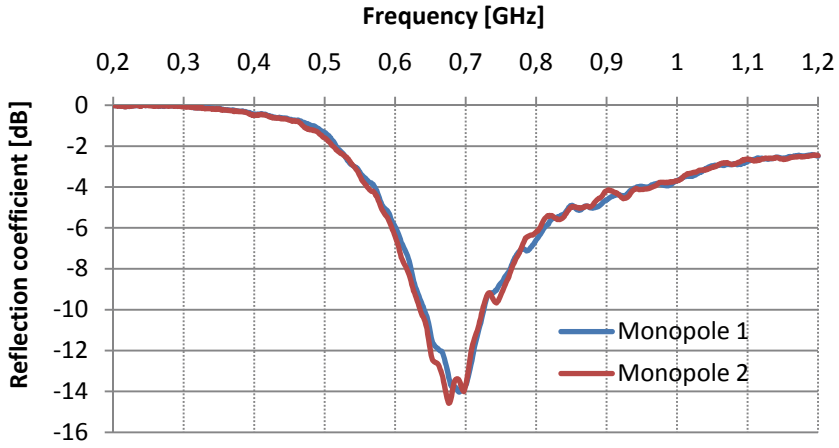

Figure 5.7. *Input reflection coefficients of the prototype monopoles.*

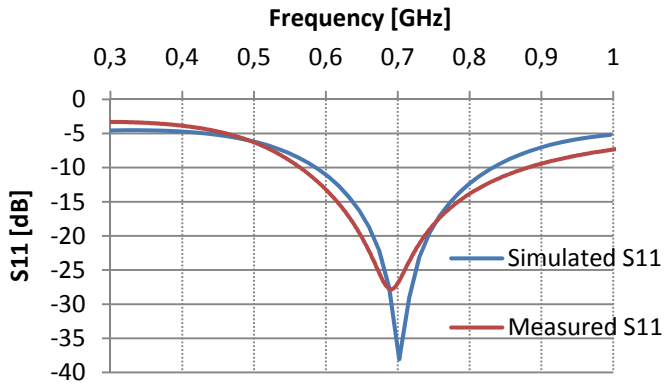

Figure 5.8. *Simulated and measured S11 of the prototype Butler matrix. The values for S22 are virtually identical, the only difference being slightly better matching at resonance for the measured S22 compared to measured S11.*

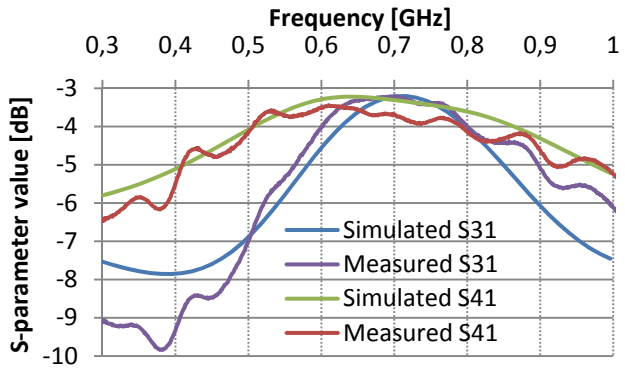

Figure 5.9. *Simulated and measured S31 and S41 of the prototype Butler matrix.*

Then, a second flat bar monopole element was prototyped and tuned, so that the 2 element array measurements with the car model could be carried out. Measured input matching characteristics of the two flat bar monopoles on a 70×70 cm ground plane are portrayed in Figure 5.7. A reflection coefficient of about −14 dB was achieved with the measured monopoles, at the centre frequency of 700 MHz, with monopole lengths of about 97 mm and 100 mm. This level of input matching is more than adequate, and enables accurate comparison to simulation results that omit the effects of input mismatch altogether. The difference in the bandwidths of the monopoles was about 5 MHz. It should be reminded

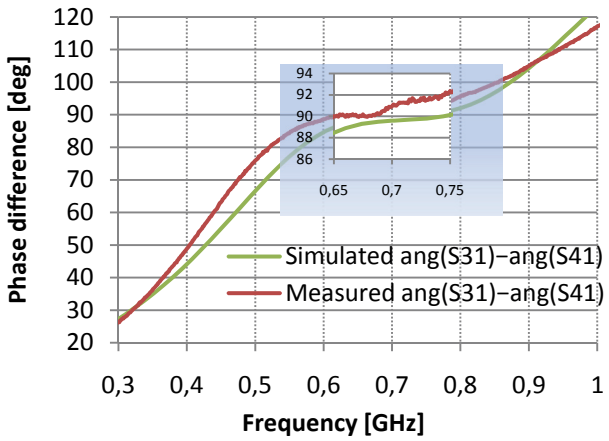

Figure 5.10. *Simulated and measured phase difference between the (output) ports 3 and 4 of the Butler matrix.*

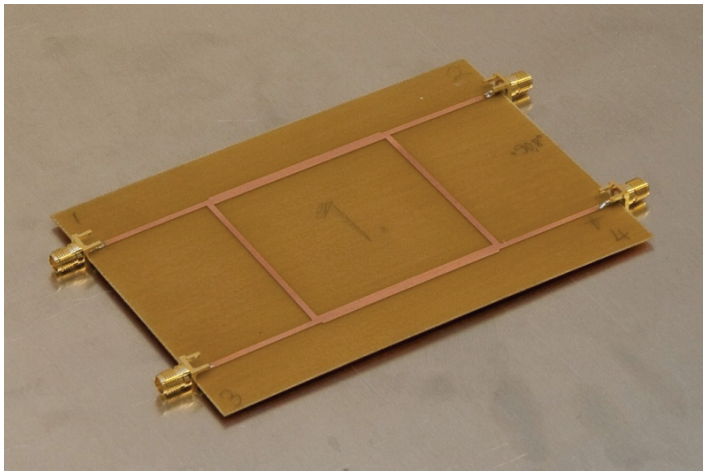

Figure 5.11. *The prototype Butler matrix. The port naming in the photograph differs from that used in the text.*

that, as evidenced in Figure 5.4, the input matching will probably change slightly once the antennas are mounted on the car model.

The feed network in the multi-antenna measurements comprised a Butler matrix (BM). The BM was used to provide the phase difference and power division that are required in beamforming arrays between the antenna elements. In the two-element case the BM is just a 90 degree hybrid, which is easy to design and build. In the case of four antenna elements, some discrete elements are also needed, and design in general is a bit more complicated.

The Butler matrix (in this case a 90 degree hybrid) that provided the power division between the two monopoles was designed at Elektrobit, and manufactured by the author at TUT facilities. The BM added some 0.5 dB of additional attenuation to the system, while there was less than one degree of phase inaccuracy between the output ports of the BM (further mitigated by the around 1 degree of phase difference between the feeding cables from the BM to the antennas). The simulated and the measured *S*-parameter plots of the Butler matrix are presented in the Figure 5.8, Figure 5.9 and Figure 5.10. Ports 1 and 2 in the BM are the input ports, and ports 3 and 4 are the outputs to the antennas. The prototype BM is photographed in Figure 5.11.

5.2. Simulation and measurement of monopole multi-antenna configurations

As discussed in Section 4.2.1 some limitations were set to the number of antenna elements at the vehicle. With these limitations in mind, simulations were made with two monopoles at different locations on the roof of the BCM and ACM. All the simulated

arrays were located symmetrically about the longitudinal roof centre line. This section presents the simulation results, and also includes a comparison to corresponding measurement results.

5.2.1. Measurement setup

Based on the simulations, a couple of array configurations were chosen to be implemented. The array configurations chosen were linear arrays in longitudinal and transverse directions versus the vehicle. Furthermore, due to the limited time available for the design and construction of the antennas and the required BM, a decision was made to only realize two-antenna monopole arrays. The linear arrays were placed at distances of 60, 220 and 770 mm from the roof rear edge, based on simulation results and aesthetic viewpoints. The interelement spacing of the antennas was varied between 0.5 and 1.25 λ. All the different antenna locations, as measured on the roof of the car model, are illustrated in Figure 5.12.

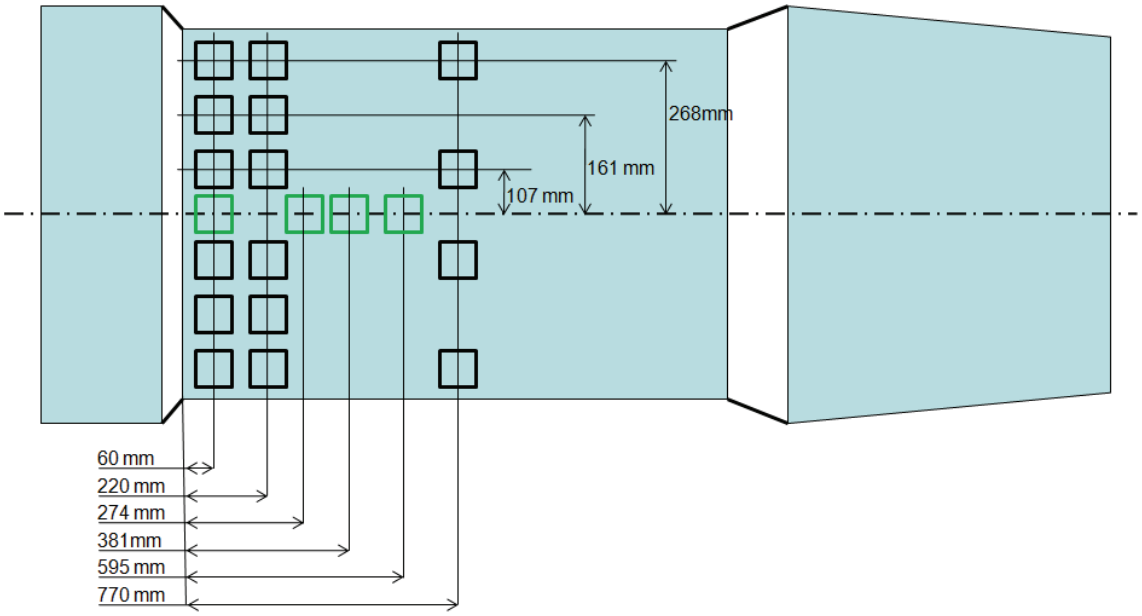

Figure 5.12. *The monopole antenna locations on the roof of the car model in the measurements. In the simulations the antennas were located 20 mm more to the rear. Transverse direction arrays are plotted in black and longitudinal arrays in green.*

Radiation pattern measurements of the antenna system were done at VTT Technical Research Centre of Finland facilities at Espoo. The anechoic antenna test chamber that was used in the measurements had dimensions of $12 \times 12 \times 17$ m^3 ($L \times W \times H$), frequency range of 100 MHz to 200 GHz and measuring distance of less than 10 m.

The monopoles were mounted on the roof of a dummy car. The dummy car consisted of a roof, a bonnet, and a trunk lid joined together with 30 mm × 30 mm beams. The body panel parts (roof, bonnet, trunk lid) were sourced from scrap cars, and represent real designs. The model is photographed in Figure 5.13, and the planes in which the measurements were made, in Figure 5.14. The car model's approximate dimensions are 365 cm × 120 cm × 65 cm (L×W×H). Due to the physical limitations of

Figure 5.13. *The dummy car model that was used in the measurements.*

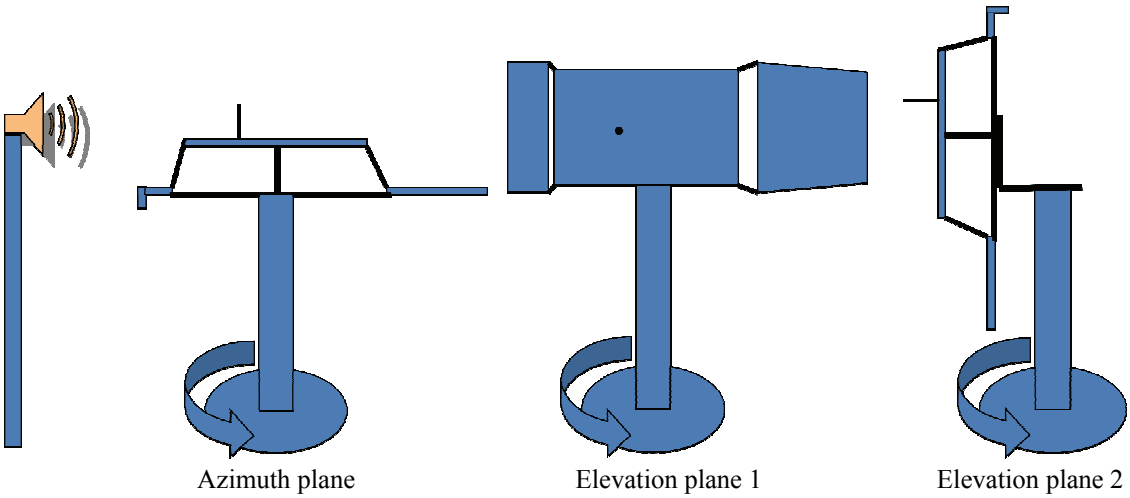

Figure 5.14. *The cut planes in which the measurements were made.*

the measurement setup (namely the movement of the measuring mast and the adjustability of the mast-to-car-model adapter), the antennas could not be mounted directly on the rotation axis in the measurements in the elevation plane 1. However, the difference between the rotation axis and the centre of the antennas was at most about 20 cm, and due to lack of time most measurements were made in the azimuth plane and the elevation plane 2 in any case.

A BF MIMO approach was chosen as the method of utilising the multiple antennas. The BF MIMO system concept is touched upon in Section 2.3. The main principle in BF MIMO is to employ parallel uncorrelated beams in a way that makes good use of multipath propagation. Compared to traditional MIMO systems where uncorrelated antenna elements are used in a similar way, BF MIMO provides additional array gain to the individual beams. As in any beamforming array, the beams are generated by feeding the elements with a suitable phase difference and amplitude taper (see Section 2.3.3). Using n antenna elements an equal number n of orthogonal beams can be generated. Generally only one of these beams will be plotted in the radiation patterns, since most

simulations and measurements were made with two elements in a transverse direction array, and due to the elements' symmetrical location on the roof of the car the other beam is near-perfectly symmetrical. On the other hand, the longitudinal direction arrays produce asymmetrical beams due to the antennas not being located symmetrically on the car roof, and for these arrays both beams will be plotted, if available.

The car model was lifted on top of an about 5 m high mast that could be rotated freely. The mast could also be moved about the rotation axis, so that the centre of the antennas could mostly be maintained at the rotation axis. Because the BER-simulation code introduced in Chapter 4 only uses data from the azimuth plane, and because the measurement time was limited, all the antenna locations were not measured in elevation planes 1 and 2. The accuracy of the elevation plane measurements probably suffered the most from the lack of side panels in the car model, and this was also one of the main reasons why azimuth plane measurements were given the highest priority.

The results of the measurements are compared to corresponding simulations in the next section. The less detailed car model was chosen as the basis of comparison because the radiation patterns of the more detailed ACM were rather distinct. Most of the features of the ACM's radiation patterns are most likely characteristic to this particular vehicle model, and thus not representative in the more general case. The BCM lacks these kinds of characteristics, and the results should be better suited for generalization.

In the simulations the antenna elements were located 20 mm closer to the roof edge than in the measurements. This apparent discrepancy was intentional, and was set because the roof panel of the measured car model was quite heavily curved at the back. The horizontal distance of the antenna elements from the roof edge was about the same in both cases.

5.2.2. Simulation and measurement results

Differences between the ACM and the BCM

The advantages of the BCM include slightly faster simulation time and considerably smaller memory footprint compared to the more detailed ACM. Consequently, the BCM was used in the majority of analyses of different aspects of the simulation, such as the effect of ground plane on far field pattern.

The simulated radiation pattern of the two-beam, two-antenna system ($\lambda/2$ spacing, 90° phase shift) located at about 200 mm from the rear edge of the roof with the BCM are presented in Figure 5.15, together with the corresponding radiation patterns with the ACM. As can be seen from the figures, the azimuth plane radiation patterns of the ACM and the BCM are remarkably similar. The direction of the peaks and nulls agree well, as do the general gain levels. As could be expected, the radiation pattern of the ACM has perhaps slightly more detail, while that of the BCM is a little smoother. The elements in the ACM were excited with discrete *S*-parameter ports while waveguide ports were used with the BCM. Elevation plane plots are also very similar, though here the BCM's pattern seems to contain a bit more detail.

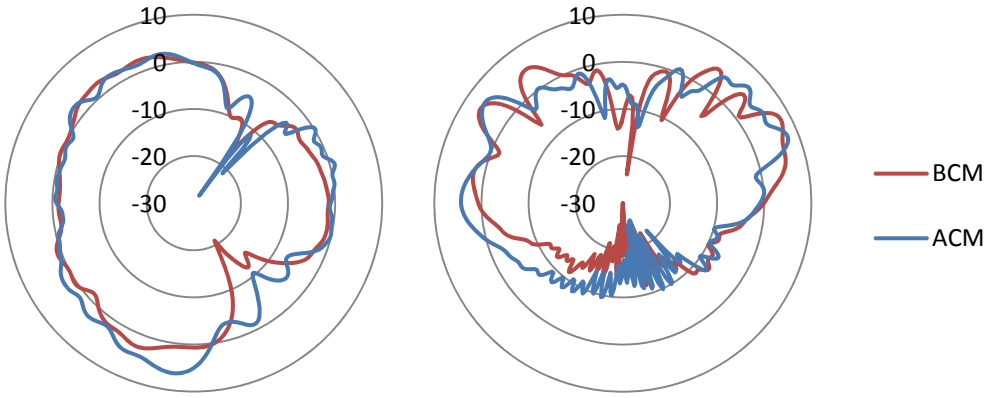

Figure 5.15. *Azimuth plane (on the left) and longitudinal elevation plane (on the right) radiation patterns with different car models. Interelement spacing is λ/2 and the distance from the roof rear edge is 200 mm.*

At the largest interelement spacing of $5\lambda/4$ the differences between the car models remain scarce. As can be seen in Figure 5.16, both the azimuth and the longitudinal elevation plane patterns are again very similar with the different car models. Transverse direction elevation plane radiation patterns are also very similar between the models, but are not presented here.

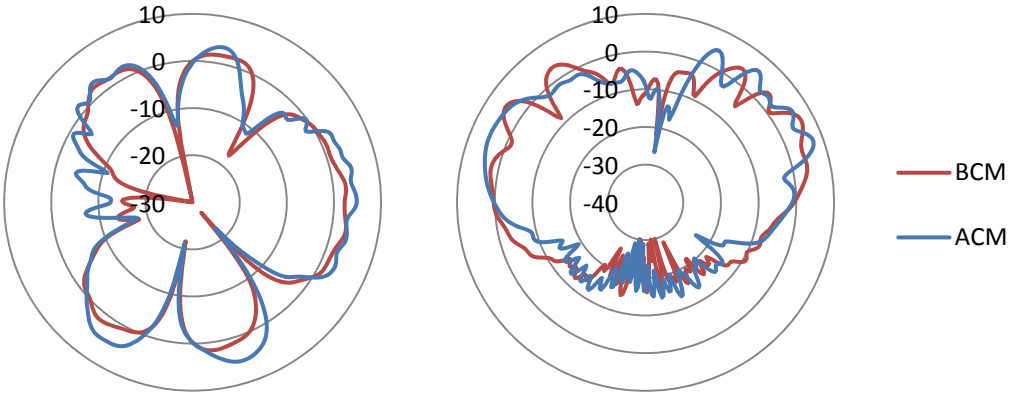

Figure 5.16. *Azimuth plane (on the left) and longitudinal elevation plane (on the right) radiation patterns with different car models. Interelement spacing is 5λ/4 and the distance from the roof rear edge is 200 mm.*

Distance from the roof rear edge

The distance of the array from the rear edge of the roof affected the radiation pattern of a given array configuration to some extent. Take, for example, the case of two monopoles with $\lambda/2$ interelement spacing on the BCM. As can be seen in Figure 5.17, some RF current extends to the edge of the roof when the elements are located about 40 mm or $\lambda/10$ from the edge such that the path of the RF currents are obstructed and this affect the radiation patterns to some extent. The simulated radiation patterns at different distances from the roof edge are portrayed in Figure 5.18. The radiation patterns are remarkably alike, with the arrays nearest to the edge having only slightly more ripple. The location of nulls and peaks is all but unaffected. On the other hand, there is a

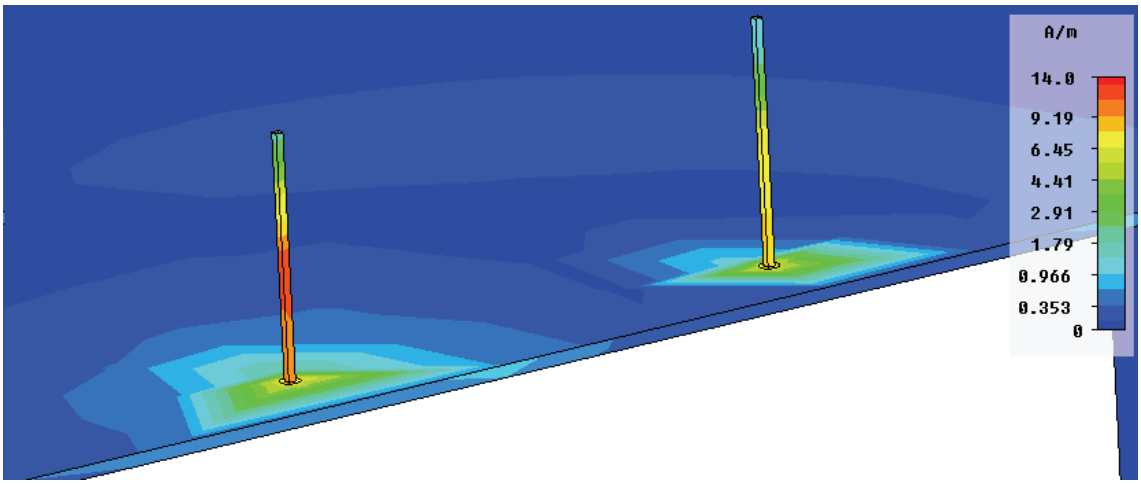

Figure 5.17. *An illustration of surface currents (absolute values) near the monopole elements on the BCM. Though the resolution of the currents is quite low, it should be apparent that the paths of the surface currents are altered at the edge of the roof.*

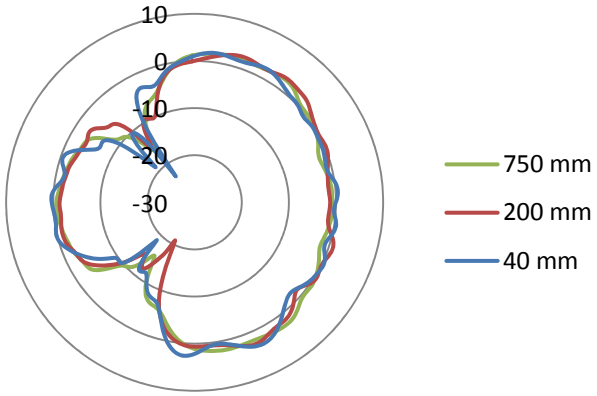

Figure 5.18. *Azimuth plane simulated radiation patterns of two 90° phased monopoles at different distances from the rear edge of the roof of the BCM.*

noticeable effect on the φ-polarization, but its levels still remain mostly under –10 dB and hence insignificant. This is likely the result of the horizontal edge of the roof contributing to the radiation of φ-polarization, but having much less of an effect on θ-polarization. Measured azimuth plane radiation pattern when antennas are located nearest to the edge of the roof is

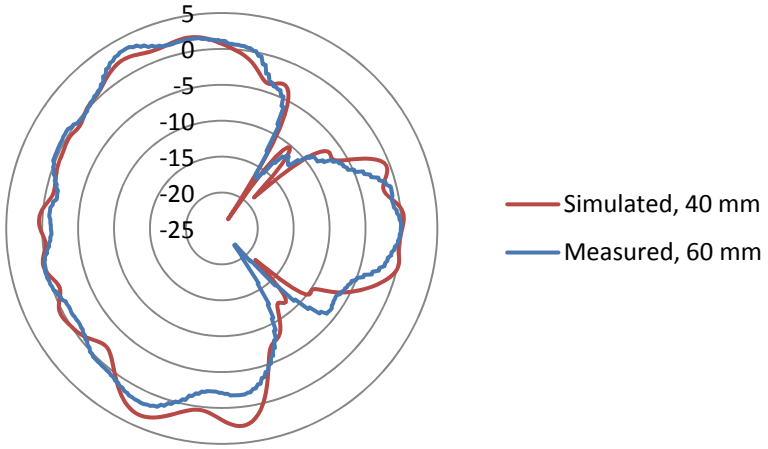

Figure 5.19. *Measured azimuth plane radiation pattern compared to corresponding simulated (BCM) radiation pattern. The simulated antennas were located 40 mm from the edge of the roof, while the measured antennas were located 60 mm from the edge of the roof.*

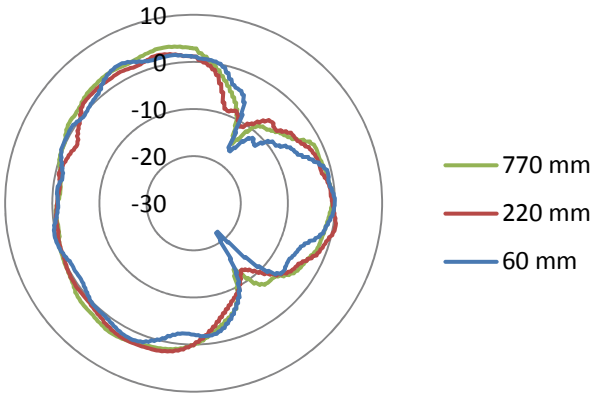

Figure 5.21. *Measured azimuth plane radiation patterns of two 90° phased monopoles at different distances from the edge of the roof.*

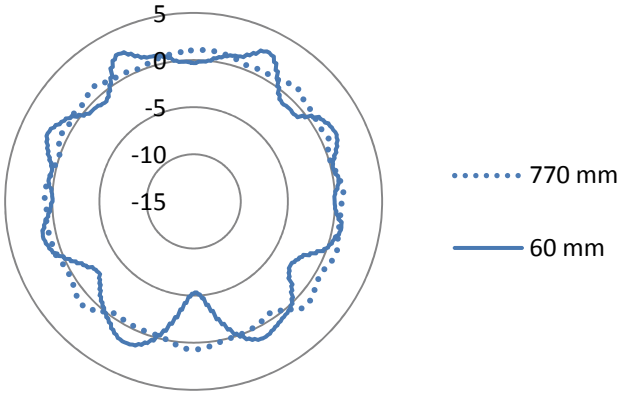

Figure 5.20. *Measured azimuth plane radiation patterns with one monopole at 770 mm or at 60 mm from the edge of the roof.*

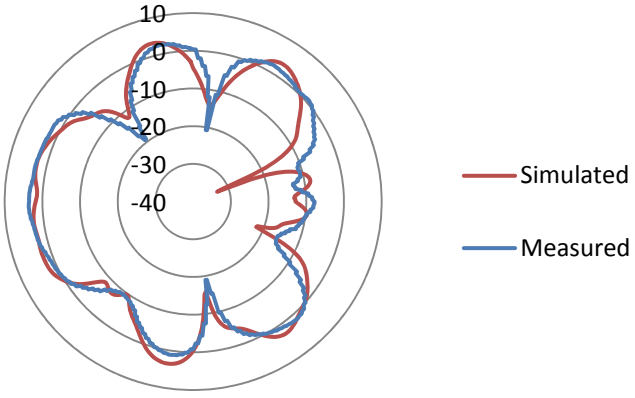

Figure 5.22. *A comparison of measured and simulated azimuth plane radiation patterns of two 90° phased monopoles at 60 mm from the edge of the roof,* $5\lambda/4$ *interelement spacing.*

compared to the corresponding simulated pattern in Figure 5.19, and the measured radiation patterns of antennas at different distances from the edge of the roof is presented in Figure 5.21.

Measurements seem to agree very well with the simulated results. It would indeed seem that, at least for the two-element BM fed array, the distance to the antenna elements from the roof rear edge is not critical. On the other hand, in the case of a single antenna, the closer the antennas are located to the edge of the roof, the more it increases the ripples. This effect is illustrated in Figure 5.20, which shows a comparison of measured radiation patterns of one monopole antenna located at 60 mm and at 770 mm from the roof edge. In the former case, the ripple is less than 2 dB peak-to-peak, while in the latter it is almost 7 dB peak-to-peak.

Figure 5.22 presents the measured radiation pattern of two monopoles at 60 mm from the roof rear edge, with interelement spacing of $5\lambda/4$. Corresponding simulation results using the BCM are plotted in the same figure, and matching elevation plane 2 results in Figure 5.23. As can be seen the correlation is extraordinary and was not

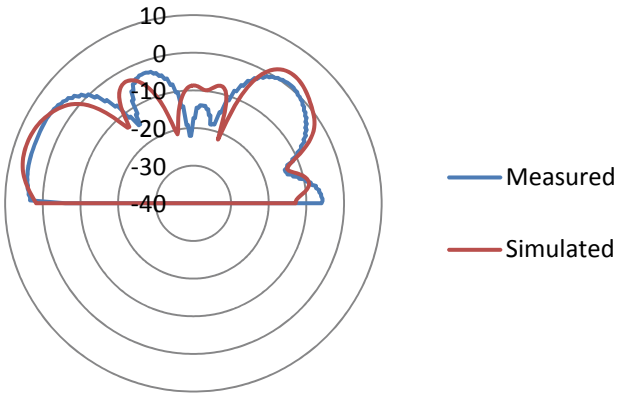

Figure 5.23. *A comparison of measured and simulated (BCM) elevation plane 2 radiation patterns of two 90° phased monopoles at 60 mm from the edge of the roof, $5\lambda/4$ interelement spacing.*

limited only to this particular case. All of the numerous nulls in the azimuth plane pattern were quite accurately predicted by the simulations, and even the elevation plane patterns are very similar, with just a slight shift in the direction of some of the nulls. Similar correlation was seen with almost every interelement spacing and antenna location. Considering the fact that the car models in the simulations and the measurements were not identical, these results are exceptional. However, further work is needed to study the effects of non-planar body panels. Based on the results presented here, it seems that the effects are reasonably small, at least if the curvature of the body panels is not excessive. What is not covered in this thesis, is the effects of the vehicle interior. According to a couple of studies referenced in Section 3.2, these effects could be noteworthy.

Antenna spacing

The radiation patterns of closely spaced antennas are affected by mutual coupling. Also, with beamforming arrays, the beam pattern (array gain) is heavily influenced by the antenna spacing. To study the effects of antenna spacing on the radiation pattern, two-element arrays with various interelement spacings were simulated. The elements were fed with identical amplitude and a 90° phase difference. Simulations were run on both the ACM and the BCM. According to the theory of phased arrays [13] large element spacing causes grating lobes to appear in the radiation pattern. The combined effect of mutual coupling and array gain on the radiation patterns was studied by progressively increasing the element spacing from $\lambda/2$ to $5\lambda/4$, in steps of $\lambda/4$. The results are presented in Figure 5.24–Figure 5.26 for the case of two monopoles in the transverse direction at 200 mm from the roof's rear edge. As is clearly visible in the figures, the number of nulls increases when the antenna

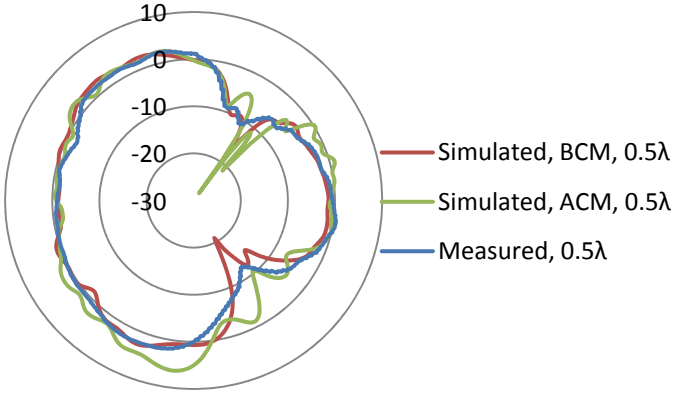

Figure 5.24. *Azimuth plane radiation patterns with the shortest interelement spacing of 0.5λ.*

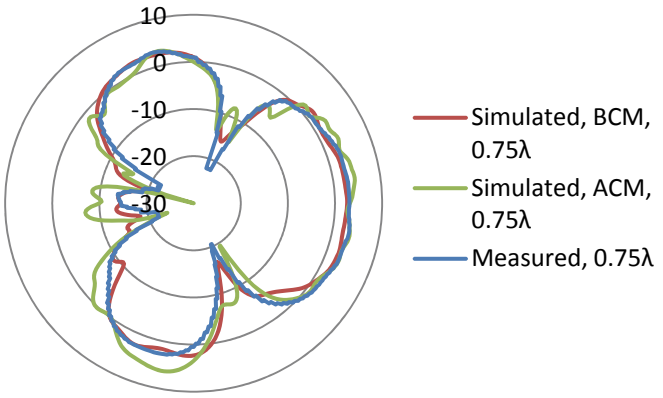

Figure 5.27. *Azimuth plane radiation patterns with interelement spacing of 0.75λ.*

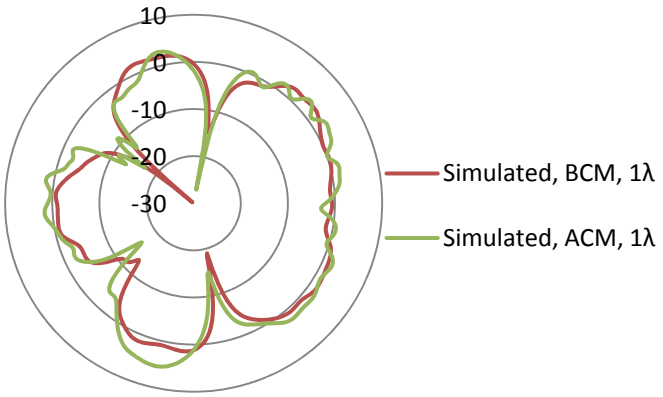

Figure 5.25. *Azimuth plane radiation patterns with interelement spacing of 1λ. Measurements were not made with this element spacing.*

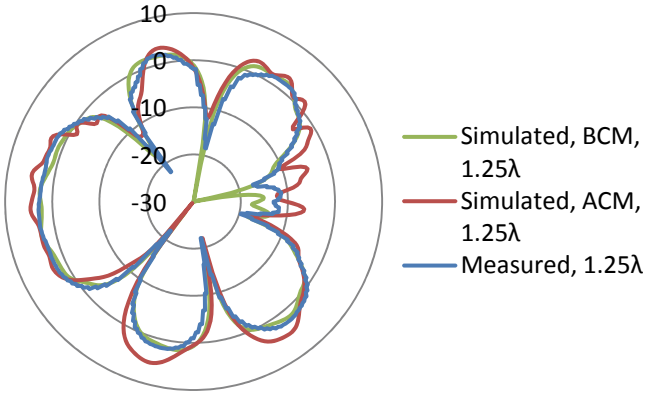

Figure 5.26. *Azimuth plane radiation patterns with interelement spacing of 1.25λ.*

spacing is increased. The peak gains of the beams are largely unaffected by the element spacing, although the direction of the peak gain does change.

The observations for the transverse linear array are also valid for the linear array in the longitudinal direction. In this case, the antennas are located in the centre of the roof in the transverse direction, and the rearmost element is in every case located at 60 mm from the roof rear edge (see Figure 5.12). Figure 5.29 presents a selection of measured and simulated radiation patterns for the longitudinal direction linear array. Longitudinal arrays were a little problematic on the ACM, as the quite heavily curved roof panel affected the input matching and mutual coupling of the antenna elements. Consequently, simulation was run only with interelement spacing of 0.5λ in the case of the ACM. The radiation patterns of the longitudinal array on both car models are illustrated in Figure 5.29. Figure 5.28 illustrates the typical differences between the two beams of the longitudinal direction array. As can be seen, for both the ACM as well as BCM the basic shape of the radiation pattern stays largely unchanged, though smaller differences are visible between the beams.

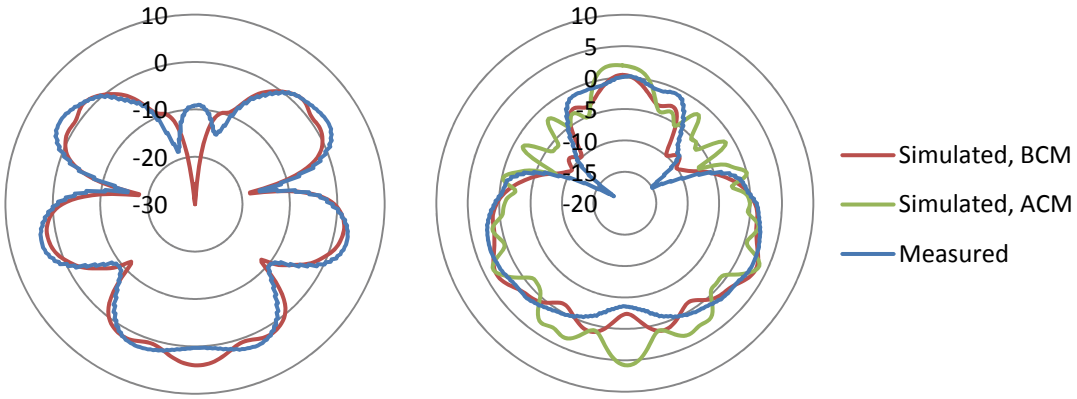

Figure 5.29. *Azimuth plane radiation patterns of the longitudinal direction array with interelement spacing of 1.25λ (on the left) and 0.5λ (on the right).*

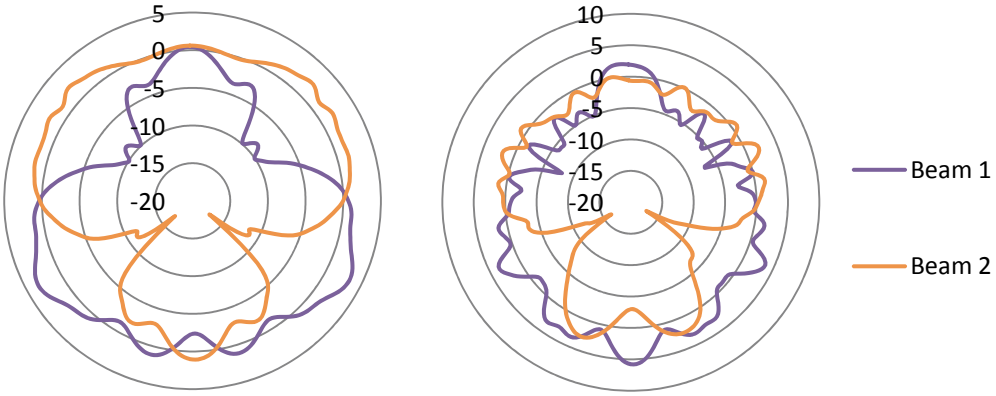

Figure 5.28. *Simulated azimuth plane beam patterns of the longitudinal direction array with interelement spacing of 0.5λ; BCM on left, ACM on the right.*

Four-element arrays

Some uniform linear and rectangular four-element arrays were also simulated and the results compared to corresponding two-element arrays. As an example, Figure 5.30 plots the azimuth plane gain with two and four antenna elements ($\lambda/2$ spacing) in a linear array at about 200 mm from the rear edge of the roof (BCM). The interelement phase difference was 90° in the case of two elements and 45° in the case of four elements. The grating lobe levels are reduced and peak gain increased, both by about 3 dB, when the

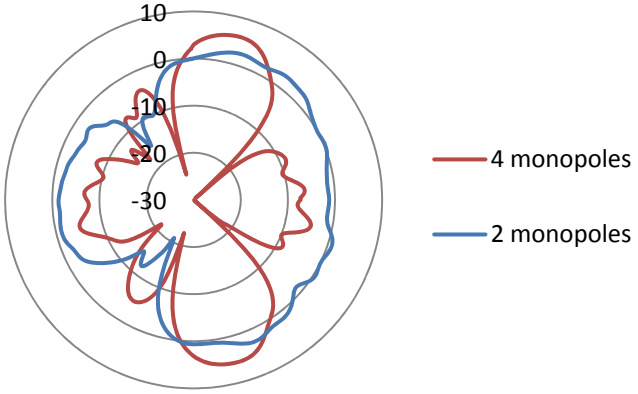

Figure 5.30. *Simulated azimuth plane radiation patterns of two and four monopole antennas.*

number of antenna elements are increased. Main lobe beam width is also significantly reduced. Very similar results were recorded with the ACM. In diversity applications the decreased side-lobe levels are as important as increased main lobe level, since it reduces the interference from neighbouring beams. Non-uniform arrays would have made an intriguing comparison, but the design of such arrays is out of the scope of this thesis.

5.3. Simulation studies of after-market and dipole antennas

In this thesis, most of the efforts are centred on integrated antennas on the roof of a vehicle. This was a conscious decision to try and keep the scope of the thesis within reason. Some after-market and dipole designs were nevertheless briefly studied through simulations. The purpose of these simulations was to at least briefly study how big of an impact locating the antenna element in the interior or on the rear window of the vehicle would have on the radiation pattern, when compared to the roof mounted monopole. The effect of window glasses (with and without heating wires) on the radiation patterns of the after-market antennas was also of interest. Due to lack of time and suitable measurement vehicles these antennas could not be extensively simulated or measured.

After-market antennas

The simulated after-market antenna designs were introduced in Section 4.2.1. A typical azimuth plane radiation pattern of an after-market antenna (model *b* in Figure 4.6) is presented in Figure 5.30. All the antenna models located near the windscreen produced radiation patterns with the widest beam pointing in the forward direction and a couple of narrower beams directed rearward. As would be expected, when compared to the roof mounted monopole, the variation in gain is far greater, with a large number of nulls present in almost all directions.

Due to the small sized ground planes of the after-market antennas, input matching was thrown amiss compared to roof mounted monopoles. The target was a −6 dB input matching, and this was achieved in most cases. Radiation efficiency in all cases was at least 98 %, except for the heated windscreen models, in which case the radiation efficiency was about 93 %. The decrease in radiation efficiency may however be purely computational, since only perfect electrically conducting (PEC) material was added to the model in the case of the heated windscreen. The car model had no prominent effect on the radiation efficiency.

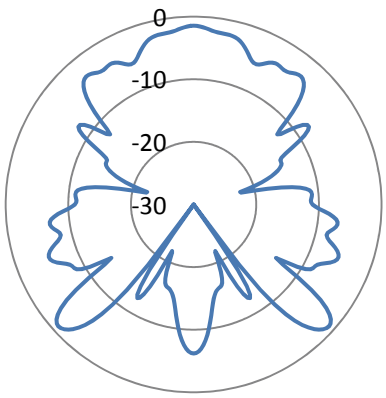

Figure 5.30. *Azimuth plane radiation pattern of the model b after-market antenna on the BCM.*

Windscreen glasses

According to a recent study [83] window glasses can attenuate the fields of an in-car antenna considerably. Thus, it was considered useful to

study the effects of window glasses on the radiation properties of the after-market antennas. Unfortunately the curved nature of the window glasses caused some problems with the "Thicken sheet" function of CST MWS, and in the end we had to settle for planar window glasses. This resulted in gaps of up to about 15 cm between the body panels and the glass in the corners of the windscreen and the rear window.

The electrical properties of the window material were: $\varepsilon_r = 6.5$, $\mu_r = 1$, $\tan\delta = 0.03$. The values of permittivity and permeability were taken from the material databank that is included in CST MWS, and the value of dissipation factor was taken from [25]. The thicknesses of the windows were set at 2 mm. The resulting radiation patterns are presented in Figure 5.31, with comparison to respective models with no window glasses. In the case of the elevation plane pattern, one should keep in mind that only the part above the ground plane ($|\theta| \leq 90°$) is significant and should be considered, although the pattern is plotted over 360° for technical reasons. While the general shape of the patterns is very similar, there are also some differences. The directions of the nulls and peaks are mostly unchanged, but the level is altered. Curiously, according to these simulations, the window glasses increase the radiation in most directions. The corresponding longitudinal direction elevation plane patterns are practically identical.

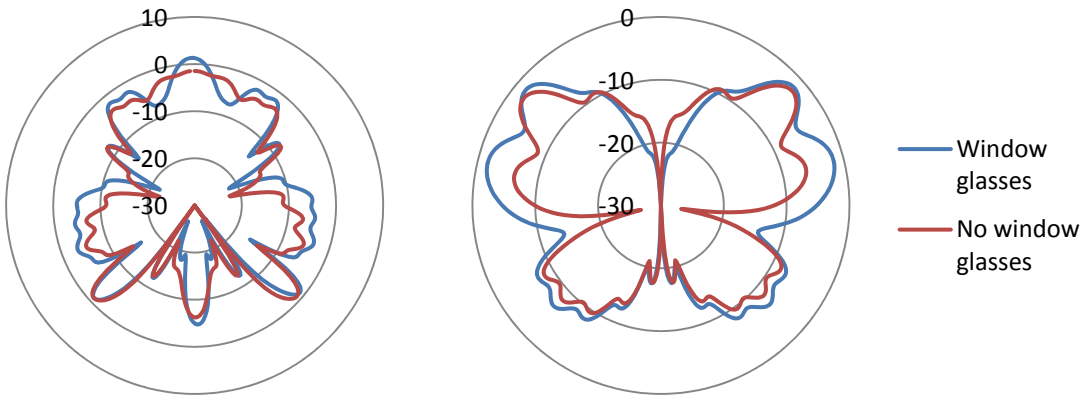

Figure 5.31. *Azimuth plane (on the left) and transverse elevation plane ($\varphi = 90°$, on the right) radiation patterns of the after-market antenna model b with window glasses on the BCM.*

The effect of the finite thickness windows on simulation time was rather profound. Typically, the simulation time for the models with the 2 mm thick glasses approximately doubled compared to the simulation time of the same model without window glasses. Additionally, it would seem that lossy windows ($\tan\delta = 0.03$) contributed a roughly 10 % increase to the simulation time and approximately 1.5 % decrease in radiation efficiency, compared to lossless window glasses ($\tan\delta = 0$), while the radiation pattern remained effectively identical.

Heated windscreen

Another new feature on some new cars is heated windscreen. These work similar to heated rear windows, but the heating element is made of much thinner wire to maintain

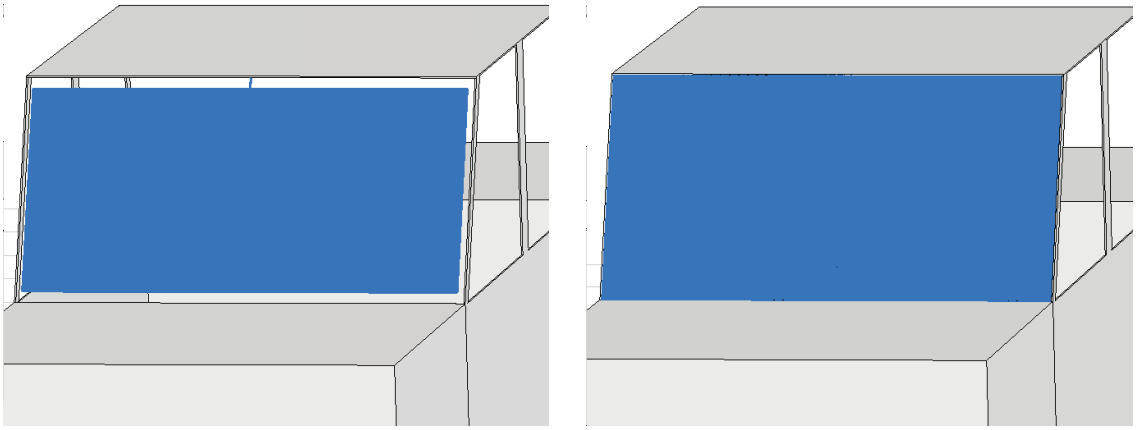

Figure 5.33. *Heated windscreen models on the BCM. The blue area is where the heating wires are located; the wires are so closely spaced that they appear as a uniform plane in these pictures. The antenna element (after-market antenna model a) was located behind the wires.*

maximum visibility. Any conducting wires in the windows are of course bound to affect the operation of antennas inside the vehicle. The effects of these wires were simulated with the interior mounted after-market antenna model *a* (see Figure 4.6). Two kinds of models were simulated: *1)* the wires were modelled as vertical "bond wires" running from the top to bottom of the windscreen, with about 5 cm between the ends of the wires and the body panels. Adjacent wires were connected to each other on the top and the bottom ends by a horizontal wire, and a single line provided a ground path to the roof panel at the top centre. Alternatively, *2)* each bond wire ran directly from the roof panel all the way to the bonnet, making electrical contact to the panels at each end. The heated windscreen models are illustrated in Figure 5.33

The bond wire model in CST treats the wires as infinitely thin, and conformal to the mesh. This does introduce some inaccuracy in the geometry, as the mesh isn't particularly dense in this region (the window glasses were not modelled to reduce simulation time). It is however computationally lighter (especially so for as thin wires as these), which is very desirable, as there are almost 500 of these wires in the windscreen with horizontal separation of 3 mm.

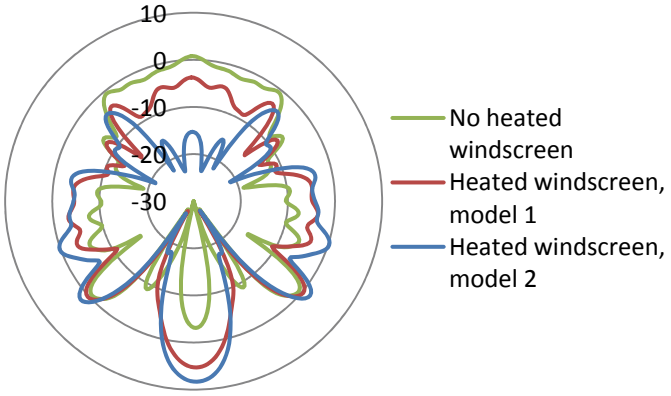

Figure 5.32. *Azimuth plane radiation patterns of the heated windscreen models with the after-market antenna model a.*

The location of the nulls and maxima are all but identical between the "base" model (without heated windscreen) and the model with the heated windscreens (Figure 5.32), although the gain levels diverge. It is quite clear from

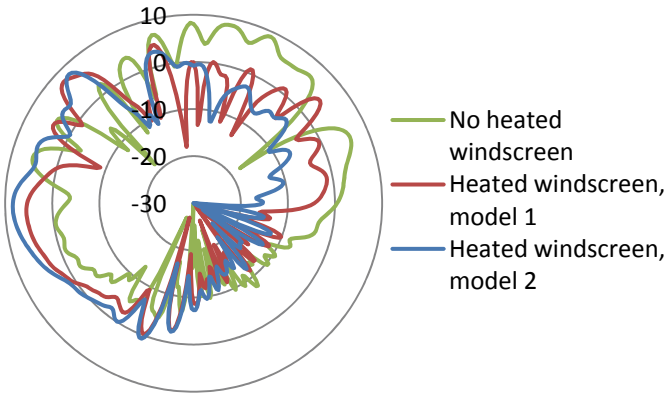

Figure 5.34. *Longitudinal elevation plane radiation patterns of the heated windscreen models with the after-market antenna model a.*

Figure 5.32 how the model *2* attenuates signals in the forward direction even more than model *1*, while there are only slight differences in the other directions. Obviously, this is to be expected, since the heating wires in model *2* span the whole height of the windscreen, whereas model *1* has the 5 cm gaps both on the top and on the bottom. The longitudinal elevation plane ($\varphi = 0°$) radiation patterns are presented in Figure 5.34. Again, the attenuating effect of the heated windscreen is clearly visible. In the forward direction, the θ-polarization ("vertical" polarization) is attenuated by about 10–15 dB, and again the model *2* is clearly showing stronger attenuation. In the rearward direction the situation is much closer with one model providing better gain in one direction and other models in other directions.

The radiation efficiency of the heated windscreen models were simulated as about 5 %-points lower compared to the other after-market models. This difference may be due to computational inaccuracies, since only PEC structures were added to the models, which should not decrease the radiation efficiency. However, in real world situations a decrease may well be expected, since the conducting materials in the windscreen reflect radiated energy back to the interior of the vehicle, where there are lossy materials that absorb a part of the energy.

Dipole antenna

The dipole antenna constituted the basis of on-glass antenna simulations of this thesis. Although a dipole array was not realized during the course of this thesis, the idea is that if a conformal antenna will be prototyped in the future, there is a fair chance that it will be of the on-glass type. As with the roof monopole, as simple and generic a design as possible will probably be required initially, and with that in mind, the dipole was chosen as the antenna element for on-glass antenna simulations in this thesis. The dipole designs themselves were mirrored from the monopoles, described above, with the main difference of being cylindrical instead of

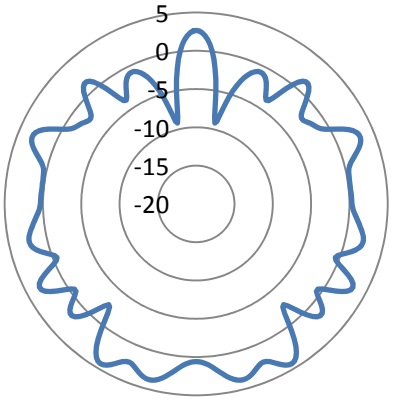

Figure 5.35. *Azimuth plane radiation pattern for a dipole element at the centre of the rear window of the BCM.*

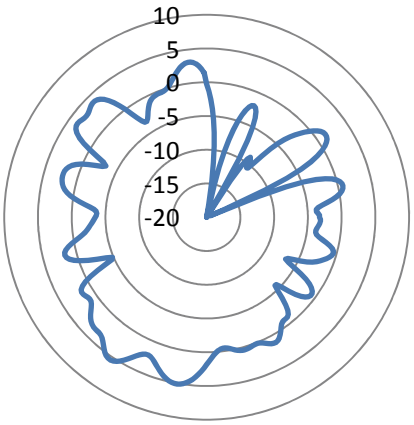

Figure 5.36. *Azimuth plane radiation pattern for two-element phased dipole array at the centre of the rear window of the BCM.*

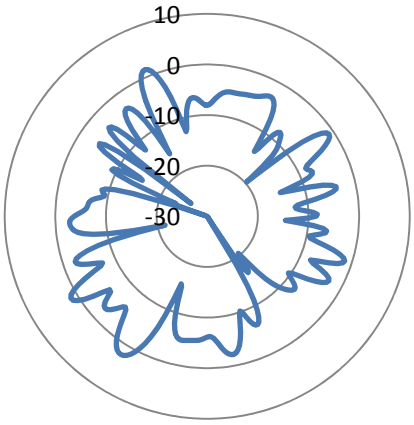

Figure 5.37. *Azimuth plane radiation pattern for two-element phased dipole array at the centre of the rear window of the ACM.*

rectangular. The shape of the dipole element however has little to no effect on the radiation pattern. The on-glass dipole simulations will be studied only in passing, as the main focus of this thesis is on the roof monopoles.

The simulated dipole antennas were located on the middle of the rear window. The radiation pattern of a single dipole element on the rear window is quite similar to that of the monopole on the roof, though expectedly there is more ripple (Figure 5.35). Also, in the forward direction the gain is worse than that of the monopole, while in the rearward direction it is perhaps slightly better. Doubling the number of elements to two, and feeding the two-element array ($\lambda/2$ interelement spacing) with a 90° phase difference results in quite a rippled radiation pattern also, with no clear main beam (Figure 5.36). The situation is even more incoherent with two dipole elements (90° phase difference) on rear window of the ACM (Figure 5.37). On the BCM, increasing the antenna spacing to $3\lambda/4$ helps somewhat, with the main beam to the rear becoming slightly more apparent, and side lobe levels decreasing a little. Further increases in the antenna spacing do not clear things up anymore, due to the side lobe levels increasing again. On the ACM, increasing the antenna spacing doesn't really provide any improvements; numerous nulls remain throughout the radiation pattern and the main beam is barely distinguishable.

5.4. Link level performance simulation results

The link level performance simulation method was presented in Chapter 4. The goal of this simulation is to estimate the bit-error rate that is achievable with a specific antenna in a specific radio channel. The simulation can also be used in a kind of a hybrid simulation-measurement mode, in which the radiation pattern is originated from measurements, instead of simulations. In addition to the measured radiation pattern data, the channel model that is used in the simulations is also based on measurements, and should be statistically accurate.

The link level performance results will be presented in this section, and are categorized to sub-sections according to the antenna type and array configuration. Contrary to the radiation pattern simulation results presented earlier in this chapter, the simulated radiation patterns that were used in the BER simulations take into account the effects of input mismatch and ohmic losses. Angular spread in the channel model is set at 8°, unless otherwise noted. The beam patterns used in the simulations based BER calculations were created with either one of the following methods: *1)* antennas were excited as if through a Butler matrix, that is, with equal amplitude and a $180°/M$ interelement phase shift, where M is the total number of antenna elements. *2)* For each beam, a single antenna was excited independently of the others, which were terminated with a matched load. Slightly differing beams are created due to the mutual coupling and individual location of each antenna on the roof. These excitation methods are denoted as "BM" and "Independent", respectively. For the measurements based BER calculation, only method *1* was used.

5.4.1. Linear monopole array in transverse direction

The BER simulation results for the linear monopole array on the roof of the BCM are presented in Figure 5.38–Figure 5.40, for antenna element distances of 40, 200 and 750 mm from the roof rear edge, respectively. As mentioned in the previous section, the antenna distance from the roof edge had little effect on azimuth plane θ-polarization

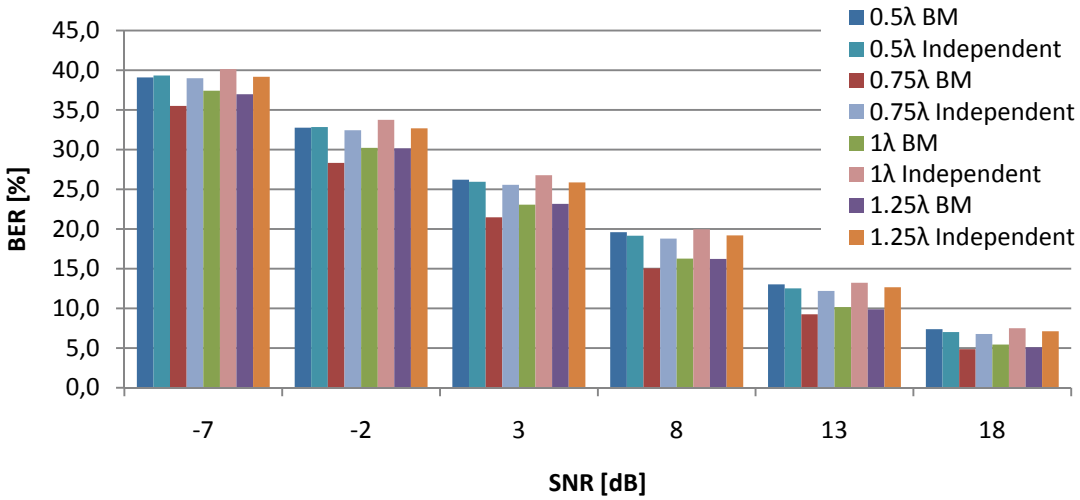

Figure 5.38. *BER performance of the two-element phased monopole array on the BCM 40 mm from the edge of the roof.*

radiation pattern. This is clearly reflected in the BER results, as there is but a small difference between the BER values at different distances. Only two interelement spacings were simulated at the 750 mm distance, due to time constraints and because the radiation pattern measurements were done only for those two spacings. Looking at the simulations based BER calculations, it seems that the coherent combining (array gain) offered by the BM affords an up to 4 %-point enhancement in BER, compared to feeding the antennas individually. This effect, nevertheless, is not seen at the smallest

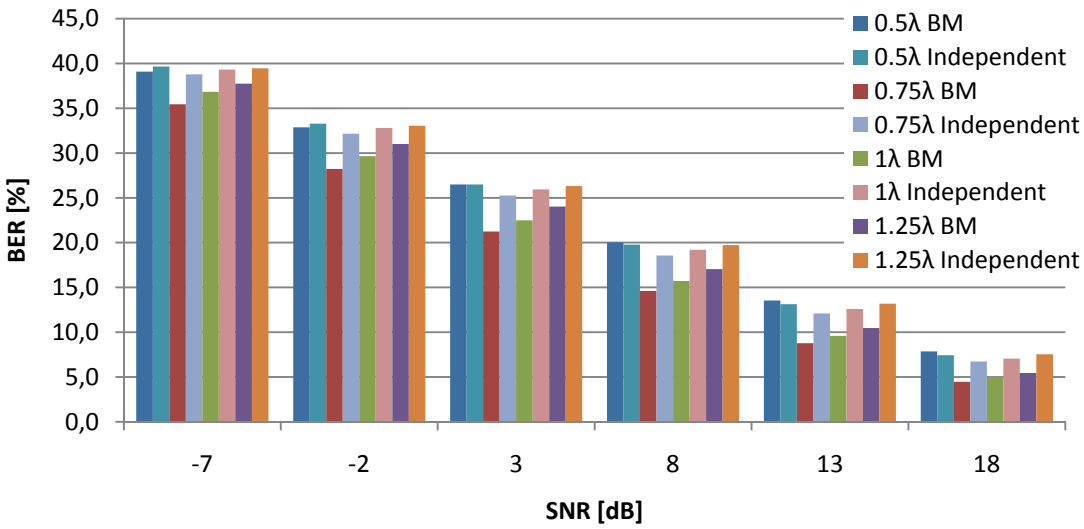

Figure 5.39 *BER performance of the two-element phased monopole array on the BCM 200 mm from the edge of the roof.*

interelement spacing of half a wavelength, where the BER of the BM fed array increases several percentage points compared to larger interelement spacings. One reason for this could be that due to the lack of nulls in the radiation pattern the orthogonal beams (that are essential to any beamforming system) cannot be taken full advantage of, or such beams are not formed effectively.

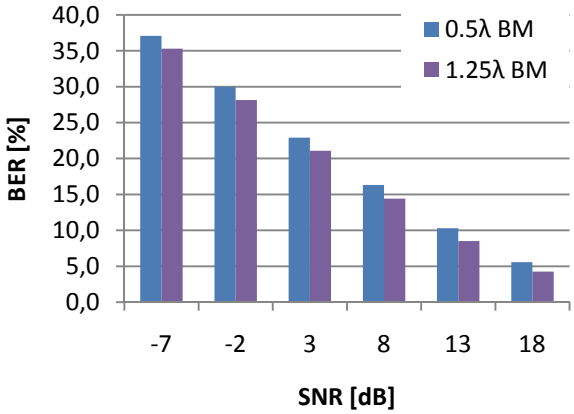

Figure 5.40. *BER performance of the two-element phased monopole array on the BCM in the centre of the roof. A reduced set of array configurations was simulated at this location.*

The BER values were also calculated for the ACM with antenna element distance of 200 mm from the roof rear edge. The results are printed in Figure 5.41. In the BM fed cases the results are quite similar to those of the BCM for interelement spacings of one-half to 1 wavelength, with the ACM having a slight advantage. BF MIMO provides again a 1−3 %-points advantage in BER, compared to feeding the elements individually. At the largest interelement spacing of 1.25λ the BER values with the BCM are significantly higher, about 5 %-points at the lower SNR values. This increase may result from the ACM's about 2 dB increase in peak gain compared to the BCM. Other than this difference in peak gain, the radiation patterns of the two models are almost identical, as can be seen in Figure 5.16.

BER values based on the measured radiation patterns are presented in Figure 5.42 for the linear array in transverse direction. The results overall are quite close to those in Figure 5.38–Figure 5.40, which is to be expected, considering the good agreement between simulated and measured radiation patterns. Still, it does seem that the

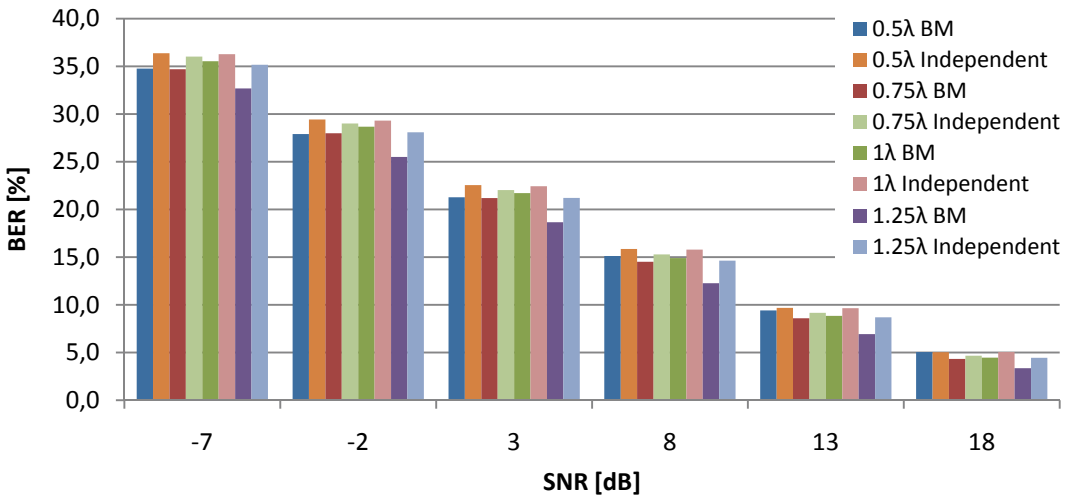

Figure 5.41. *BER performance of the two-element phased monopole array on the ACM 200 mm from the rear edge of the roof.*

measurement based BER values are consistently slightly lower, up to about 4 %-points in some cases, than corresponding simulations based BER values. The results are most discordant at 0.75λ interelement spacing. It is also interesting to note that locating the antennas further away from the edge of the roof enhances BER performance by a couple of %-points.

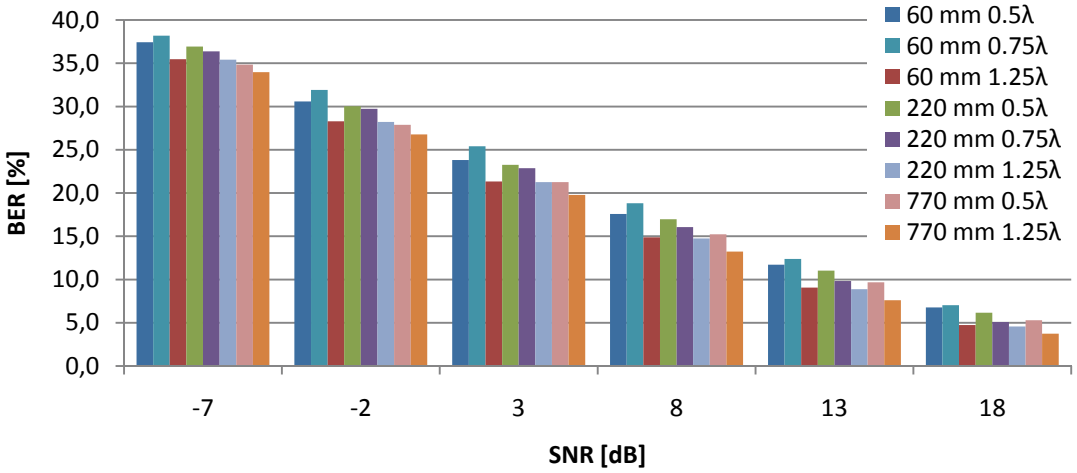

Figure 5.42. *Measurement based BER values at different interelement spacing and distances from the rear edge of the roof.*

The simulations described so far have used angular spread (AS) of 8°. To simulate the effect of a richer multipath environment, a couple of simulations were run at an increased AS of 15°. For the ACM the results with the increased angular spread are presented in Figure 5.44. The first thing to notice is that increasing the angular spread does not really change the order of the different arrays. That is, the array configuration that achieved the best BER with the smaller AS achieves the best BER with the increased AS as well; the array that was second best in terms of BER with the smaller AS is second best with the increased AS, and so on. The next thing to notice is that the advantage provided by the AS increases with increasing SNR. At the lowest SNR the difference in BER between an 8° AS and a 15° AS is only about 5 %. At an

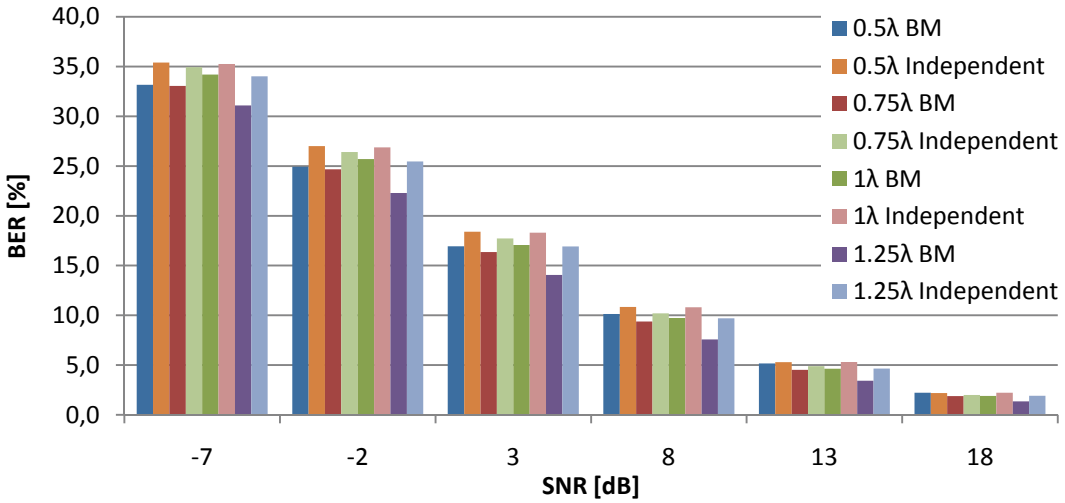

Figure 5.44. *BER performance of the two-element phased monopole array on the ACM 200 mm from the rear edge of the roof, with increased AS of 15°.*

intermediate SNR of 8 dB, the difference is already about 50 % in favour of the larger AS. Increasing the SNR further, to the largest simulated value of 18 dB, a remarkable 130 % enhancement in BER is achieved with the 15° AS, when compared to the same results with the smaller AS of 8°. Similar numbers are recorded for the BCM, for which the BER values obtained with AS of 15° are presented in Figure 5.43.

This behaviour results from the fact that increased AS means increased angular diversity, and diversity gives the more gain the larger is the SNR. The increased angular diversity results from larger phase angle differences between different antennas for the

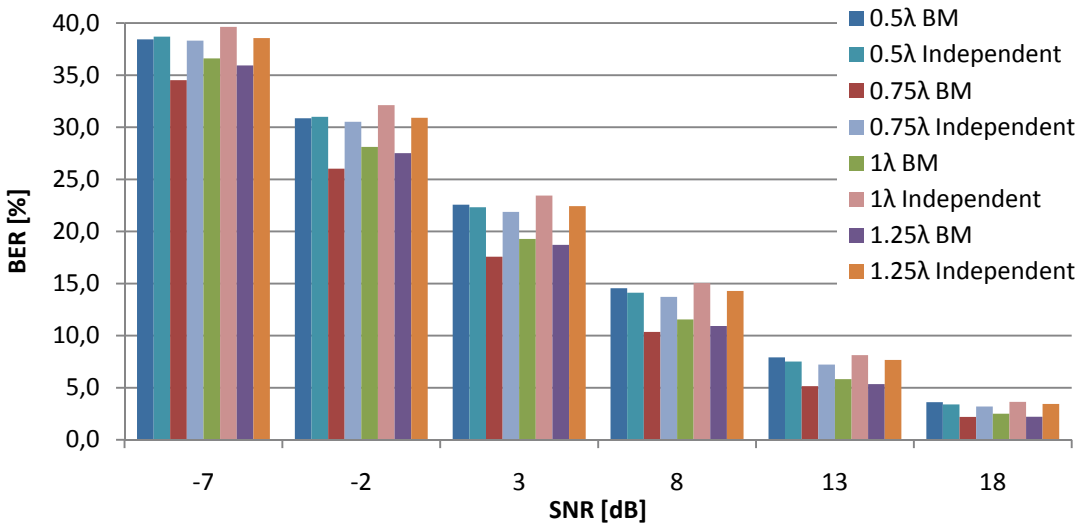

Figure 5.43. *BER performance of the two-element phased monopole array on the BCM 40 mm from the rear edge of the roof, with increased AS of 15°.*

multipaths from different local scatterers. If the SNR is sufficiently high, the diversity gain can be significant. On the other hand, if the SNR is low, the correlation between different antenna signals is dominated by the AWGN noise rather than the angular spread of multipaths.

5.4.2. Linear monopole array in the longitudinal direction

The BER calculations for the longitudinal direction linear array are presented in Figure 5.45. Compared to the corresponding case of linear array in the transverse direction (Figure 5.38) the BER values are very similar overall. What is interesting is that in the case of the longitudinal direction array, with antenna element spacings of 0.75λ and 1λ, the individual feed system provides significantly better BER values than the BM feed system. The cause of such a behaviour is unknown, since the radiation patterns with the BM feed seem to indicate a similar, if not larger gain overall than with the individual feed.

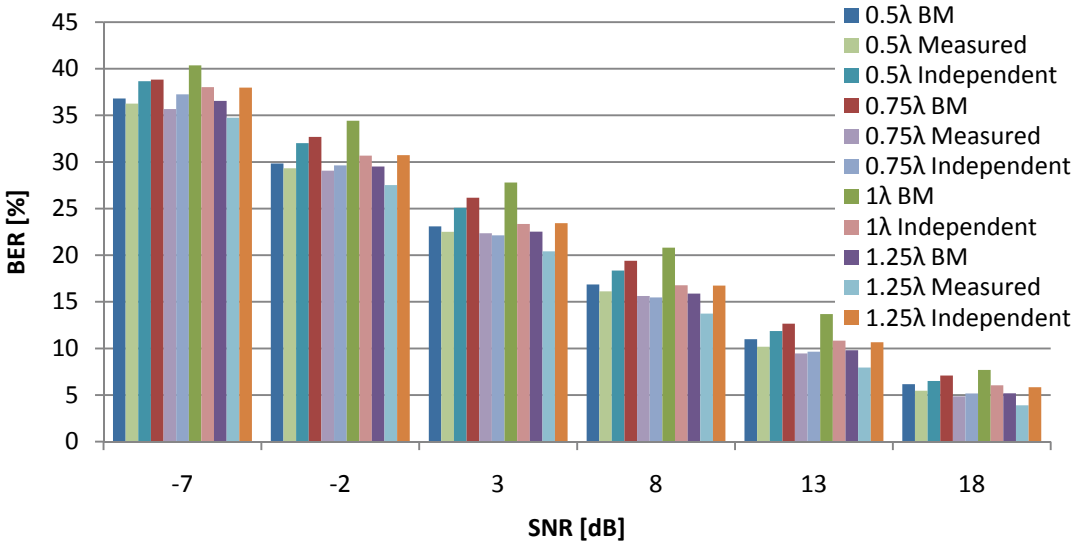

Figure 5.45. *BER performance of the two-element longitudinal direction monopole array on the BCM and measurement based BER values.*

Except for the results for 0.75λ antenna spacing, the results in Figure 5.45 with the BCM are quite well in line with the measurements based BER calculations in the same figure, although the measurement based values are generally 1–2 %-points better. The effects of increasing the angular spread to 15° are practically identical to those with the linear array in the transverse direction, and hence will not be presented here.

5.4.3. Rear window dipole element array

The radiation patterns of the dipole arrays on the rear window of the BCM were more irregular and uneven compared to those of the monopole arrays. With the ACM, the dipole array radiation patterns were a lot more irregular. The BER results for the rear window dipole array are presented in Figure 5.46 and Figure 5.47 for the BCM and the ACM, respectively. Here, BF MIMO does not seem to provide a noteworthy advantage over traditional MIMO. It does perform slightly better at the larger interelement spacings in the BCM, but slightly worse at the intermediate element spacings in the ACM. The BER values with the BCM are quite similar to those of the monopole element arrays. Disregarding the results with the 0.5λ interelement spacing, the results are markedly even. For some reason, BF MIMO with the smallest element spacing in

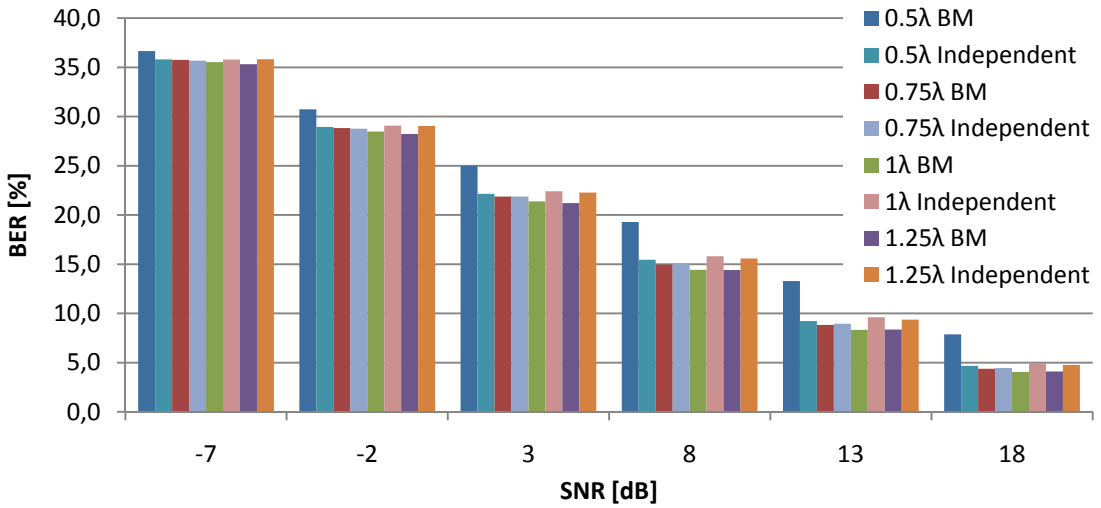

Figure 5.46. *BER performance of phased two dipole-element array on the rear window of the BCM.*

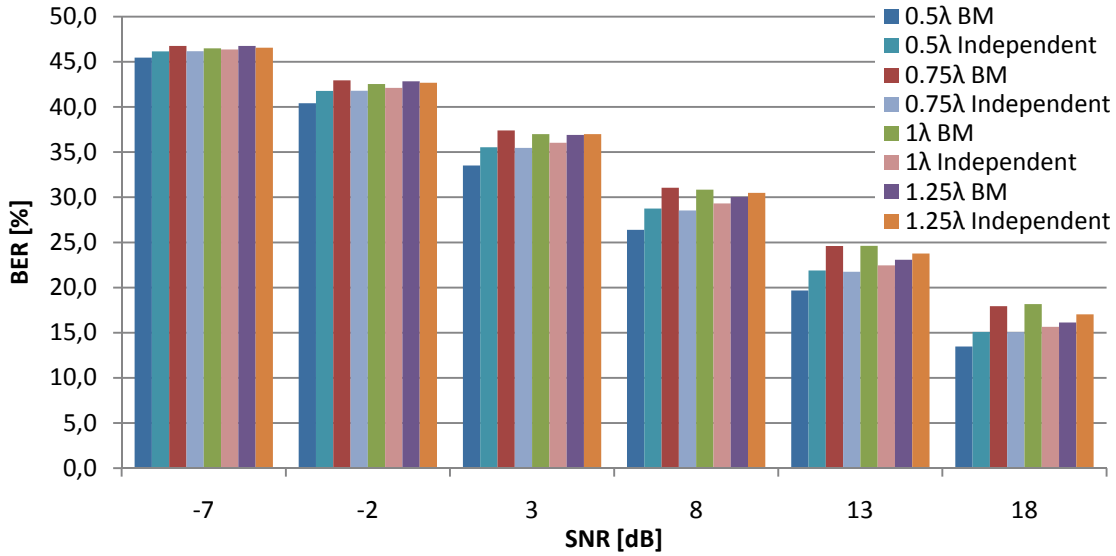

Figure 5.47. *BER performance of phased two dipole-element array on the rear window of the ACM.*

the BCM provides notably lower performance. The results with the ACM are noticeably worse than with the BCM. This is not surprising, as the overall gain levels of the ACM were more than 5 dB worse than those of the BCM. A further interesting discrepancy between the BER results of the ACM and the BCM is that while BCM achieved the best BER performance at the largest interelement spacing, the exact opposite is true in the case of the ACM. Measurements based BER calculations are better in line with the BCM results, although the BER values of the BCM with the smallest interelement spacing are peculiarly high.

5.4.4. After-market antennas

Some BER simulations were also run for after-market antennas. As is remembered, these are single antenna elements. The BER calculation code, on the other hand, was

originally developed for the simulation of multi-antenna systems. If only one antenna element is used the whole wireless transmission system changes fundamentally. While the BER calculation code was successfully adapted to the one antenna case, it does not mean that the results are comparable. In fact, because of the inherently different interference and noise characteristics of the MIMO and SISO systems, the BER results presented in this subsection are not directly comparable to those presented in the earlier subsections. Additionally, most of the after-market antennas were matched quite poorly, which may decrease the BER performance of the affected models by up to 5 %-points.

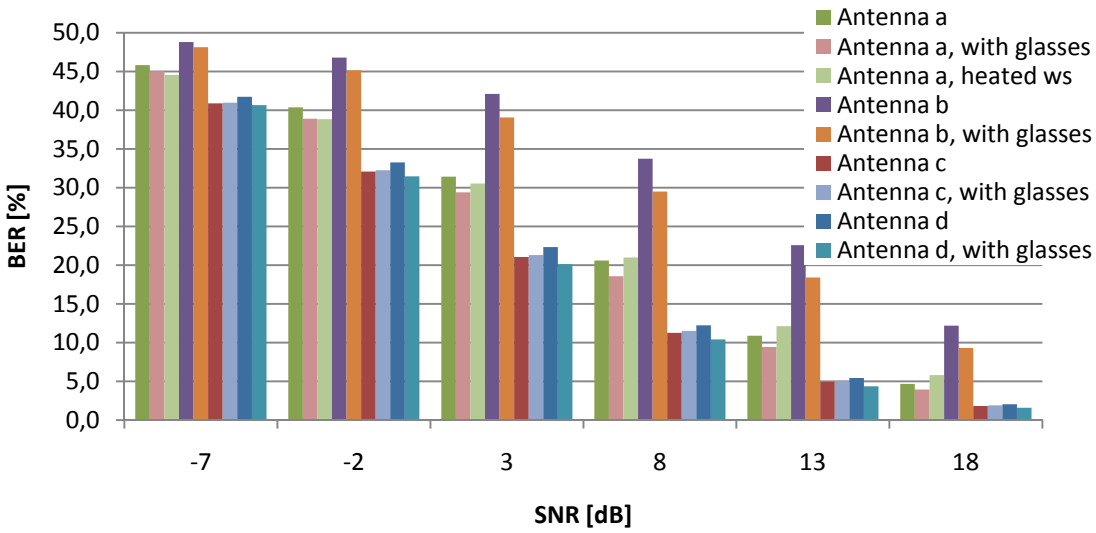

Figure 5.48. *BER performance of the after-market antennas in the BCM.*

The BER performance of the after-market antennas is presented in Figure 5.48 with the BCM. The BER results with the ACM are presented in Figure 5.49. Simulations with the window glasses and heated windscreen were only run with the BCM. The after-market antenna models referenced in the above mentioned figures were presented in Figure 4.6. The results with and without window glasses as well as with the heated windscreen (no window glasses) are included. The reader is not encouraged to make far-reaching conclusions about the relative performance of the different antenna elements, since the input matching, location in the vehicle, antenna element design and the ground planes of each antenna were anything but optimized. However, what should draw the reader's attention is how the window glasses and the heated windscreen affect the BER performance:

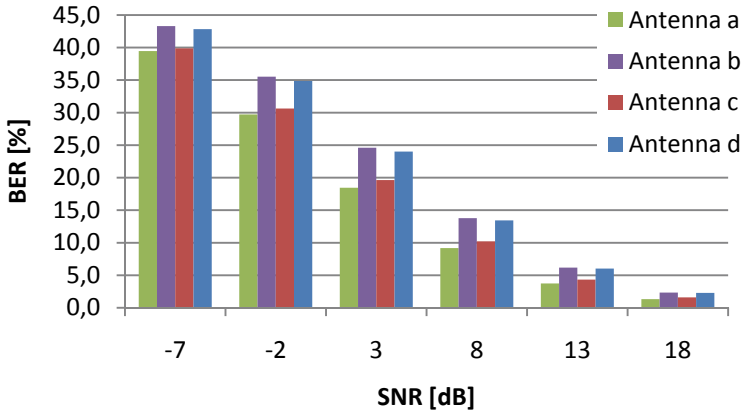

Figure 5.49. *BER performance of the after-market antennas on the ACM.*

not very much at all. In fact, in most cases it would seem that the window glasses actually enhance the performance. Any increases in the performance due to window glasses are more probably erroneous than not, but these results do suggest that the window glasses might not have a profound, adverse effect on the link level performance of the car interior mounted antennas. On the other hand, it could be that the thickness of the window glasses, relative to the wavelength, was not modelled accurately enough to show the actual effects of the glasses. On the other hand, with a simulation time of nearly 70 hours with the current model, a significantly more accurate model was not very attractive. It should be noted that simulation times counted in the tens of hours were highly unusual.

It is very interesting to note that the heated windscreen does not have a too significant adverse effect on the BER values. This is in spite of the considerably weaker gain in the forward direction, which is however offset to some extent with a stronger gain in the rearward direction. It would seem that a weak gain in certain angles is not necessarily critical to link level performance of BF MIMO systems.

6. CONCLUSIONS

This thesis had three primary objectives: to develop a procedure for the design of multi-antenna systems, to study the simulation of antennas in automotive environment using a commercial electromagnetic simulation tool and to compare the benefits of different multi-antenna systems in vehicles from the point of view of link level performance.

The FIT based CST MWS provided very accurate radiation pattern results with a simplistic car model, and could also handle a significantly detailed car model, though these simulation results could not be verified due to lack of appropriate car model for measurements. The modelling detail could be even further improved, but this would increase the computer memory requirements accordingly. All in all, FIT can be judged a fitting and accurate technique for the EM simulation of automotive antennas at the frequency of 700 MHz. Nevertheless, there are situations where other simulation methods are more effective, and cases where FIT is not applicable at all. For these cases, it is useful to acknowledge that everything that can be done with FIT can also be done with FEM (although at reduced performance in some cases), but not the other way around. Indeed, FIT can be regarded as a special case of FEM with the assumption of local orthogonality. On the other hand, simulation software and modelling methods are two very different things, and all the capabilities of a modelling method are rarely utilized by one software package, meaning that FEM-based software packages are not necessarily any better or more comprehensive than FIT-based solutions.

Link level performance simulations were based on a MATLAB implementation of the SCME channel model. Link level BER calculations were conducted with simulated and also with measured radiation patterns. The BF MIMO implementation of the multiple antenna elements was used, as it promises significant benefits in many circumstances compared to traditional MIMO. The BF MIMO uses a beam domain approach to creating parallel orthogonal paths, while traditional MIMO systems rely on antenna domain implementation. According to the link level performance simulations in this thesis, the BF MIMO approach enhances BER performance over traditional MIMO in most situations. These are the first link level simulation results for BF MIMO arrays in automotive environment that the author is aware of.

The objective was also to study the effect of antenna array configuration on the BER, and to see if an optimal configuration could be found. The results of the link level performance simulations were for the most part non-conclusive. Differences between antenna configurations were rather small in most cases, and changing the car model could change the order of the best antenna configurations. While an optimal array configuration was not found, some interesting remarks can be made based on the BER

results. It was found that the distance of the antenna array from the edge of the roof had only a small effect on the BER performance. This implies that locating the antennas quite near to the edge of the roof, for example due to improved aesthetics, does not significantly impede link level performance. Many case examples also indicate that a larger interelement spacing for the antennas may be beneficial. Yet, this is not conclusive, since some simulations point to the contrary. Using antennas located inside the car, it was found that window glasses and a heated windscreen (with wires of electrically conducting material) had little effect on the attained BER levels. The result for the case of the heated windscreen is especially interesting, because its radiation pattern clearly showed very weak gain in the forward direction. So, it seems that weak gain in certain (range of) directions does not automatically imply inferior performance. However, the models of the antennas located inside the vehicle were quite crude, and more detailed models should be used to confirm these findings.

Performance comparison of different MIMO antenna configurations is problematic. In single-antenna wireless systems the effects of the radio channel on the performance of the system can be accurately modelled with just a few quantities, like SNR and fading. Due to the added degrees of freedom associated with multi-channel propagation, describing the propagation environment of a multi-antenna system involves a lot more variables. These variables are fundamentally different in different propagation environments—indoors, outdoors, office, hall, urban, rural, and so on. Major differences were noted between measurements in different environments, and so it would seem that the channel properties affect the performance results in such a significant way that no definite conclusions can be made based on a single a measurement made under certain channel conditions and/or propagation environment. For example, a particular antenna configuration may perform well in some environments, while being markedly sub-optimal in others. The same problem exists in simulation based performance evaluation: while a certain antenna configuration may give very good results with a certain channel model, the situation may change profoundly by switching to another channel model. At the moment it seems that it must simply be accepted that—much like an antenna element should always be measured on final location—the performance of a multi-antenna system should be evaluated in a propagation environment that matches that of the intended final location of use. Of course, in the case of mobile (non-fixed) antennas, such an environment does not necessarily exist and perhaps the only choice is to evaluate the performance in diverse propagation environments, and see if a certain antenna configuration performs better than the others in most situations. A similar approach might be the only appropriate course of action with simulations as well. This means that the performance simulations should perhaps be carried out using multiple channel models (or a single channel model with scenarios for different channel conditions) to give an accurate representation of the performance of an antenna configuration in different environments. To this end, more measurements with MIMO antenna systems are needed, so that more accurate channel models can be developed.

REFERENCES

[1] McLean, J.S. A Re-Examination of the Fundamental Limits on the Radiation Q of Electrically Small Antennas. IEEE Transactions on Antennas and Propagation 44(1996)5, pp. 672–676.

[2] Chu, L.J. Physical Limitations of Omni-Directional Antennas. Journal of Applied Physics 19(1948)12, pp. 1163-1175.

[3] Hansen. R.C. Fundamental Limitations in Antennas. Proceedings of the IEEE 69(1981)2, pp. 170-182.

[4] Balanis, C.A. Antenna Theory Analysis And Design 3rd ed. Hoboken 2005, Wiley. 1117 p.

[5] Vainikainen, P. Multi-System and Multi-Element Antennas for Mobile Terminals. Oulu 2007, TKK Library. Lecture slides, PG Course in Radio Engineering. 96 p.

[6] Ollikainen, J. Design and Implementation Techniques of Wideband Mobile Communications Antennas. Dissertation. Espoo 2004. Helsinki University of Technology, Department of Electrical and Communications Engineering, Report S 266, 70 p.

[7] El Zooghby, A. Smart Antenna Engineering. Boston 2005, Artech House. 330 p.

[8] Jakes, W.C. Microwave Mobile Communications. New York 1974, Wiley. 642 p.

[9] Tse, D., Viswanath, P. Fundamentals of Wireless Communications. New York 2005, Cambridge University Press. 586 p.

[10] Gesbert, D., Shafi, M., Da-Shan, S., Smith, P.J., Naguib, A. From theory to practice: an overview of MIMO space-time coded wireless systems. IEEE Journal on Selected Areas in Communications, 21(2003)3, pp. 281-302.

[11] Paulraj, A.J., Gore, D.A., Nabar, R.U., Bolcskei, H. An Overview of MIMO Communications – A Key to Gigabit Wireless. Proceedings of the IEEE 92(2004)2, pp. 198-218.

[12] Foschini, G.J., Gans, M.J. On Limits of Wireless Communications in a Fading Environment when Using Multiple Antennas Wireless Personal Communications, 6(1998)3, pp. 311-335.

[13] Johnson, R.C. Antenna Engineering Handbook 3rd ed., New York 1993, McGraw-Hill. 1532 p.

[14] Ylitalo, J. Double-Directional Beamforming MIMO: A Simulation Study. IEEE Vehicular Technology Conference, Dublin, Ireland, April 22-25, 2007. pp. 2063-2067.

[15] Lee, W.C.Y. Mobile Communications Engineering Theory and Applications. New York 1998, McGraw-Hill. 689 p.

[16] Jankiraman, M. Space-Time Codes and MIMO Systems. Norwood 2004, Artech House. 327 p.

[17] Kyösti, P., Meinilä, J., Hentilä, L., Zhao, X., Jämsä, T., Schneider, C., Narandzić, M., Milojević, M., Hong, A., Ylitalo, J., Holappa, V., Alatossava, M., Bultitude, R., de Jong, Y., Rautiainen, T. WINNER-II Channel Models. 2007, WINNER, IST-4-027756 WINNER II D1.1.2 V1.2. 82 p.

[18] Huang, H. Spatial channel model for multiple input multiple output (MIMO) simulations. 2003, 3GPP, TR 25.996. 40 p.

[19] Gschwendtner, E. Wiesbeck,W. Ultra-Broadband Car Antennas for Communications and Navigation Applications. IEEE Transactions on Antennas and Propagation, 51(2003)8, pp. 2020-2027.

[20] Walbeoff, A., Langley, R.J. Multiband PCB antenna. IEE Proceedings Microwaves, Antennas and Propagation, 153(2005)6, pp. 471-475.

[21] Gamage, J.K., Jensen, I.A. Double-Fed Wideband Printed Monopole Antenna. International ITG Conference on Antennas, Munich, Germany, March 28-30, 2007. pp. 76-80.

[22] Azaro, R., De Natale, F.G.B., Donelli, M., Massa, A., Zeni, E. Optimized Design of a Multifunction/Multiband Antenna for Automotive Rescue Systems. IEEE Transactions on Antennas and Propagation, 54(2006)2, pp. 392-400.

[23 Brzeska, M., Chakam, G. Compact Dual Band Reduced Size PIFA Antenna for Automotive Applications. European Conference on Antennas and Propagation, Nice, France, November 6-10, 2006. pp. 1-4.

[24] Al-Khateeb, B., Rabinovich, V., Oakley, B., Alexandrov, N. Compact Planar Antennas for Short-Range Wireless Automotive Communication IEEE Transactions on Vehicular Technology, 55(2006)4, pp. 1425-1435.

[25] Economou, L. Langley, J. Circular Microstrip Patch Antennas on Glass for Vehicle Applications. IEE Proceedings Microwaves, Antennas and Propagation, 145(2005)5, pp. 416-420.

[26] Low, L. Modelling Automotive Antennas. IEEE Antennas and Propagation Society International Symposium, Volume 3, 2004, pp. 3171-3174.

[27] Low, L., Callaghan, P., Langley, R., Breden, R. Hidden Automotive Antenna Performance and Simulation. IEEE Transactions on Antennas and Propagation, 54(2006)12, pp. 3707-3712.

[28] Savia, S., Walbeoff, A., Langley, R. Automotive antenna simulation. Proceedings of the European Conference on Antennas and Propagation, Edinburgh, United Kingdom, November 11-16, 2007. pp. 1-4.

[29] Low, L., Langley, R., Batchelor, J. Modelling and Performance of Conformal Automotive Antennas. Microwaves, Antennas & Propagation, IET, 1(2007)5, pp. 973-979.

[30] Batchelor, J.C., Langley, R.J., Endo, H. On-Glass Mobile Antenna Performance Modelling. IEE Proceedings Microwaves, Antennas and Propagation, 148(2001)4, pp. 233-238.

[31] Cerretelli, M., Biffi G. Progress in Compact Multifunction Automotive Antennas International Conference on Electromagnetics in Advanced Applications, Torino, Italy, September 17-21, 2007. pp. 93-96.

[32] Filipovic, D.S., Volakis, J.L. Novel Slot Spiral Antenna Designs for Dual-Band/Multiband Operation. IEEE Transactions on Antennas and Propagation, 51(2003)3, pp. 430-440.

[33] Hopf, J.F., Reiter, L.M., Lindenmeier, S.M. Compact Multi-Antenna System for Cars With Electrically Invisible Phone Antennas for SDARS Frequencies. International INICA Conference on Antennas, Munich, Germany, March 28-30, 2007. pp. 171-175.

[34] Svantesson, T. Correlation and Channel Capacity of MIMO Systems Employing Multimode Antennas. IEEE Transactions on Vehicular Technology, 51(2002)6, pp. 1304-1312.

[35] Lambrecht, A., Schulteis, S., Wiesbeck, W. Diversity Antenna System for Radio Reception in Automative Applications. International Conference on Electromagnetics in Advanced Applications, Torino, Italy, September 17-21, 2007. pp. 21-24.

[36] Gardner, P., Hall, P.S., Lee, E., Lee, T.Y., Foster, R. Millimetre Wave Antennas Using Microstrip and Air Spaced Suspended Line Techniques for Vehicular Communications and Radar. European Conference in Antennas and Propagation, Nice, France, November 6-10, 2006. pp. 1-5

[37] Huang, J., Densmore, A.C. Microstrip Yagi Array Antenna for Mobile Satellite Vehicle Aapplication. IEEE Transactions on Antennas and Propagation, 39(1991)7, pp. 1024-1030.

[38] Swanson, D.G. Jr., Hoefer, W.J.R. Microwave Circuit Modeling using Electromagnetic Field Simulation. Norwood 2003, Artech House, 474 p.

[39] Harrysson, F. A Simple Directional Path Loss Model for a Terminal Inside a Car. IEEE 58th Vehicular Technology Conference, Orlando, USA, October 6-9, 2003. pp. 119-122.

[40] Schoof, A., Stadtler, T., Haseborg, J.L Simulation and Measurement of the Propagation of Bluetooth Signals in Automobiles. IEEE International Symposium on Electromagnetic Compatibility, Volume 2, 2003, pp. 1297-1300.

[41] Tanaka, M. A Study on the Electric Field Distribution in an Automobile Body for an Antenna System Mounted Inside the Body. IEEE Transactions on Vehicular Technology, 37(1988)2, pp. 114-119.

[42] Blöcher, H., Beilenhoff, K., Wenger, J. Simulation of the Electromagnetic Wave Propagation in Cars. European Microwave Conference, Munich, Germany, October 7-9, 2003. pp. 1151-1154.

[43] Bach Andersen, J. Antenna Arrays in Mobile Communications: Gain, Diversity, and Channel Capacity. IEEE Antennas and Propagation Magazine, 42(2000)2, pp. 12-16.

[44] Salvekar, A., Sandhu, S., Qinghua, L., Minh-Anh, V., Xiaoshu, Q. Multiple-Antenna Technology in WiMAX Systems. Intel Technology Journal, 8(2004)3, pp. 229-239.

[45] Choi, R.L., Murch, R.D., Letaief, K.B. MIMO CDMA Antenna System for SINR Enhancement. IEEE Transactions on Wireless Communications, 2(2003)2, pp. 240-249.

[46] Jeong, W., Chung, J. Analysis of Macroscopic Diversity Combining of MIMO Signals in Mobile Communications. International Journal of Electronics and Communications, 59(2005)8, pp. 454-462.

[47] Jensen, M.A., Wallace, J.W. A Review of Antennas and Propagation for MIMO Wireless Communications. IEEE Transactions on Antennas and Propagation, 52(2004)11, pp. 2810-2824.

[48] Wallace, J.W., Jensen, M.A. The Capacity of MIMO Wireless Systems With Mutual Coupling. IEEE 56th Vehicular Technology Conference, Vancouver, Canada, September 24-28, 2002. pp. 696-700.

[49] Wallace, J.W., Jensen, M.A., Swindlehurst, A.L., Jeffs, B.D. Experimental Characterization of the MIMO Wireless Channel: Data Acquisition and Analysis. IEEE Transactions on Wireless Communications, 2(2003)2, pp. 335-343.

[50] Wallace, J.W., Jensen, M.A. Termination-Dependent Diversity Performance of Coupled Antennas: Network Theory Analysis. IEEE Transactions on Antennas and Propagation, 52(2004)1, pp. 98-105.

[51] Kurpjuhn, T.P., Joham, M., Utschick, W., Nossek, J.A. Comparison of Transmission Approaches in Vehicular Standardization MIMO Channels. IEEE 59th Vehicular Technology Conference, Milan, Italy, May 17-19, 2004. pp. 784-788.

[52] Zhou, Y., Chin, F., Liang, Y.C., Ko, C.C. Performance Comparison of Transmit Diversity and Beamforming for the Downlink of DS-CDMA system. IEEE Transactions on Wireless Communications, 2(2003)2, pp. 320-334.

[53] Fettweis, G., Zimmermann, E., Jungnickel, V., Jorswieck, E.A. Challenges in Future Short Range Wireless Systems. IEEE Vehicular Technology Magazine, 1(2006)2, pp. 24-31.

[54] Boche, H., Bourdoux, A., Fonollosa, J.R., Kaiser, T., Molisch, A. Smart Antennas: State of the Art. IEEE Vehicular Technology Magazine, 1(2006)1, pp. 8-17.

[55] Laurila, J.K. Multi-Antenna Techniques in Cellular Systems. In: Nousiainen, M. (ed.). Signal Processing Advances and Smart Antenna Systems., Ylöjärvi 2003, Puolustusvoimien teknillinen tutkimuslaitos. 12 p.

[56] Sulonen, K., Suvikunnas, P., Vuokko, L., Kivinen, J., Vainikainen, P. Comparison of MIMO Antenna Configurations in Picocell and Microcell Environments. IEEE Journal on Selected Areas in Communications, 21(2003)5, pp. 703-712.

[57] Bhagavatula, R., Heath, R.W., Vishwanath, S. Optimizing MIMO Antenna Placement and Array Configurations for Multimedia Delivery in Aircraft. IEEE 65th Vehicular Technology Conference, Dublin, Ireland, April 22-25, 2007. pp. 425-429.

[58] Janaswamy, R. Effect of Element Mutual Coupling on the Capacity of Fixed Length Linear Arrays. IEEE Antennas and Wireless Propagation Letters, Volume 1, 2002, pp. 157-160.

[59] Chiurtu, N., Rimoldi, B., Telatar, E., Pauli, V. Impact of Correlation and Coupling on the Capacity of MIMO Systems. Proceedings of the 3rd IEEE International Symposium on Signal Processing and Information Technology, 2003, pp. 154-157.

[60] Munawwar, M.S. Impact of Antenna Array Geometry on the Capacity of MIMO Communication System. International Conference on Electrical and Computer Engineering, Dhaka, Bangladesh, December 19-21, 2006. pp. 80-83.

[61] Karamalis, P.D., Skentos, N.D., Kanatas, A.G. Selecting Array Configurations for MIMO Systems: an Evolutionary Computation Approach. IEEE Transactions on Wireless Communications, 3(2004)6, pp. 1994-1998.

[62] Thaysen, J., Jakobsen, K.B. Mutual Coupling Between Identical Planar Inverted-F Antennas. International Journal on Electronics and Communications, 61(2007)8, pp. 540-545.

[63] Getu, B.N., Andersen, J.B. The MIMO Cube - A Compact MIMO Antenna. IEEE Transactions on Wireless Communications, 4(2005)3, pp. 1136-1141.

[64] Jungnickel, V., Pohl, V., von Helmolt, C. Capacity of MIMO Systems with Closely Spaced Antennas. IEEE Communications Letters, 7(2003)8, pp. 361-363.

[65] Martin, C.C., Winters, J.H., Sollenberger, N.R. MIMO Radio Channel Measurements: Performance Comparison of Antenna Configurations. IEEE 54th Vehicular Technology Conference, Atlantic City, USA, October 7-11, 2001. pp. 1225-1229.

[66] Song, H.J., Sievenpiper, D., Hsu, H.P., Tangonan, G., Pikulski, J. Diversity Antenna Atudies at 2.3 GHz for Automotive Applications, and MEMS-Based Antenna Diversity Switching Circuit. IEEE 56th Vehicular Technology Conference, Vancouver, Canada, September 24-28, 2002. pp. 1096-1099.

[67] Kronberger, R., Lindenmeier, H., Reiter L., Hopf, J. Adaptive Low Profile Array Antennas for Smart Car Antenna Systems. IEEE Vehicular Technology Conference, Rhodes, Greece, May 6-9, 2001. pp. 63-67.

[68] Kronberger, R., Lindenmeier, H.K., Hopf, J.F., Reiter, L.M. Design Method for Antenna Arrays on Cars With Electrically Short Elements Under Incorporation of the Radiation Properties of the Car Body. IEEE Antennas and Propagation Society International Symposium. Volume 1, 1997, pp. 418-421.

[69] Reiter, L., Lindenmeier, H., Hopf, J., Kronberger, R. Antenna-Diversity Techniques in Cars for FM-Radio, TV and Cellular Phone. European Microwave Conference, Munich, Germany, October 4-8, 1999. pp. 147-150.

[70] Muharemovic, T., Sabharwal, A., Aazhang, B. Antenna Packing in Low-Power Systems: Communication Limits and Array Design. IEEE Transactions on Information Theory, 54(2008)1, pp. 429-440.

[71] Norklit, O., Teal, P.D., Vaughan, R.G. Measurement and Evaluation of Multi-Antenna Handsets in Indoor Mobile Communication. IEEE Transactions on Antennas and Propagation, 49(2001)3, pp. 429-437.

[72] Gao, Y., Chiau, C.C., Chen, X., Parini, C.G. Modified PIFA and Its Array for MIMO Terminals. IEE Proceedings Microwaves, Antennas and Propagation, 152(2005)4, pp. 255-259.

[73] Jofre, L. Miniature Multi-Element Antenna for Wireless Communications. IEEE Transactions on Antennas and Propagation, 50(2002)5, pp. 658-669.

[74] Manteghi, M., Rahmat-Samii, Y. A Novel Miniaturized Triband PIFA for MIMO Applications. Microwave Optical Technology Letters, 49(2007)3, pp. 724-731.

[75] Sugiura, S., Iizuka, H. Reactively Steered Ring Antenna Array for Automotive Application. IEEE Transactions on Antennas and Propagation, 55(2007)7, pp. 1902-1908.

[76] Cetiner, B.A. Multifunctional Reconfigurable MEMS Integrated Antennas for Adaptive MIMO Systems. IEEE Communications Magazine, 42(2004)12, pp. 62-70.

[77] CST Studio Suite 2008 Help. 2007. Computer Simulation Technology. Software help files.

[78] Mailloux, R.J. Phased Array Antenna Handbook 2nd ed. Norwood Mass 2005, Artech House. 508 p.

[79] Mobile WiMAX – Part I: A Technical Overview and Performance Evaluation [WWW]. WiMAX Forum. August, 2006 [referenced 10.1.2009]. Available: http://www.wimaxforum.org/documents/downloads/.

[80] Fernandes, E. User Equipment Radio Transmission and Reception (Release 7), version 7.14.0. 2008, 3GPP, TS 25.101.

[81] Baum, D.S., Salo, J., Milojevic, M., Kyösti, P., Hansen, J. MATLAB Implementation of the Interim Channel Model for Beyond-3G Systems (SCME)

[WWW]. 2005 [referenced 10.1.2009]. Available: http://radio.tkk.fi/en/research/rf_applications_in_mobile_communication/radio_channel/scm.html.

[82] Guidelines for Evaluation of Radio Interface Technologies for IMT-Advanced. 2008, International Telecommunications Union, ITU-R M.2135. 67 p.

[83] Berens, F., Dunger, H., Czarnecki, S., Bock, T., Reuter, R., Zeisberg, S., Weber J., Guasch, J.F. UWB Car Attenuation Measurements. 16th IST Mobile and Wireless Communications Summit, Budapest, Hungary, July 1-5, 2007. pp. 1-5.